A Lanczos Study of Superconducting Correlations on a Honeycomb Lattice

by

Thomas Edward McIntosh

A thesis submitted to the
Department of Physics, Engineering Physics and Astronomy
in conformity with the requirements for
the degree of Master of Science

Queen's University
Kingston, Ontario, Canada
March 2008

Abstract

In this thesis superconducting correlations on both a one-dimensional chain and a two-dimensional honeycomb lattice are analyzed using the $t - J$ model Hamiltonian. Both systems use periodic boundary conditions and different electron fillings, and both are solved numerically using the Lanczos algorithm. In order to search for superconducting correlations in the ground state the pair-pair correlation and susceptibility functions are defined. In one dimension the correlation function, at lower electronic fillings, displayed appreciable, non-zero values for all pair-pair separations. In general, the one-dimensional results were consistent with the literature. However, the honeycomb results did not show such strong superconducting correlations, as the correlation function remained close to zero for most separation distances.

Acknowledgments

The author would like to thank his supervisor, Dr. Robert J. Gooding, for his patience and guidance throughout the completion of this thesis. Thanks are also due to P. W. Leung (*University of Science and Technology of Hong Kong*) for providing his personal course notes which aided in the writing of the Lanczos code used in this study. The author would also like to thank the current members his research group, Avid Farhoodfar, Chen Xi and Wu Zhigang for their help and suggestions. Finally, the author would like to acknowledge his family (Mom, Dad, John, James, and Andy), as well as the support of his girlfriend Alison Browne.

Statement of Originality

Other than reviews of standard material contained within Appendices A, B, C, and D, the thesis is entirely the work of the author in collaboration with his supervisor, Dr. Robert J. Gooding. Any other sources used in the completion of this work have been appropriately cited.

Table of Contents

List of Figures

Chapter 1

Introduction

The first high-temperature (T_c) superconductor was discovered in 1986 [1]. Subsequently, a whole family of high-T_c superconductors have been found, with new materials being found to this day. Unlike the conventional superconductors, which were eventually explained using the Bardeen, Cooper, and Schrieffer (BCS) theory [2] (see Appendix C), high-temperature superconductivity (HTSC) has yet to gain a full description. The two types of superconductors are not considered to be completely different, and BCS theory is not excluded as a possible explanation of HTSC [3]. There are elements common to both conventional superconductivity and HTSC, such as both involve Cooper pairing [4]; there are also differences, the key difference being the mechanism causing the Cooper pairing. It is this mechanism which has eluded an explanation. In addition, there are other types of superconductors, such as heavy fermion and exotic superconductors, which are not fully described by BCS theory [3]. They are, however, not considered high-T_c, and form a sort of grey area between high-T_c and conventional superconductors. One such exotic compound is lithium titanate, $LiTi_2O_4$, which is of interest for various reasons described below, a

key reason being it is a spinel-oxide, which is rare for a superconductor. It is hoped that through an understanding of this compound, and others like it, more insight into the mechanism underlying HTSC will be found.

This study is intended to be a preliminary step in a theoretical examination of superconductivity in lithium titanate. This chapter serves as an introduction and outline of the general problem to be considered. The first section includes a brief introduction to the concepts of High-T_c superconductivity, as well as a discussion of some of the research done in this area. The second section discusses lithium titanate and its properties. The last section outlines what is to follow in the thesis.

1.1 High-T_c Superconductivity

The search for a theoretical explanation of HTSC has generated an immense number of papers. There are some reviews which attempt to gather and put in perspective this large amount of work. Reference [3] is cited numerous times in this study, and another review can be found in [5]. These reviews make it clear that there is still much work to be done, and reflect the generally inconclusive state of the research in this area.

Despite a lack of overall explanation, a large amount of experimental information has been gathered[1]. As a result many common properties have been found in these materials that have led to the general high-T_c phase diagram shown in Fig. 1.1. The defining feature of all high-T_c superconductors is the presence of copper oxide planes, which are separated from each other by layers of other atoms. This common

[1]See sections I and VI of [3] and Chapter 9 of [4] for an overview and further references.

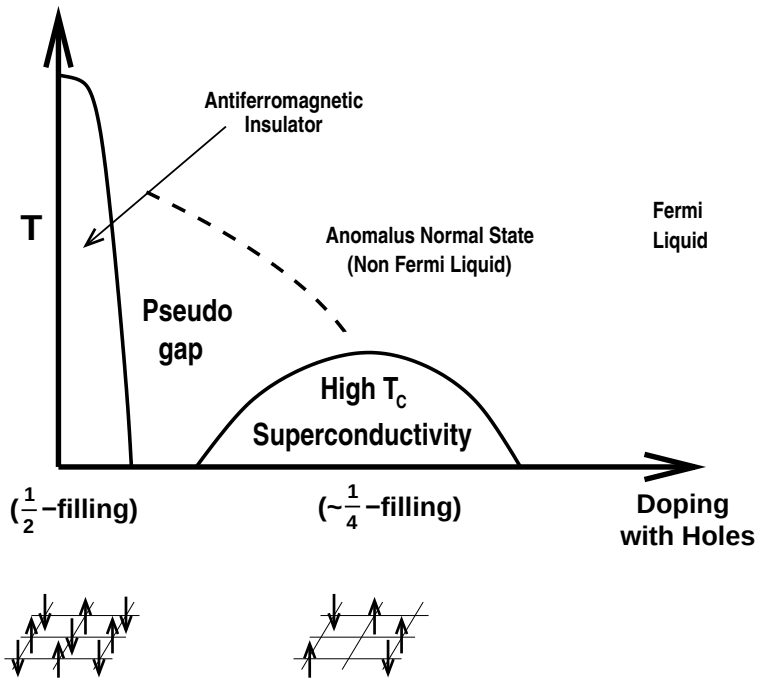

Figure 1.1: A typical high-T_c phase diagram, taken from [6]. Antiferromagnetic order is present at low temperature and low doping. Upon doping, long range spin order is destroyed, giving way first to a pseudo gap phase and eventually the superconducting phase. At higher temperatures than those that allow for superconductivity, a non-Fermi-liquid state appears. Eventually, at all temperatures, the system settles into a Fermi-liquid state.

element has led to the term "cuprate superconductors" being synonymous with high-T_c superconductors. The phenomenon responsible for HTSC is thought to occur in the copper oxide planes, with the other layers providing the charge carriers [3].

For theoretical studies, physicists turn to model Hamiltonians which are defined to describe a system of fermions residing on a lattice. The Hamiltonian together with the lattice comprise a system which attempts to mimic the properties of the high-T_c superconductors. The lattice used is usually a simplified version of the structure of the material; for instance, since the copper-oxide planes of the cuprates form a square lattice, much research considers these lattices; e.g. [7, 8, 9, 10]. The key

property that most studies strive to explain is Cooper pairing, and the mechanism causing the pairs to form. Some reviews focusing on the question of the pairing mechanism can found in [11] and [12]. It was known prior to the discovery of HTSC that singlet-pairing was enhanced in the strong on-site coupling limit of the Hubbard model [13] and that this led to an effective attractive interaction between antiparallel spins on nearest neighbour sites. This effective attractive interaction, as discussed in Appendix B, is the key to the Cooper pairing problem[14]. In part because of this, Anderson suggested the appropriate model to study the cuprates is the nearly half-filled two-dimensional Hubbard model, with moderately large on-site repulsion U, and antiferromagnetic exchange J [15].

Following this suggestion, extensive studies on the Hubbard and $t-J$ models were carried out[2]. Many of these studies focus on the large-U limit of the Hubbard model [16, 17, 18], where at half-filling it becomes equivalent to the Heisenberg model, a result that had been known for some time, e.g. [19, 13]. However, it was rigorously restated in [20] and will be derived for the simple two-site case in the next chapter. By adding holes to the Heisenberg model one gets the $t-J$ model.

It is generally agreed that both the Hubbard and $t-J$ models describe the normal state features of the cuprates [12]. For instance, antiferromagnetic order was also observed in the Heisenberg model [21, 22] using both Monte Carlo (MC) and renormalization group (RG) methods. The superconducting state, however, has not been described by these models; specifically, evidence of Cooper pair formation has not been conclusive. Several studies have approached the problem from different theoretical perspectives that find "conclusive" evidence of pairing, be it exact diagonalization [23, 24, 25, 26, 27], Monte Carlo [8, 28, 17, 27], or simply by direct analysis

[2]These models will be discussed in more detail in Chapter 2.

[29, 30]. However, there are other studies which either find no evidence of pair formation, or refute the claim that the $t - J$ or Hubbard models superconduct at all [10, 7, 31]. In fact, there is at least one example where two separate groups openly debated certain results in Physical Review Letters [28, 32, 33], which continued further into another group's paper [34]. This is simply indicative of the general HTSC debate that continues to this day.

1.2 $LiTi_2O_4$

Lithium titanate is a transition metal oxide (TMO) with a face-centred-cubic spinel crystal structure – see Fig. 1.2. In a conventional unit cell there are 32 oxygen atoms arranged in an approximate cubic-close-packed structure, forming 32 octahedra and 64 tetrahedra. The structure of $LiTi_2O_4$ is such that one-half of the octahedra are occupied by TiO_6 and one-eighth of the tetrahedra are occupied by LiO_4. Two one-band local density calculations [35, 36] of lithium titanate have shown that the $3d$ titanium orbitals are separated from the oxygen $2p$ bands by $2.4eV$. The octahedral field of the crystal around the titanium atom splits these bands into two lower t_{2g} bands and one e_g band. It was found that the Fermi energy lies within the lower t_{2g} band. Therefore, electronic conduction will take place mainly on the titanium atoms which form a corner sharing tetrahedral lattice (CSTL). As the sites of electronic conduction, the titanium sublattice is of the most interest for investigating electronic properties. With only one-half of an electron per Ti atom, this is a quarter-filled system.

$LiTi_2O_4$ was discovered to superconduct in 1973 [37], and was classified as an

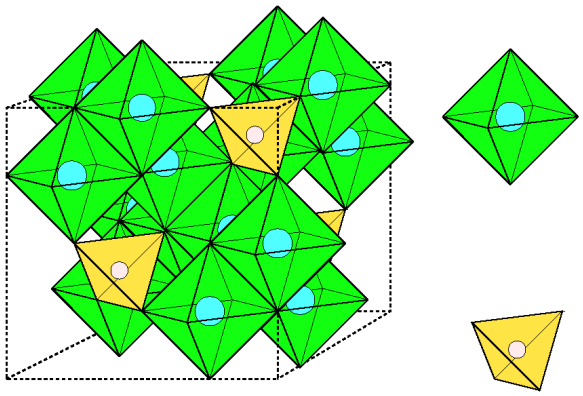

Figure 1.2: One unit cell of lithium titanate, taken from [6]. In a conventional unit cell there are 32 oxygen atoms arranged in an approximate cubic-close-packed structure, forming 32 octahedra and 64 tetrahedra. The structure of $LiTi_2O_4$ is such that one-half of the octahedra are occupied by TiO_6, seen in the top right corner, and one-eighth of the tetrahedra are occupied by LiO_4, seen in the bottom right corner. The corresponding Li or Ti atom are found in the center of the shapes, and the oxygen atoms occupy the corners which are shared with neighbouring shapes.

exotic superconductor[3] [38]. $LiTi_2O_4$ is a d-band superconductor with properties that are well described by BCS theory [39], however, the condensation mechanism is not [36]. It was found in a previous group member's Ph.D. thesis [6, 40] that strong electronic correlations play a role in the metal-to-insulator transition of $LiTi_2O_4$. Perhaps strong electronic correlations also play a role in the superconducting phase transition. Such a possibility is the main motivation for the work in this thesis.

Experimental data [41, 42, 43] from the two compounds $Li_{1+x}Ti_{2-x}O_4$ and $LiAl_yTi_{2-y}O_4$ has led to the phase diagram in Fig. 1.3. At low temperatures it has a metallic ground state, with a superconducting transition temperature of approximately 11K at zero doping. Upon doping, the system first becomes an insulator at

[3]The difference between a conventional and an exotic superconductor is characterized by the value of $\frac{T_c}{T_f}$ [38], where T_f is the Fermi temperature. For a conventional superconductor it is generally found that $\frac{T_c}{T_f} \leq \frac{1}{1000}$, and for an exotic superconductor it is considerably larger, between $\frac{1}{10}$ to $\frac{1}{100}$.

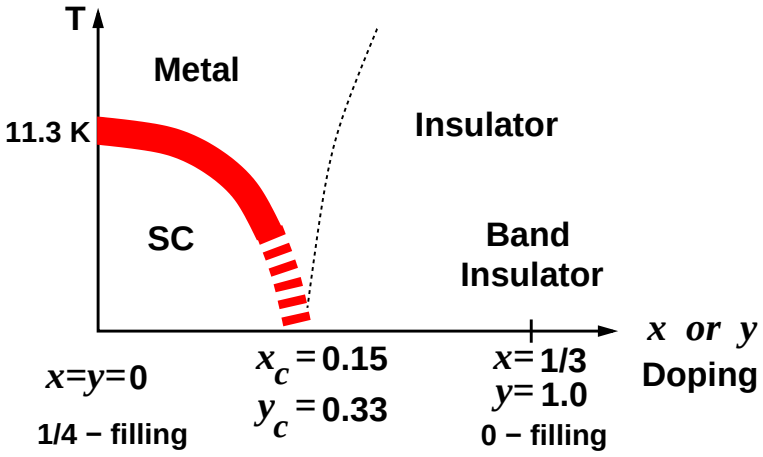

Figure 1.3: The phase diagram of lithium titanate, taken from [6]. At low temperatures it has a metallic ground state, with a superconducting transition temperature of approximately 11K at zero doping. Upon doping the system first becomes an insulator at the respective doping values of $x = 0.15$ and $y = 0.33$. Then as each doping is increased to $x = 0.33$ and $y = 1.0$, bringing the filling factor to zero, the system becomes a band insulator.

$x = 0.15$ and $y = 0.33$, then at $x = 0.33$ and $y = 1.0$; when the filling factor is zero, the system becomes a band insulator[4].

While not a high-T_c superconductor, lithium titanate, $LiTi_2O_4$, is of particular interest for its many unique features. Of the 300 or so known spinels it is one of only four having superconducting properties, and has the highest T_c of the four. It is one of the few spinels to have a metallic ground state, as well as being the only known spinel-oxide superconductor. It is also one of the few low-T_c superconducting oxides. For a thorough discussion of this compound see [38], and references therein.

An understanding of superconductivity in lithium titanate would provide a unique perspective on superconductivity due to its many unique properties. In particular, it would be interesting to find out if the pairing mechanism of lithium titanate is the same as that of high-T_c superconductors. This knowledge could provide more

[4]A band insulator means there are no electrons left in the conduction bands.

insight into HTSC, as well as the superconducting problem in general. As mentioned, in its superconducting state lithium titanate is a quarter-filled system. Studies have shown that, in some cases, the $t - J$ model has the largest pairing susceptibility[5] at quarter-filling [23, 24], suggesting the $t - J$ model may be appropriate to describe this system.

This study proposes to start from a simple Lanczos study of the system, then work up to more complicated, advanced studies, such as Monte Carlo (MC). Unfortunately, the level of computation used in this study forbids a quantitative study of the CSTL, so the honeycomb lattice will be studied instead, for reasons discussed in Chapters 2 and 3. The goal of this thesis is to understand electronic correlations on the honeycomb lattice using the $t - J$ model Hamiltonian.

1.3 Contributions and Conclusions

In this thesis a one-dimensional chain and a honeycomb lattice were analyzed to find indications of superconductivity, using a superconducting pair-pair correlation function, and the corresponding susceptibility. Our one-dimensional results did show indications of superconductivity. For the lower electronic fillings, the correlations displayed appreciable, non-zero values for all pair-pair separations. These results are consistent with other data in the literature, e.g. Ref. [23]. The honeycomb results, however, did not show strong signs of superconductivity, as the correlations quickly died off and remained close to zero for most pair-pair separations. In addition to contributing to the existing studies on the superconducting phenomenon, this thesis contributes to the study of electronic correlations on a variety of one- and

[5] See Appendix D and Chapter 4.

two-dimensional structures.

1.4 Outline of thesis presentation

The second chapter discusses the honeycomb lattice and compares it to the other lattices related to the problem. The Hubbard model and the $t-J$ model are then introduced and discussed. The chapter concludes by presenting the formal development of the $t-J$ model from the Hubbard model.

The third chapter focuses on the numerical aspects of our study. It first covers the good quantum numbers for the system, then moves on to a discussion of size of the Hilbert spaces being encountered along with some measures taken to reduce the sizes. Finally, the Lanczos method is reviewed, followed by some diagnostic considerations taken to ensure converged and reliable numerical results.

In the fourth chapter the numerical results are presented. First, a general discussion of electron pairing is given, then the pair-pair correlation and susceptibility functions are introduced. For the remainder of the chapter, the results of the pairing correlations and susceptibility as function of $\frac{J}{t}$ are presented and discussed at length for the one-dimensional chain and the two-dimensional honeycomb lattice.

The final chapter provides a summary and conclusions. This is followed by plans for future work which will be built on the study contained within this thesis.

Chapter 2

Background

As mentioned in the last chapter, in attempting to mimic the properties of transition metal-oxides (TMOs) physicists construct a model system which includes a model Hamiltonian describing electrons residing on a lattice. The intention of this chapter is to give appropriate background knowledge on the system considered in this study, which consists of the $t - J$ model Hamiltonian acting on electrons residing on a honeycomb lattice.

The first section of the chapter is divided into two subsections. The first discusses the reasons for using the honeycomb lattice and compares it to the other lattices related to the problem. The second subsection presents the mathematical description of the honeycomb lattice. The Hubbard model is presented in the second section, with two example systems given afterwards. The first example is non-interacting electrons on a honeycomb lattice. The second example is a simple two-site system containing two electrons which serves to show an important result that will carry over to the remaining sections. The third section presents the $t - J$ model, giving arguments leading to its development from the Hubbard model. The chapter concludes

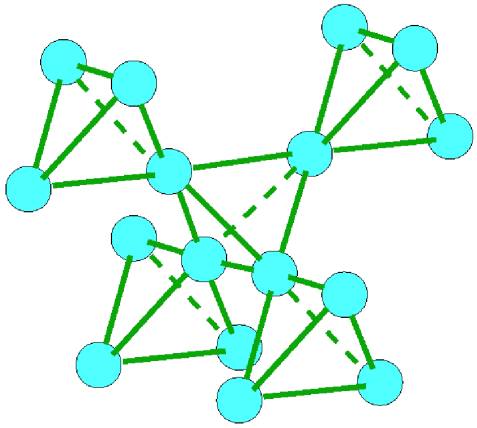

Figure 2.1: One unit cell of the corner sharing tetrahedral lattice, taken from [6], illustrating the arrangement of Ti atoms in $LiTi_2O_4$.

by presenting the formal development of the Heisenberg model from the Hubbard model.

2.1 Relevant Crystalline Lattices

The sites of electronic conduction of $LiTi_2O_4$ are found on the Ti atoms which form a CSTL, shown in Fig. 2.1. One unit cell of the CSTL contains sixteen sites. With this many sites even one unit cell is too large for the level of computing used in this study[1]. If a model system is supposed to capture the physics of a bulk material one would like to include more than one unit cell. With this in mind, a simpler system needs to be considered.

[1]The reason for this will be discussed in the next chapter, as well as in Chapter 4 where a one-dimensional system containing sixteen sites is shown to take, on a computer, anywhere between two to three weeks to find a single ground state.

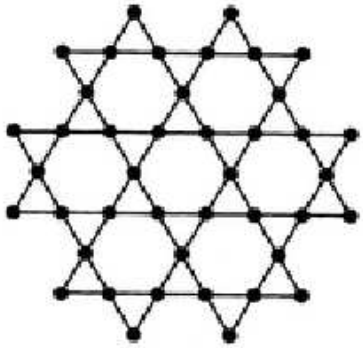

Figure 2.2: A portion of the kagomé lattice, taken from [46].

2.1.1 Lattices Related to the CSTL

Bulk CSTL can be viewed as an ...ABCABC... stacking of two-dimensional kagomé lattices (see Figs. 2.2 and 2.3). Whereas a kagomé lattice would have been an ideal structure to study, the honeycomb lattice (Fig. 2.4) will be used instead; it has two basis sites per unit cell as opposed to three for the kagomé lattice. This allows a greater number of unit cells to be considered. The kagomé and honeycomb lattices are similar, both having a triangular Bravais lattice and the same symmetries. However, the kagomé is frustrated, or non-bipartite[2], whereas the honeycomb is not.

The honeycomb lattice is a much simpler structure than the CSTL. For example, the CSTL has four basis sites per unit cell and is frustrated, whereas the honeycomb lattice only has two basis sites and is not frustrated. Also, the CSTL only has three-fold rotational symmetry, whereas the honeycomb has six-fold. However, the honeycomb lattice retains some of the features of the CSTL, most notably the

[2]A bipartite lattice is a lattice that may be divided into two sub-lattices such that no site on a sub-lattice is a nearest-neighbour to a site on the same sub-lattice. If this is not the case the lattice is considered to be non-bipartite, or frustrated. As such, no configuration exists that simultaneously satisfies all of the interactions between spins, usually resulting in a highly degenerate ground state. See Refs. [44] and [45] for further discussions.

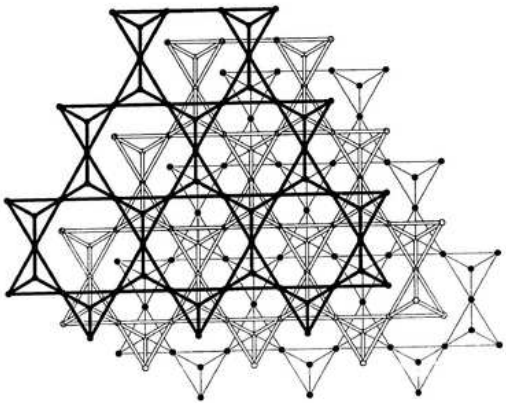

Figure 2.3: An "overhead" view of the CSTL illustrating how it can be viewed as a stacking of kagomé lattices, taken from [46].

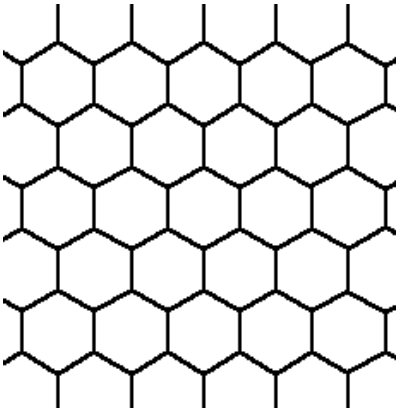

Figure 2.4: A portion of the honeycomb lattice.

underlying triangular basis and, in general, the multi-sited basis. Most importantly it provides a simple starting point with which to build up to a study of the CSTL.

Despite the simpler structure, the study of the honeycomb lattice is interesting in its own right. There are some superconducting compounds for which the study of the honeycomb lattice is relevant. The underlying triangular structure of $Na_xCoO_2yH_2O$ is noted in [47] as a reason to consider the honeycomb lattice. Another, more concrete example is graphene, which has been observed to superconduct [48], and is a

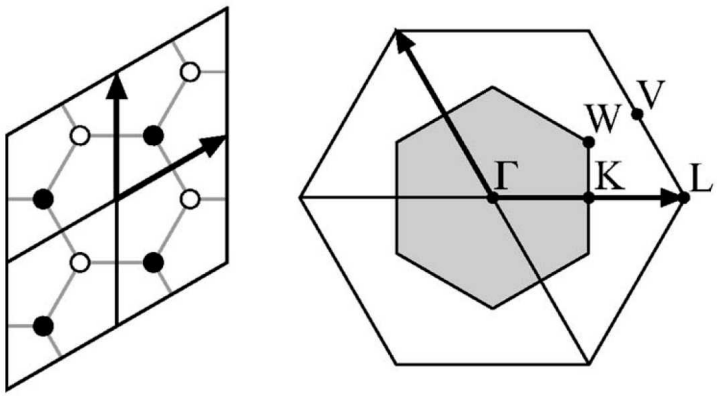

Figure 2.5: On the left is an illustration of the unit cells of the honeycomb lattice, taken from [47]. The two arrows represent the Bravais lattice vectors: note the triangular shape of the basis. Within the arrows the two-site basis is indicated by the circles and each site is differentiated by the different colouring. On the right is the honeycomb lattice in reciprocal space. The high-symmetry points are indicated, where $\Gamma = (0, 0)$, $K = \left(\frac{2\pi}{3}, 0\right)$, $L = \left(\frac{4\pi}{3}, 0\right)$, $V = \left(\pi, \frac{\pi}{\sqrt{3}}\right)$, and $W = \left(\frac{2\pi}{3}, \frac{2\pi}{3\sqrt{3}}\right)$.

honeycomb lattice. The honeycomb lattice is also a natural choice for comparing and contrasting results with other commonly studied two-dimensional lattices, such as square and the other types of triangular lattices.

2.1.2 The Honeycomb Lattice

The honeycomb lattice is represented as a two-dimensional triangular Bravais lattice with a two-point basis, as shown in Fig. 2.5. The unit cell of a triangular lattice may be defined by the vectors

$$\mathbf{d}_1 = \frac{\sqrt{3}a}{2}\left(\sqrt{3}\hat{x} + \hat{y}\right) \qquad \mathbf{d}_2 = \sqrt{3}a\hat{y}\ , \tag{2.1}$$

where $\hat{x}$ and $\hat{y}$ are the usual unit vectors of the Cartesian plane. For simplicity, below the lattice constant, a, which specifies the size of the unit cell, is set equal to one. The Bravais lattice is then

$$\mathbf{R}_{m,n} = m\mathbf{d}_1 + n\mathbf{d}_2. \tag{2.2}$$

The basis sites within the unit cell are given by the vectors

$$\mathbf{r}_1 = 0 \qquad \mathbf{r}_2 = \frac{1}{3}\left(\mathbf{d}_1 + \mathbf{d}_2\right), \tag{2.3}$$

and thus any atom may be found at the positions

$$\mathbf{R}_{m,n,\alpha} = \mathbf{R}_{m,n} + \mathbf{r}_\alpha \ , \tag{2.4}$$

where $\alpha = 1, 2$ labels the two atoms within each unit cell.

The basis vectors for the reciprocal lattice are

$$\mathbf{b}_1 = \frac{4\pi}{3}\hat{\mathbf{x}} \quad \mathbf{b}_2 = -\frac{2\pi}{3}\hat{\mathbf{x}} + \frac{2\pi}{\sqrt{3}}\hat{\mathbf{y}} \ , \tag{2.5}$$

and the reciprocal lattice vectors are then

$$\mathbf{G} = (g_1\mathbf{b}_1 + g_2\mathbf{b}_2) = \frac{2\pi}{3}\left(2g_1 - g_2\right)\hat{\mathbf{x}} + \frac{2\pi}{\sqrt{3}}g_2\hat{\mathbf{y}} \ , \tag{2.6}$$

where $g_i = 0, \pm 1, \pm 2, ...$ See Fig. 2.5, which illustrates reciprocal space and the high-symmetry points: $\Gamma = (0, 0)$, $K = \left(\frac{2\pi}{3}, 0\right)$, $L = \left(\frac{4\pi}{3}, 0\right)$, $V = \left(\pi, \frac{\pi}{\sqrt{3}}\right)$, and $W = \left(\frac{2\pi}{3}, \frac{2\pi}{3\sqrt{3}}\right)$. These points are important for a plot of the energy band structure[3]

[3]For a review of some elementary solid state topics, such as Bloch's theorem and energy bands, see Appendix A.

given in the next section.

2.2 The Hubbard Model

Attempting to describe the interactions of many-electron systems is very complicated, and often theorists turn to simplified models which retain some of the important features of the system while ignoring other, hopefully less important features. Perhaps the simplest model of an interacting many-electron system is the Hubbard model [49].

2.2.1 General Discussion

The Hubbard model uses tight-binding arguments that exploit the fact that the electron density in a d-band transition metal is concentrated close to the nuclei and sparse in between. In effect, one can view the electrons as residing on a particular atom. The location of an atom in the material is referred to as a lattice site, or simply a site, where at most two electrons may occupy any single site provided they have opposite spin. The electrons may "hop" between nearest neighbour sites, contributing an off-diagonal element, $-t$, to the Hamiltonian. In addition, in the Hubbard model electrons interact only through Coulombic repulsion when residing on the same site.

The hopping constitutes the kinetic energy part of the Hamiltonian. By itself it is sometimes called the "hopping term," which using occupation number formalism is given by

$$H_{hop} = -t \sum_{<i,j>,\sigma} (c^{\dagger}_{i,\sigma} c_{j,\sigma} + c^{\dagger}_{j,\sigma} c_{i,\sigma}) \ , \tag{2.7}$$

where i and j label the sites, and σ labels the spin. The brackets, $<,>$, indicate the sum is performed over nearest neighbour sites only, with each pair of sites only

counted once.

The Coulombic interaction between electrons comprises the potential energy of the Hamiltonian. In its most general form it is given by

$$V_{ee} = U \sum_i n_{i,\uparrow} n_{i,\downarrow} + \sum_{i \neq j} V_{|i-j|} n_i n_j \ , \tag{2.8}$$

where i and j run over the lattice sites. The first term, or U-term, considers only on-site interactions. The second term, or V-term, considers all other interactions, and, in general, $V_{|i-j|} \sim \frac{1}{|\mathbf{r}_i - \mathbf{r}_j|}$, where $\mathbf{r}_i$ is the position of the ith atom. U and V are energy scales which define the strength of the interaction. If U or V is positive (negative) the respective interaction is repulsive (attractive).

The Hubbard model only considers repulsive, on-site interactions and so only the U-term is retained. Finally, the nearest-neighbour-hopping Hubbard model is given by,

$$H_{Hub} = -t \sum_{<i,j>,\sigma} (c^\dagger_{i,\sigma} c_{j,\sigma} + c^\dagger_{j,\sigma} c_{i,\sigma}) + U \sum_i n_{i,\uparrow} n_{i,\downarrow} \ . \tag{2.9}$$

It will be shown below that in the large U limit, where the on-site repulsion is effectively so large that no site can accommodate two electrons, the ground state is a singlet. Furthermore, at half-filling and in this large U limit the Hubbard model becomes equivalent to the Heisenberg model. This will be derived explicitly in § 2.4.

2.2.2 Example System - Non-Interacting Electrons on a Honeycomb Lattice

To tie in the topics of the last two sections, and indeed with the overall purpose of this study, a system of non-interacting electrons moving on a honeycomb lattice

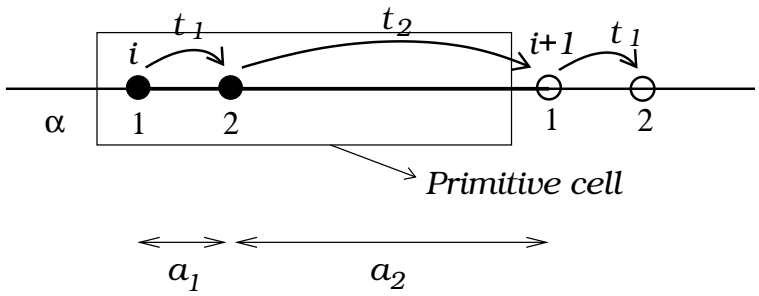

Figure 2.6: An illustration of hopping on a two-site basis in one-dimension, taken from [6]. In general, two different hopping energies, t_1 and t_2, are required since the distance between the two sites in the unit cell might be different than the distance between the unit cells.

will be considered. The honeycomb lattice has a two-site basis, which makes matters a little more complicated. So consider first the simpler situation of hopping on a one-dimensional chain with a two-site basis. This situation is depicted in Fig. 2.6.

For the case of non-interacting electrons, U is set to zero in Eq. (2.9), leaving only the hopping term, i.e. Eq. (2.7). Hopping on a two-site basis requires a slight modification to account for two different hopping energies, t_1 and t_2, reflecting that the distance between the two sites in the unit cell might be different than the distance between the unit cells[4]. The Hamiltonian may be expressed

$$H_{hop} = -\sum_{i,\nu,\sigma} \left(t_1 c^\dagger_{i,1,\sigma} c_{i,2,\sigma} + t_2 c^\dagger_{i,2,\sigma} c_{i+1,1,\sigma} + h.c. \right) \ . \tag{2.10}$$

In this case i labels the primitive cell, the second subscript labels the atom within the primitive cell and h.c. indicates the corresponding Hermitian conjugate.

For the two-dimensional honeycomb lattice, all sites are equivalent, and so there is only one hopping energy, i.e. $t_1 = t_2 = t$. However, each atom has three nearest neighbours (as opposed to two for the one-dimensional case), so this adds another

[4]For real materials this would be due to the possibility that the atoms in the unit cell are different.

hopping term into the Hamiltonian,

$$H_{hop} = -t \sum_{m,n,\sigma} \left(c^{\dagger}_{m,n,2,\sigma} c_{m,n,1,\sigma} + c^{\dagger}_{m,n,2,\sigma} c_{m+1,n,1,\sigma} + c^{\dagger}_{m,n,2,\sigma} c_{m,n+1,1,\sigma} + h.c. \right) \ . \tag{2.11}$$

Inserting the Fourier transforms

$$c_{m,n,1,\sigma} = \frac{1}{\sqrt{N}} \sum_{\mathbf{k}} e^{i\mathbf{k}\cdot\mathbf{R}_{m,n}} a_{\mathbf{k},\sigma} \tag{2.12}$$

$$c_{m,n,2,\sigma} = \frac{1}{\sqrt{N}} \sum_{\mathbf{k}} e^{i\mathbf{k}\cdot\mathbf{R}_{m,n}} b_{\mathbf{k},\sigma} \tag{2.13}$$

the Hamiltonian becomes

$$H_{hop} = -t \sum_{\mathbf{k},\sigma} \left(b^{\dagger}_{\mathbf{k},\sigma} a_{\mathbf{k},\sigma} \left(1 + e^{-i\mathbf{k}\cdot\mathbf{d}_1} + e^{-i\mathbf{k}\cdot\mathbf{d}_2} \right) + h.c. \right) \ . \tag{2.14}$$

By setting

$$A_{\mathbf{k}} = |A_{\mathbf{k}}| e^{i\phi_{\mathbf{k}}} = \left(1 + e^{-i\mathbf{k}\cdot\mathbf{d}_1} + e^{-i\mathbf{k}\cdot\mathbf{d}_2} \right) \ , \tag{2.15}$$

and introducing

$$a_{\mathbf{k},\sigma} = \frac{1}{\sqrt{2}} \left(f_{\mathbf{k},\sigma} + g_{\mathbf{k},\sigma} \right) e^{-i\frac{\phi_{\mathbf{k}}}{2}} \tag{2.16}$$

$$b_{\mathbf{k},\sigma} = \frac{1}{\sqrt{2}} \left(f_{\mathbf{k},\sigma} - g_{\mathbf{k},\sigma} \right) e^{+i\frac{\phi_{\mathbf{k}}}{2}} \ , \tag{2.17}$$

where f and g are fermion field operators representing the two bands arising from the two sites per unit cell. The Hamiltonian may now be expressed in diagonal form

$$H_{hop} = -t \sum_{\mathbf{k},\sigma} |A_{\mathbf{k}}| \left(f^{\dagger}_{\mathbf{k},\sigma} f_{\mathbf{k},\sigma} - g^{\dagger}_{\mathbf{k},\sigma} g_{\mathbf{k},\sigma} \right) \ . \tag{2.18}$$

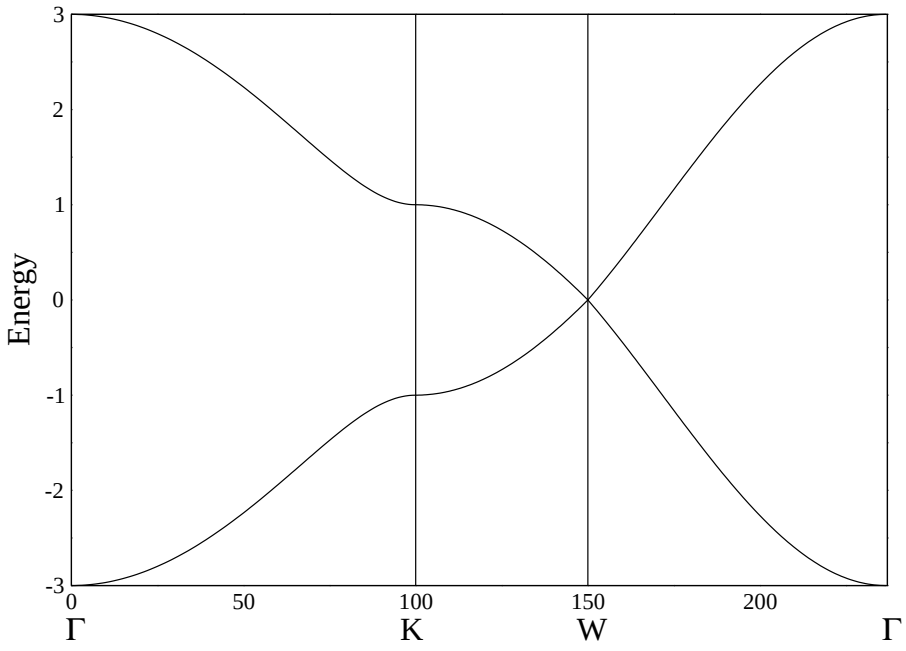

Figure 2.7: A plot of the energy bands for a system of non-interacting electrons on a honeycomb lattice. Referring to Fig. 2.5, the points correspond to $\Gamma = (0, 0)$, $K = \left(\frac{2\pi}{3}, 0\right)$, and $W = \left(\frac{2\pi}{3}, \frac{2\pi}{3\sqrt{3}}\right)$.

The energies of the two bands are then seen to be given by $\pm|A_{\mathbf{k}}|t$. A plot of the energy bands can be found in Fig. 2.7.

2.2.3 Example System - Two Sites, Two Electrons

Previously, a two-atom basis was considered. Now electron-electron interaction will be included on a simpler system consisting of two interacting electrons on a two-site lattice. Fully expanded, the Hubbard model of Eq. (2.9) reads

$$H_{Hub} = -t(c^{\dagger}_{1,\uparrow}c_{2,\uparrow} + c^{\dagger}_{2,\uparrow}c_{1,\uparrow} + c^{\dagger}_{1,\downarrow}c_{2,\downarrow} + c^{\dagger}_{2,\downarrow}c_{1,\downarrow}) + U(n_{1,\uparrow}n_{1,\downarrow} + n_{2,\uparrow}n_{2,\downarrow}) \ . \qquad (2.19)$$

To aid the analysis further, and to tie in with the overall discussion of the thesis, we select the subspace of zero magnetization to work in. To be more concrete, let m_z be the eigenvalue of the operator S_z^{tot} in the ground state, $|\psi\rangle$, i.e. $S_z^{tot}|\psi\rangle = m_z|\psi\rangle$. Then we select the subspace $m_z = 0$. In this case, there are only four possible arrangements of the electrons on the lattice:

$$c^\dagger_{1,\uparrow}c^\dagger_{1,\downarrow}|0\rangle, \quad c^\dagger_{1,\uparrow}c^\dagger_{2,\downarrow}|0\rangle, \quad c^\dagger_{2,\uparrow}c^\dagger_{1,\downarrow}|0\rangle, \text{ and } c^\dagger_{2,\uparrow}c^\dagger_{2,\downarrow}|0\rangle \ . \tag{2.20}$$

The ground state of the system is then some linear combination of these four states.

The matrix representing the Hamiltonian has the form

$$H = \begin{pmatrix} U & -t & -t & 0 \\ -t & 0 & 0 & -t \\ -t & 0 & 0 & -t \\ 0 & -t & -t & U \end{pmatrix} , \tag{2.21}$$

and has eigenvalues 0, U, $\frac{1}{2}\left(U + \sqrt{U^2 + 16t^2}\right)$, and $\frac{1}{2}\left(U - \sqrt{U^2 + 16t^2}\right)$. The last yields the lowest eigenvalue for all U, with corresponding eigenvector

$$|\psi_{gs}\rangle = \begin{pmatrix} -\frac{1}{4}\left(U/t - \sqrt{(U/t)^2 + 16}\right) \\ 1 \\ 1 \\ -\frac{1}{4}\left(U/t - \sqrt{(U/t)^2 + 16}\right) \end{pmatrix} . \tag{2.22}$$

Now, consider these results in the large U/t limit

$$|\psi_{gs}\rangle = c^\dagger_{1,\uparrow}c^\dagger_{2,\downarrow}|0\rangle + c^\dagger_{2,\uparrow}c^\dagger_{1,\downarrow}|0\rangle + O\left(t/U\right) + \ldots \approx \begin{pmatrix} 0 \\ 1 \\ 1 \\ 0 \end{pmatrix} . \tag{2.23}$$

Thus, the ground state can be approximated as

$$|\psi_{gs}\rangle \approx (c^\dagger_{1,\uparrow}c^\dagger_{2,\downarrow} - c^\dagger_{1,\downarrow}c^\dagger_{2,\uparrow})|0\rangle \ . \tag{2.24}$$

This is a singlet state with zero double-occupancy.

The energy of this state in this limit is given by the expression $\frac{1}{2}\left(U - \sqrt{U^2 + 16t^2}\right)$ $\xrightarrow[\infty]{U} -\frac{4t^2}{U}$. With U taken to be large, this energy is clearly quite small. The two states corresponding to the energies U and $\frac{1}{2}\left(U + \sqrt{U^2 + 16t^2}\right)$ are also singlets. However, in this large U/t limit these energies are large compared with $-\frac{4t^2}{U}$. The other state corresponding to the energy of 0 is a triplet, with $m_z = 0$. Had we not restricted ourselves to the $m_z = 0$ subspace, the other two states $c^\dagger_{1,\uparrow}c^\dagger_{1,\uparrow}|0\rangle$ and $c^\dagger_{1,\downarrow}c^\dagger_{1,\downarrow}|0\rangle$ would have also been included. These states would have $m_z = 1$ $m_z = -1$ as eigenvalues of the S^{tot}_z operator, respectively, and would therefore make up the remaining triplet states. The energy eigenvalues of these states would clearly be zero, since in both states neither electron could hop, nor could both electrons occupy the same site, due to the Pauli exclusion principle.

The energy spectrum for this system consists of one singlet state of energy $E_s = -\frac{4t^2}{U}$, three triplets of energy $E_t = 0$, and two more high energy singlet states. The difference in energy between the lowest singlet and the three triplets may be expressed

as $J = E_t - E_s = \frac{4t^2}{U}$. It will be shown in the final section of this chapter that, in this same large U/t limit the Hubbard model becomes equivalent to the Heisenberg model, and the characteristic energy scale is given by $J = \frac{4t^2}{U}$.

2.3 $t - J$ Model - Qualitative Development

The Heisenberg model is defined as

$$H_{Heis} = J \sum_{<i,j>} \mathbf{S}_i \cdot \mathbf{S}_j \ . \tag{2.25}$$

$\mathbf{S}_i$ is the total spin operator on the ith lattice site, and is given by

$$\mathbf{S}_i = \frac{1}{2} c^\dagger_{i,\alpha} \boldsymbol{\sigma}_{\alpha,\beta} c^\dagger_{i,\beta} \ , \tag{2.26}$$

where $\boldsymbol{\sigma}_{\alpha,\beta} = \sigma^x_{\alpha,\beta}\hat{\mathbf{x}} + \sigma^y_{\alpha,\beta}\hat{\mathbf{y}} + \sigma^z_{\alpha,\beta}\hat{\mathbf{z}}$, and the $\sigma^k_{\alpha,\beta}$ are the Pauli spin matrices. In this model the lattice is considered half-filled, with no doubly occupied sites, i.e. each site contains one, and only one, electron. The energy scale, $J = \frac{4t^2}{U}$, is the same as that just mentioned in the last section; this result will be derived in the next section.

The Heisenberg model presents an alternative interaction between electrons, where they interact magnetically, through spin, as opposed to electronically, through charge, as in the Hubbard model. To make explicit the action of this Hamiltonian, the term $\mathbf{S}_i \cdot \mathbf{S}_j$ will be expanded using Eq. (2.26) and the commutation relations for the Pauli spin matrices. This yields

$$\mathbf{S}_i \cdot \mathbf{S}_j = S^z_i S^z_j + \frac{1}{2}\left(S^+_i S^-_j + S^-_i S^+_j\right) \ , \tag{2.27}$$

where,

$$S_i^z = \frac{1}{2}\left(n_{i,\uparrow} - n_{i,\downarrow}\right) \tag{2.28}$$

$$S_i^+ = c_{i,\uparrow}^\dagger c_{i,\downarrow} \tag{2.29}$$

$$S_i^- = c_{i,\downarrow}^\dagger c_{i,\uparrow} \ . \tag{2.30}$$

S_i^+ and S_i^- are the usual raising and lowering operators which effectively flip the spin of the electron residing on the ith site.

The Hamiltonian is seen to have both diagonal and off-diagonal terms, both representing the interaction between electrons on neighbouring sites via anti-ferromagnetic exchange. The diagonal element is $\frac{J}{4}$ $\left(-\frac{J}{4}\right)$ if the two electrons on nearest neighbour sites have parallel (anti-parallel) spin. The off-diagonal term is $-\frac{J}{2}$ and exchanges electrons of opposite spin on nearest neighbour sites.

To illustrate this model, again consider a system of two sites and two electrons. With double occupancy eliminated there are only two possible states,

$$c_{1,\uparrow}^\dagger c_{2,\downarrow}^\dagger|0\rangle \quad c_{2,\uparrow}^\dagger c_{1,\downarrow}^\dagger|0\rangle, \tag{2.31}$$

and the matrix representing the system is then

$$H = \begin{pmatrix} -\frac{J}{4} & -\frac{J}{2} \\ -\frac{J}{2} & -\frac{J}{4} \end{pmatrix} \ . \tag{2.32}$$

Diagonalizing this yields a ground state energy of $-3\frac{J}{4}$, with singlet ground state

eigenvector

$$|\psi_{gs}\rangle = (c^{\dagger}_{1,\uparrow}c^{\dagger}_{2,\downarrow} - c^{\dagger}_{1,\downarrow}c^{\dagger}_{2,\uparrow})|0\rangle \ . \tag{2.33}$$

Note the same result was found for the half-filled Hubbard model, in the large $\frac{U}{t}$ limit, in § 2.3. This indeed foreshadows the equivalency of the Hubbard and Heisenberg models at half-filling and large $\frac{U}{t}$, as shown in the next section.

It is worth noting that sometimes the Heisenberg model is written as

$$H_{Heis} = J \sum_{<i,j>} \left(\mathbf{S}_i \cdot \mathbf{S}_j - \frac{1}{4} \right) \ . \tag{2.34}$$

The operator $\mathbf{S}_i \cdot \mathbf{S}_j$ has eigenvalue $-\frac{3}{4}$ in the singlet and eigenvalue $\frac{1}{4}$ in the triplet. Thus the above will have an eigenvalue $-J$ in a singlet state and 0 in a triplet. This extra factor reflects the connection with the Hubbard model in the large $\frac{U}{t}$ limit, as will be shown in the next section.

Consider now the Heisenberg model away from half-filling, but still retaining the no double occupancy restriction. With vacancies present the electrons can move around the lattice, this is represented by adding the hopping term back into the Hamiltonian. One then arrives at the $t-J$ model,

$$H = -t \sum_{<i,j>,\sigma} (c^{\dagger}_{i,\sigma}(1-n_{i,\bar{\sigma}})(1-n_{j,\bar{\sigma}})c_{j,\sigma} + h.c.) + J \sum_{<i,j>} \mathbf{S}_i \cdot \mathbf{S}_j \ . \tag{2.35}$$

This will be the model used in this study [3]. The extra terms, $(1-n_{i,\bar{\sigma}})$ and $(1-n_{j,\bar{\sigma}})$ appearing in the hopping term are projection operators which serve to prohibit double occupany, where $\bar{\sigma} = \uparrow$ ($\downarrow$) if $\sigma = \downarrow$ ($\uparrow$), and h.c. is the corresponding Hermitian conjugate. One should keep in mind that it is common to find the $t-J$ model defined

in the literature without this projection operator, where the hopping restriction is to be implicitly understood.

As a concluding note, there are many variations and modifications of this model that can be found in the literature. For example, one could also consider an electronic interaction between electrons on nearest-neighbour sites. This is the so-called $t-J-V$ Hamiltonian [23, 24],

$$H = -t \sum_{<i,j>,\sigma} (c^{\dagger}_{i,\sigma}(1-n_{i,\bar{\sigma}})(1-n_{j,\bar{\sigma}})c_{j,\sigma}+h.c.)+J \sum_{<i,j>} \mathbf{S}_i \cdot \mathbf{S}_j + V \sum_{<i,j>} n_{i,\uparrow} n_{j,\downarrow} \ . \quad (2.36)$$

One could further lift the no double occupancy restriction and allow an on-site repulsion, this is the $t-J-U$ model [30]

$$H = -t \sum_{<i,j>,\sigma} (c^{\dagger}_{i,\sigma} c_{j,\sigma} + h.c.) + J \sum_{<i,j>} \mathbf{S}_i \cdot \mathbf{S}_j + U \sum_{i} n_{i,\uparrow} n_{i,\downarrow} \ . \quad (2.37)$$

As these models are not used in this study no further mention of them will be made.

2.4 $t-J$ Model - Formal Development

The equivalency of the Hubbard model and the Heisenberg model will now be derived. As mentioned this result is achieved in a half-filled system, with double occupancy restricted, in the large-$\frac{U}{t}$ limit. The result has been known since the mid-1970's [19], and was shown in alternative ways thereafter, e.g. see Ref. [13]. However, it was rigorously restated, with HTSC in mind, in Ref. [20], and this is the approach that will be followed below.

Starting with the Hubbard model in Eq. (2.9),

$$H = -t \sum_{<i,j>,\sigma} (c^{\dagger}_{i,\sigma} c_{j,\sigma} + c^{\dagger}_{j,\sigma} c_{i,\sigma}) + U \sum_{i} n_{i,\uparrow} n_{i,\downarrow} = T + V \ , \tag{2.38}$$

one then decomposes the T term into three distinct hoppings: one which increases the number of doubly occupied sites by one, T_1, one which decreases the number of doubly occupied sites by one, T_{-1}, and one which leaves the number of doubly occupied sites the same, T_0. This is achieved by multiplying the T-term on the left by $n_{i,\bar{\sigma}} + h_{i,\bar{\sigma}} = 1$, and on the right by $n_{j,\bar{\sigma}} + h_{j,\bar{\sigma}} = 1$, where $\bar{\sigma} = \uparrow (\downarrow)$ if $\sigma = \downarrow (\uparrow)$, and $h_{i,\bar{\sigma}} = 1 - n_{i,\bar{\sigma}}$ is the number operator for holes. Hence,

$$T = T_1 + T_0 + T_{-1} \ , \tag{2.39}$$

where,

$$T_1 = -t \sum_{<i,j>,\sigma} n_{i,\bar{\sigma}} (c^{\dagger}_{i,\sigma} c_{j,\sigma} + c^{\dagger}_{j,\sigma} c_{i,\sigma}) h_{j,\bar{\sigma}} \tag{2.40}$$

$$T_0 = -t \sum_{<i,j>,\sigma} \Big(h_{i,\bar{\sigma}} (c^{\dagger}_{i,\sigma} c_{j,\sigma} + c^{\dagger}_{j,\sigma} c_{i,\sigma}) h_{j,\bar{\sigma}} + n_{i,\bar{\sigma}} (c^{\dagger}_{i,\sigma} c_{j,\sigma} + c^{\dagger}_{j,\sigma} c_{i,\sigma}) n_{j,\bar{\sigma}} \Big) \tag{2.41}$$

$$T_{-1} = -t \sum_{<i,j>,\sigma} h_{i,\bar{\sigma}} (c^{\dagger}_{i,\sigma} c_{j,\sigma} + c^{\dagger}_{j,\sigma} c_{i,\sigma}) n_{j,\bar{\sigma}} \ . \tag{2.42}$$

Thus Eq. (2.9) becomes

$$H = T_1 + T_0 + T_{-1} + V. \tag{2.43}$$

The goal is to transform this Hamiltonian into a form

$$H' = \exp(iS)\, H \exp(-iS) = H + \frac{[iS, H]}{1!} + \frac{[iS, [iS, H]]}{2!} + ... \tag{2.44}$$

which does not allow hops between states of differing numbers of doubly occupied sites; in effect, this removes the T_1 and T_{-1} terms. This may be done by choosing

$$iS = U^{-1}\left(T_1 - T_{-1}\right) \ . \tag{2.45}$$

Putting Eqs. (2.45) and (2.43) into Eq. (2.44) and using the relation $[V, T_m] = mUT_m$ [20] it is found that

$$H' = V + T_0 + U^{-1}\left([T_1, T_{-1}] + [T_0, T_{-1}] + [T_1, T_0]\right) + O\left(U^{-2}\right) \ . \tag{2.46}$$

However, this still contains terms which change the number of doubly occupied sites, i.e. the $[T_0, T_{-1}]$ and $[T_1, T_0]$ terms. In the approach found in Refs. [20] and [18] a general expression for $iS^{(k)}$, for a kth order transformation ($H'^{[k]} = \exp\left(iS^{(k)}\right) H \exp\left(-iS^{(k)}\right)$) is given which eliminates such terms up to order k. This will not be discussed here as only a first-order transformation is desired, and is beyond the scope of this discussion. It will suffice to simply drop the terms which do not maintain the same number of doubly occupied sites. The desired transformed Hamiltonian is

$$H' = V + T_0 + U^{-1}\left([T_1, T_{-1}]\right) \ . \tag{2.47}$$

Working in the singly occupied subspace, the operator T_{-1} acting on any state will then be zero, since there are no doubly occupied states to reduce. For the same reason, V operating on any state will also give zero. Thus, the above equation may be further simplified to

$$H' = T_0 - \frac{T_{-1}T_1}{U} \ . \tag{2.48}$$

If we consider a half-filled system there is no allowed hopping, thus $\langle T_0 \rangle = 0$ and therefore

$$H' = -\frac{T_{-1}T_1}{U} \ . \tag{2.49}$$

In this subspace there are only two possible configurations, $c^\dagger_{1,\uparrow}c^\dagger_{2,\downarrow}|0\rangle = |\uparrow,\downarrow\rangle$ and $c^\dagger_{1,\downarrow}c^\dagger_{2,\uparrow}|0\rangle = |\downarrow,\uparrow\rangle$. $T_{-1}T_1$ acting on these yield

$$T_{-1}T_1|\uparrow,\downarrow\rangle = 2t^2\left(|\uparrow,\downarrow\rangle - |\downarrow,\uparrow\rangle\right) \tag{2.50}$$

$$T_{-1}T_1|\downarrow,\uparrow\rangle = -2t^2\left(|\uparrow,\downarrow\rangle - |\downarrow,\uparrow\rangle\right) \ . \tag{2.51}$$

We may now transform Eq. (2.49) to the basis $|\uparrow,\downarrow\rangle, |\downarrow,\uparrow\rangle$ by introducing a complete set $1 = |\uparrow,\downarrow\rangle\langle\uparrow,\downarrow| + |\downarrow,\uparrow\rangle\langle\downarrow,\uparrow|$ on both sides of Eq. (2.49),

$$H' = -\frac{t^2}{U}\left(|\uparrow,\downarrow\rangle\langle\uparrow,\downarrow| + |\downarrow,\uparrow\rangle\langle\downarrow,\uparrow|\right)\left(T_{-1}T_1\right)\left(|\uparrow,\downarrow\rangle\langle\uparrow,\downarrow| + |\downarrow,\uparrow\rangle\langle\downarrow,\uparrow|\right) \ . \tag{2.52}$$

Expanding and using Eq. (2.50) leads to

$$H' = -\frac{2t^2}{U}\left(|\uparrow,\downarrow\rangle - |\downarrow,\uparrow\rangle\right)\left(\langle\uparrow,\downarrow| - \langle\downarrow,\uparrow|\right) \ . \tag{2.53}$$

Now to convert to a spin Hamiltonian, H_S, the relation (see Ref. [18])

$$H_S = \frac{1}{2^N}\sum_{\alpha_1,\alpha_2,\ldots,\alpha_N=0}^{3}\left(\prod_{\ell=1}^{N}\sigma_\ell^{\alpha_\ell}\right)Tr\left(\sigma_1^{\alpha_1}\sigma_2^{\alpha_2}\ldots\sigma_N^{\alpha_N}H^{(k)}\right) \ , \tag{2.54}$$

is used, where ℓ labels the site, and σ^α refers to the Pauli spin matrices[5]. For two

[5]That is $\alpha = 1,2,3$ refers to σ^x, σ^y and σ^z respectively, and $\alpha = 0$ refers to the identity matrix σ^0.

sites we then have

$$\begin{aligned} H_S = \frac{1}{2^2}\big(&\sigma_1^0\sigma_2^0 Tr\left(\sigma_1^0\sigma_2^0 H'\right) + \sigma_1^x\sigma_2^x Tr\left(\sigma_1^x\sigma_2^x H'\right) \\ &+\sigma_1^y\sigma_2^y Tr\left(\sigma_1^y\sigma_2^y H'\right) + \sigma_1^z\sigma_2^z Tr\left(\sigma_1^z\sigma_2^z H'\right)\big) \ . \end{aligned} \tag{2.55}$$

For each of the Pauli matrices, $Tr\left(\sigma_1^\alpha\sigma_2^\alpha H'\right) = 4\frac{t^2}{U}$, and for the σ_i^0, i.e. the identity matrix, $Tr\left(\sigma_1^0\sigma_2^0 H'\right) = -4\frac{t^2}{U}$, leading to

$$\begin{aligned} H_S &= -\frac{1}{4}\left(4\frac{t^2}{U}\sigma_1^0\sigma_2^0 - 4\frac{t^2}{U}\sigma_1^x\sigma_2^x - 4\frac{t^2}{U}\sigma_1^y\sigma_2^y - 4\frac{t^2}{U}\sigma_1^z\sigma_2^z\right) \\ &= -\frac{t^2}{U}\left(\sigma_1^0\sigma_2^0 - \sigma_1^x\sigma_2^x - \sigma_1^y\sigma_2^y - \sigma_1^z\sigma_2^z\right) \\ &= \frac{t^2}{U}\left(\sigma_1\cdot\sigma_2 - 1\right) \end{aligned} \tag{2.56}$$

Using the relation $\mathbf{S} = \frac{1}{2}\boldsymbol{\sigma}$ the version of the Heisenberg model given in Eq. (2.34) is found

$$H_S = J\left(\mathbf{S}_1\cdot\mathbf{S}_2 - \frac{1}{4}\right) \tag{2.57}$$

where

$$J = \frac{4t^2}{U} \ . \tag{2.58}$$

Thus we see that the half-filled Hubbard model, under the conditions outlined above, yields the Heisenberg model, where the energy scale is given by J, which is equivalent to $\frac{4t^2}{U}$.

Chapter 3

Lanczos Studies of Interacting Electrons

The systems considered in our study have a Hilbert space that is much too large to diagonalize exactly. This, therefore, requires the use of the Lanczos algorithm [50], a common method which is used to find the ground state of a system. The Lanczos method was largely ignored when it was first published in the 1950's, due to it being numerically unstable [51]. In the 1970's the algorithm was revised [52], leading to a more stable version that had faster convergence [53].

This chapter focuses on the numerical aspects of our study. The first section will cover the good quantum numbers for the system; in the second section the size of the Hilbert spaces being encountered will be addressed along with some measures taken to reduce the sizes; in the final section the Lanczos method will be reviewed, along with a discussion of some important aspects of its implementation. This is followed by some diagnostic considerations taken to ensure converged and reliable numerical results.

3.1 Good Quantum Numbers of the $t-J$ model

A first step in studying any quantum mechanical system is finding good quantum numbers which allow for an efficient representation of the system. For reasons that will become clear in the next section, the eigenvalues of the operators S^z_{tot} and S^2 are a convenient choice. Thus, it is necessary to show that the Hubbard and $t-J$ Hamiltonians commute with the operators S^z_{tot} and S^2. Since the hopping term (Eq. (2.7)) appears in both models, it will be shown to commute with both of these operators first, after which the U and J terms of their respective models will be shown to commute with these operators.

First, we consider $[H_{hop}, S^z_{tot}]$, where

$$S^z_{tot} = \sum_i S^z_i = \frac{1}{2}\sum_i \left(n_{i,\uparrow} - n_{i,\downarrow}\right) \ . \tag{3.1}$$

We then have,

$$\begin{aligned}
[H_{Hop}, S^z_{tot}] &= \left[-t \sum_{<i,j>,\sigma} (c^\dagger_{i,\sigma} c_{j,\sigma} + c^\dagger_{j,\sigma} c_{i,\sigma}), \frac{1}{2}\sum_\ell \left(n_{\ell,\uparrow} - n_{\ell,\downarrow}\right)\right] \\
&= -\frac{t}{2} \sum_{<i,j>,\sigma} \sum_\ell \Big(\left[c^\dagger_{i,\sigma} c_{j,\sigma}, n_{\ell,\uparrow}\right] - \left[c^\dagger_{i,\sigma} c_{j,\sigma}, n_{\ell,\downarrow}\right] \\
&\qquad + \left[c^\dagger_{j,\sigma} c_{i,\sigma}, n_{\ell,\uparrow}\right] - \left[c^\dagger_{j,\sigma} c_{i,\sigma}, n_{\ell,\downarrow}\right] \Big) \ .
\end{aligned} \tag{3.2}$$

The expanded form allows use of the number operator commutation property

$$\sum_{<i,j>,\sigma} \sum_{\ell,\alpha} \left[c^\dagger_{i,\sigma} c_{j,\sigma}, n_{\ell,\alpha}\right] = 0 \ . \tag{3.3}$$

This property will be used throughout this section. This gives

$$[H_{hop}, S^z_{tot}] = 0 \ . \tag{3.4}$$

For the U-term of the Hubbard model,

$$\left[U \sum_i n_{i,\uparrow} n_{i,\downarrow}, S^z_{tot} \right] = 0 \tag{3.5}$$

because the number operator must commute with itself. Therefore,

$$[H_{Hub}, S^z_{tot}] = 0 \ . \tag{3.6}$$

Similarly, for the J-term of the $t-J$ model,

$$\begin{aligned} \left[J \sum_{<i,j>} \mathbf{S}_i \cdot \mathbf{S}_j, S^z_{tot} \right] &= \frac{J}{2} \sum_{<i,j>} \sum_{\ell} \left[S^z_i S^z_j + \frac{1}{2} \left(S^+_i S^-_j + S^-_i S^+_j \right), n_{\ell,\uparrow} - n_{\ell,\downarrow} \right] \qquad (3.7) \\ &= J \sum_{<i,j>} \sum_{\ell} \Big(\left[S^z_i S^z_j, S^z_\ell \right] + \frac{1}{2} \Big(\left[S^+_i S^-_j, n_{\ell,\uparrow} \right] \\ &\qquad - \left[S^+_i S^-_j, n_{\ell,\downarrow} \right] + \left[S^-_i S^+_j, n_{\ell,\uparrow} \right] - \left[S^-_i S^+_j, n_{\ell,\downarrow} \right] \Big) \Big) \end{aligned}$$

Now, obviously $\left[S^z_i S^z_j, S^z_\ell \right] = 0$, since S^z_i must commute with itself. For the other terms, consider the term $\left[S^+_i S^-_j, n_{\ell,\uparrow} \right]$, which can be expanded to

$$\left[S^+_i S^-_j, n_{\ell,\uparrow} \right] = S^+_i \left[S^-_j, n_{\ell,\uparrow} \right] + \left[S^+_i, n_{\ell,\uparrow} \right] S^-_j \ . \tag{3.8}$$

Since $S^+_i = c^\dagger_{i,\uparrow} c_{i,\downarrow}$ and $S^-_i = c^\dagger_{i,\downarrow} c_{i,\uparrow}$, this is seen to contain specific cases of the

property in Eq. (3.3). Thus,

$$\left[J \sum_{<i,j>} \mathbf{S}_i \cdot \mathbf{S}_j, S^z_{tot} \right] = 0 \ . \tag{3.9}$$

Finally

$$[H_{t-J}, S^z_{tot}] = 0 \ . \tag{3.10}$$

Now consider the S^2 operator. The spin operator $\mathbf{S}$ defined on an N-site lattice is

$$\mathbf{S} = \sum_i^N \mathbf{S}_i \ , \tag{3.11}$$

and so,

$$\mathbf{S}^2 = \sum_i \mathbf{S}_i^2 + 2 \sum_{i \neq j} \mathbf{S}_i \cdot \mathbf{S}_j \ . \tag{3.12}$$

Again, the hopping term will be shown to commute first. Consider,

$$\left[H_{hop}, \mathbf{S}^2 \right] = \sum_i \left[H_{hop}, \mathbf{S}_\ell^2 \right] + 2 \sum_{\ell \neq m} \left[H_{hop}, \mathbf{S}_\ell \cdot \mathbf{S}_m \right] \ . \tag{3.13}$$

Each term will be dealt with separately. Rewriting $\mathbf{S}_\ell^2 = (S_\ell^z)^2 + \frac{1}{2} \left(S_\ell^+ S_\ell^- + S_\ell^- S_\ell^+ \right)$ we find

$$\sum_\ell \left[H_{hop}, \mathbf{S}_\ell^2 \right] = \sum_\ell \left[H_{hop}, (S_\ell^z)^2 \right] + \sum_\ell \left[H_{hop}, \frac{1}{2} \left(S_\ell^+ S_\ell^- + S_\ell^- S_\ell^+ \right) \right] \ . \tag{3.14}$$

It was already shown that H_{hop} commutes with S_ℓ^z, and therefore

$$\sum_\ell \left[H_{hop}, (S_\ell^z)^2 \right] = 0 \ . \tag{3.15}$$

For the second term in Eq. (3.14), consider the general form of a ladder operator, $S^{\pm}_{\ell} = c^{\dagger}_{\ell,\alpha} c_{\ell,\bar{\alpha}}$ where $\bar{\alpha} = \uparrow(\downarrow)$ if $\alpha = \downarrow(\uparrow)$ and $\alpha = \uparrow(\downarrow)$ corresponds to $S^{+}_{\ell}\left(S^{-}_{\ell}\right)$. Thus, in general commutators of the form $\sum_{<i,j>\ell,\sigma,\alpha}\left[c^{\dagger}_{i,\sigma}c_{j,\sigma}, c^{\dagger}_{\ell,\alpha}c_{\ell,\bar{\alpha}}\right]$ must be computed,

$$
\begin{aligned}
&\sum_{<i,j>\ell,\sigma,\alpha}\left[c^{\dagger}_{i,\sigma}c_{j,\sigma}, c^{\dagger}_{\ell,\alpha}c_{\ell,\bar{\alpha}}\right] = \sum_{<i,j>\ell,\sigma,\alpha}\left(c^{\dagger}_{i,\sigma}c_{j,\sigma}c^{\dagger}_{\ell,\alpha}c_{\ell,\bar{\alpha}} - c^{\dagger}_{\ell,\alpha}c_{\ell,\bar{\alpha}}c^{\dagger}_{i,\sigma}c_{j,\sigma}\right) \\
= &\sum_{<i,j>\ell,\sigma,\alpha} c^{\dagger}_{i,\sigma}c_{j,\sigma}c^{\dagger}_{\ell,\alpha}c_{\ell,\bar{\alpha}} - \sum_{<i,j>\ell,\sigma,\alpha} c^{\dagger}_{\ell,\alpha}\left(\delta_{\ell,i}\delta_{\bar{\alpha},\sigma} - c^{\dagger}_{i,\sigma}c_{\ell,\bar{\alpha}}\right)c_{j,\sigma} \\
= &\sum_{<i,j>\ell,\sigma,\alpha} c^{\dagger}_{i,\sigma}c_{j,\sigma}c^{\dagger}_{\ell,\alpha}c_{\ell,\bar{\alpha}} - \sum_{<i,j>,\alpha} c^{\dagger}_{i,\alpha}c_{j,\bar{\alpha}} + \sum_{<i,j>\ell,\sigma,\alpha} c^{\dagger}_{\ell,\sigma}c^{\dagger}_{i,\sigma}c_{\ell,\bar{\alpha}}c_{j,\sigma} \\
= &\sum_{<i,j>\ell,\sigma,\alpha} c^{\dagger}_{i,\sigma}c_{j,\sigma}c^{\dagger}_{\ell,\alpha}c_{\ell,\bar{\alpha}} - \sum_{<i,j>,\alpha} c^{\dagger}_{i,\alpha}c_{j,\bar{\alpha}} + \sum_{<i,j>\ell,\sigma,\alpha} c^{\dagger}_{i,\sigma}c^{\dagger}_{\ell,\sigma}c_{j,\sigma}c_{\ell,\bar{\alpha}} \\
= &\sum_{<i,j>\ell,\sigma,\alpha} c^{\dagger}_{i,\sigma}c_{j,\sigma}c^{\dagger}_{\ell,\alpha}c_{\ell,\bar{\alpha}} - \sum_{<i,j>,\alpha} c^{\dagger}_{i,\alpha}c_{j,\bar{\alpha}} + \sum_{<i,j>\ell,\sigma,\alpha} c^{\dagger}_{i,\sigma}\left(\delta_{\ell,j}\delta_{\alpha,\sigma} - c_{j,\sigma}c^{\dagger}_{\ell,\sigma}\right)c_{\ell,\bar{\alpha}} \\
= &\sum_{<i,j>\ell,\sigma,\alpha} c^{\dagger}_{i,\sigma}c_{j,\sigma}c^{\dagger}_{\ell,\alpha}c_{\ell,\bar{\alpha}} - \sum_{<i,j>,\alpha} c^{\dagger}_{i,\alpha}c_{j,\bar{\alpha}} + \sum_{<i,j>,\alpha} c^{\dagger}_{i,\alpha}c_{j,\bar{\alpha}} - \sum_{<i,j>\ell,\sigma,\alpha} c^{\dagger}_{i,\sigma}c_{j,\sigma}c^{\dagger}_{\ell,\sigma}c_{\ell,\bar{\alpha}} \\
= &\ 0\ .
\end{aligned}
$$

This gives

$$\sum_{\ell}\left[H_{hop}, S^{\pm}_{\ell}\right] = 0\ , \tag{3.16}$$

and using this property yields,

$$\sum_{\ell}\left[H_{hop}, \frac{1}{2}\left(S^{+}_{\ell}S^{-}_{\ell} + S^{-}_{\ell}S^{+}_{\ell}\right)\right] = 0\ . \tag{3.17}$$

Therefore,

$$\sum_{\ell}\left[H_{hop}, S^{2}_{\ell}\right] = 0\ . \tag{3.18}$$

Now consider the $[H_{hop}, \mathbf{S}_\ell \cdot \mathbf{S}_m]$ term; since $\mathbf{S}_\ell \cdot \mathbf{S}_m = S^z_\ell \cdot S^z_m + \frac{1}{2}\left(S^+_\ell S^-_m + S^-_\ell S^+_m\right)$,

$$\sum_{\ell \neq m} \left[H_{hop}, S^2_\ell\right] = \sum_{\ell \neq m} \left[H_{hop}, S^z_\ell S^z_m\right] + \frac{1}{2} \sum_{\ell \neq m} \left[H_{hop}, \left(S^+_\ell S^-_m + S^-_\ell S^+_m\right)\right] \ . \tag{3.19}$$

We already know that $\sum_\ell \left[H_{hop}, S^z_\ell\right] = 0$, and therefore $\sum_{\ell \neq m} \left[H_{hop}, S^z_\ell S^z_m\right] = 0$. Finally we note that

$$\sum_{\ell \neq m} \left[H_{hop}, \left(S^+_\ell S^-_m + S^-_\ell S^+_m\right)\right] = \sum_{\ell \neq m} \left[H_{hop}, S^+_\ell S^-_m\right] + \sum_{\ell \neq m} \left[H_{hop}, S^-_\ell S^+_m\right] \ , \tag{3.20}$$

where expanding $\sum_{\ell \neq m} \left[H_{hop}, S^+_\ell S^-_m, \right] = \sum_{\ell \neq m} S^+_\ell \left[H_{hop}, S^-_m, \right] + \sum_{\ell \neq m} \left[H_{hop}, S^+_\ell\right] S^-_m$, and invoking the property of Eq. (3.16) leads to

$$\sum_{\ell \neq m} \left[H_{hop}, \left(S^+_\ell S^-_m + S^-_\ell S^+_m\right)\right] = 0 \ , \tag{3.21}$$

Thus,

$$\left[H_{hop}, \mathbf{S}^2\right] = 0 \ . \tag{3.22}$$

From the property in Eq. (3.3), the Hubbard term $U n_{i\uparrow} n_{i\downarrow}$ will commute with $\mathbf{S}^2$ since the commutator is easily reduced down to terms of the form $\left[n_{\ell,\gamma}, c^\dagger_{i,\alpha} c_{j,\beta}\right]$, giving

$$\left[H_{Hub}, \mathbf{S}^2\right] = 0 \ . \tag{3.23}$$

For the J-term of the $t-J$ model,

$$\left[J\sum_{<i,j>}\mathbf{S}_i\cdot\mathbf{S}_i,\mathbf{S}^2\right] = \left[J\sum_{<i,j>}\mathbf{S}_i\cdot\mathbf{S}_i,\sum_{\ell}\mathbf{S}_\ell^2+\sum_{\ell\neq m}\mathbf{S}_\ell\cdot\mathbf{S}_m\right] \quad (3.24)$$

$$= J\sum_{<i,j>,\ell}\left[\mathbf{S}_i\cdot\mathbf{S}_i,\mathbf{S}_\ell^2\right]+J\sum_{<i,j>,\ell\neq m}\left[\mathbf{S}_i\cdot\mathbf{S}_i,\mathbf{S}_\ell\cdot\mathbf{S}_m\right]. \quad (3.25)$$

It is clear that $[\mathbf{S}_i\cdot\mathbf{S}_j,\mathbf{S}_\ell\cdot\mathbf{S}_m]=0$, for all i, j, ℓ, and m. Therefore

$$\left[J\sum_{<i,j>}\mathbf{S}_i\cdot\mathbf{S}_i,\mathbf{S}^2\right]=0\ , \quad (3.26)$$

and so

$$\left[H_{t-J},\mathbf{S}^2\right]=0\ . \quad (3.27)$$

With both the Hubbard and $t-J$ models commuting with the operators S^z_{tot} and S^2, the eigenvalues of these operators may be selected to label the states. The commutation relation with S^z_{tot} is especially important since it implies that these Hamiltonians do not change the value of total magnetization, and so the convenient choice restriction to the $m_z=0$ subspace may be used[1].

3.2 Dimensionality of the Hilbert Space

The total number of states appearing in the system is given by the number of ways the electrons can arrange themselves on the lattice. For the N_{up} up-spin electrons

[1]Recall, as mentioned in the last chapter m_z is the eigenvalue of S^z_{tot} with respect to the ground state eigenvector. Selecting $m_z=0$ guarantees that one will find the true ground state. For example, for a system of two electrons in a bound state in free space one can only have a singlet ($s=0$, $m_z=0$), or one of three triplets ($s=1$, $m_z=-1$,0,1), where s is the eigenvalue of S^2 with respect to the ground state. So if one selected some $m_z\neq 0$, for instance $m_z=-1$, automatically one is restricted to the triplet subspace, and there is no possibility of finding a singlet ground state.

this is given by the binomial relation, $\binom{N_{sites}}{N_{up}}$ and similarly for the N_{down} down-spin electrons, $\binom{N_{sites}}{N_{down}}$, where $N_{up} = \sum_i n_{i\uparrow}$, $N_{down} = \sum_i n_{i\downarrow}$, and N_{sites} is the number of sites in the lattice. Then if double occupancy is allowed the number of states for some general value of m_z is

$$N_{m_z} = \binom{N_{sites}}{N_{up}} \binom{N_{sites}}{N_{down}} . \tag{3.28}$$

The total dimensionality of the Hilbert space is given by summing all of the N_{m_z} over all possible values for m_z. It is clear how the Hilbert space can get extremely large even for a relatively small system.

However, since the Hubbard and $t-J$ Hamiltonians do not change the value of m_z, the problem can be restricted to the m_z subspace, where $N_{up} = N_{down} = \frac{N_e}{2}$. Subject to this restriction the total number of states can be found through

$$N_{states} = \binom{N_{sites}}{\frac{N_e}{2}}^2 . \tag{3.29}$$

This greatly reduces the number of possible states.

Furthermore, as was shown in the last chapter, in the $t-J$ model the system is restricted to the subspace of unoccupied and singly occupied sites, further reducing the number of possible arrangements. Considering the down-spin electrons first they can arrange themselves in $\binom{N_{sites}}{\frac{N_e}{2}}$ ways. This leaves $N_{sites} - \frac{N_e}{2}$ sites for the up-spin electrons to go on, in $\binom{N_{sites}-\frac{N_e}{2}}{\frac{N_e}{2}}$ ways. Then the total number of states in the singly occupied $m_z = 0$ Hilbert space of the $t-J$ model is given as,

$$N_{states} = \binom{N_{sites}}{\frac{N_e}{2}} \binom{N_{sites} - \frac{N_e}{2}}{\frac{N_e}{2}} . \tag{3.30}$$

Under appropriate conditions, further reductions can be made by using various symmetries of the system [54, 53]; however, these methods were not attempted in this study.

The number of states, however, can still become very large, as was the case in this study. For a honeycomb lattice of length $L = 3$, i.e. 18 lattice sites, with $N_e = 6$ electrons the Hilbert space will have $N_{states} = 371,280$ states. To store the entire Hamiltonian matrix, which has over 130 billion elements, would require over half of a terabyte of RAM. This we do not have. Consequently, the Lanczos technique was required to find the ground state of the system.

3.3 Lanczos Diagonalization

The Lanczos method[2] is widely used in theoretical investigations into superconductivity. It works especially well for matrices which are large and sparse (most of the elements are zero) [51]. As opposed to storing an $N_{states} \times N_{states}$ matrix, one need only store a few vectors of length N_{states}. This is ideal in situations where there is insufficient memory to store the Hamiltonian matrix. In this case, one must devise a way to generate the matrix without storing it, which reduces to defining its action on a general state vector for the system. One drawback to this is that it becomes time consuming to generate the matrix during each iterative step of the algorithm. However, an attractive feature is that the extreme eigenvalues will converge relatively fast. Even if there is enough memory to store and diagonalize the entire Hamiltonian, if only the ground state of a system is desired this method can be used to quickly get results that could take a conventional routine much, much longer.

[2]It is common to find the Lanczos method referred to as "exact diagonalization" in the literature.

The first part of this section outlines and discusses the structure of the Lanczos routine used in this study. The second part focuses on the topic of binary labelling, a key aspect in executing the code. The third section discusses some diagnostic measures taken in ensuring converged and reliable numerical results. Some articles and books that were used throughout the writing of the code contain more detailed and thorough discussions than given here. For instance, Refs. [3], [54], [53], and [55] focus on the Lanczos method as applied to the Hubbard and $t - J$ models. For general discussions see Refs. [56] and [57]. Chapter 9 from Ref. [51] contains a concise discussion.

3.3.1 The Lanczos Procedure

The Lanczos method is an iterative algorithm for tridiagonalizing a matrix, H. During the procedure the eigenvalues of each successively generated tridiagonal matrix, T, will converge to those of H. With enough time the entire matrix, H, could be diagonalized in this way. However, the key feature of this method is that the extreme eigenvalues converge long before the entire tridiagonalization is complete. As a result, reasonably accurate information about the ground state can be found relatively quickly, usually within $n = 150$ steps. Hence, only partial tridiagonalization is needed.

The version of the code followed here is one slightly modified [58] from Ref. [51],

and goes as follows:

$$
\begin{aligned}
|w_0\rangle &= \text{normalized trial state} \\
|v\rangle &= H|w_0\rangle \\
a_0 &= \langle w_0|v\rangle \ , \quad |v\rangle = |v\rangle - a_0|w_0\rangle \ , \quad b_0 = \sqrt{\langle v|v\rangle} \\
\text{for i} &= 1 \text{ to N} \\
|t\rangle &= |w_{i-1}\rangle \ , \quad |w_i\rangle = b_{i-1}^{-1}|v\rangle \ , \quad |v\rangle = -b_{i-1}|t\rangle \\
|v\rangle &= |v\rangle + H|w_i\rangle \\
a_i &= \langle w_i|v\rangle \ , \quad |v\rangle = |v\rangle - a_i|w_i\rangle \ , \quad b_i = \sqrt{\langle v|v\rangle} \\
&\text{end}
\end{aligned}
$$

Loosely speaking, in performing the Lanczos procedure one is constructing an orthogonal basis of vectors, $|w_i\rangle$, called the Lanczos vectors. Initially, $|w_0\rangle$ is chosen randomly, with a new $|w_i\rangle$ generated recursively according to

$$|w_{i+1}\rangle = H|w_i\rangle - a_i|w_i\rangle - b_i^2|w_{i-1}\rangle \ , \tag{3.31}$$

where $a_i = \frac{\langle w_i|H|w_i\rangle}{\langle w_i|w_i\rangle}$ and $b_i^2 = \frac{\langle w_i|w_i\rangle}{\langle w_{i-1}|w_{i-1}\rangle}$. In this basis the Hamiltonian becomes tridiagonal. For instance, at the Nth step of the procedure one is left with an $N \times N$

matrix

$$T = \begin{pmatrix} a_0 & b_0 & 0 & ... & 0 \\ b_0 & a_1 & b_1 & ... & 0 \\ . & . & . & . & . \\ . & . & . & a_{N-1} & b_{N-1} \\ . & . & . & b_{N-1} & a_N \end{pmatrix} , \tag{3.32}$$

which is much smaller than the original Hamiltonian.

One may then easily diagonalize T and yield its lowest eigenvalue, θ, and corresponding eigenvector,

$$|\tau\rangle = \sum_{i=0}^{N} c_i |i\rangle \ . \tag{3.33}$$

The $|i\rangle$ represent the orthogonal basis in the N-dimensional eigenspace of T. If λ is the true ground state eigenvalue of H, it can be shown [51] that

$$|\lambda - \theta| \leq ||H|\psi\rangle - \theta|\psi\rangle|| = |b_{N-1}c_{N-1}| \ . \tag{3.34}$$

This provides a condition, $|b_{N-1}c_{N-1}|$, termed here the *tolerance*, under which the code may be terminated. At each step the tolerance condition is checked to see if the desired accuracy has been achieved. Once achieved, the value of θ has presumably reached a sufficient approximation of the true eigenvalue λ. The tolerance for this study was set to 10^{-7}; § 3.3 contains a further discussion of the tolerance.

The approximate ground state eigenvector of H is found through

$$|\psi\rangle = \sum_{i=0}^{N} c_i |w_i\rangle \ , \tag{3.35}$$

where $|w_i\rangle$ are the Lanczos vectors generated at each step of the Lanczos procedure,

and the c_i are the components of the final vector $|\tau\rangle$, in Eq. (3.33), computed at the terminating step, N. So, if memory permits, one may save the $|w_i\rangle$ at each step and construct the ground state after the terminating step. However, when memory is a serious consideration, the code must be run over again, continuously constructing the ground state vector at each step. The latter was the case in this study, and, in fact, two separate codes were used to find the eigenvalues and eigenvectors. The code for finding the eigenvalue may be found in Appendix E.

3.3.2 Binary Labelling

In order to effectively generate the Hamiltonian at each step an efficient representation of the basis states is needed. The S^z_{tot} representation is ideal for this as it allows one to represent the states as a list of all possible arrangements of the electrons on the lattice. Each individual arrangement of electrons on the lattice in turn may be represented by a unique binary number. This is referred to as binary representation, or binary labelling [55]. Section 3 of Appendix E contains the code for generating the binary states.

The conversion to binary labelling can be read directly from the order of the operators appearing in a given basis state,

$$|\psi\rangle = \prod_{i'} c^\dagger_{i',\uparrow} \prod_{j'} c^\dagger_{j',\downarrow} |0\rangle \ . \tag{3.36}$$

The prime on the site label indicates that only the occupied sites are considered in

the product. Equation (3.36) becomes in binary form[3]

$$|\psi\rangle = b_{2N_{site}-1}b_{2N_{site}-2}...b_{N_{site}}b_{N_{site}-1}...b_1b_0 \tag{3.37}$$

where $b_i = 0$ or 1 is a bit. If the creation operator for an electron on a particular site appears in a basis state then the corresponding bit is set to 1, if it does not appear then the bit is set to 0. As is indicated the down spins are added first, filling bits 0 to $N_{sites} - 1$, followed by the up spins in the bits N_{sites} to $2N_{sites} - 1$. For example, consider the four site, four electron state given by, $|\psi_1\rangle = c^\dagger_{2,\uparrow}c^\dagger_{1,\uparrow}c^\dagger_{2,\downarrow}c^\dagger_{1,\downarrow}|0\rangle$; the corresponding binary state would read, $|01100110\rangle$.

However, it requires too much memory to store each of the binary states. To overcome this each binary number is converted to a base-ten number. The total state vector describing the system is then a list of all of the possible base-ten numbers corresponding to all of the possible binary numbers representing the arrangement of the electrons.

3.3.3 Numerical Considerations

As a first measure the code was tested to verify that the correct eigenvalues and eigenvectors were being found. For this, the Lanczos results were compared to exact results of small systems which could be easily diagonalized exactly. Several different system sizes were checked for both the honeycomb and one-dimensional chain. For both the Hubbard and $t - J$ models it was found that the Lanczos code was yielding

[3]The site-labelling starts at zero since in the programming language C the counting loops start at zero.

accurate results for both the eigenvalues and eigenvectors. The accuracy of the eigenvalues were generally consistent with the tolerance condition found in Eq. (3.34). Some size dependence was found, where larger systems were yielding less accurate results. However, all satisfied the tolerance condition.

During the actual execution of the code, a step-by-step diagnosis of the algorithm is carried out, and can be viewed while the code is running, or after the code has completed. This is important when no exact value is known as it provides a way of ensuring the code has run properly. Initial testing of this diagnosis was done on a system size that allowed for quick results. Three different tolerances were used on a honeycomb lattice of length $L = 2$, with four and six electrons. Two different values of J (0.1 and 0.3) were considered.

For the eigenvalue, at each step the current approximation of the eigenvalue, θ_i, is printed out, and one may see the gradual convergence of the eigenvalue to a particular number. The vectors, on the other hand, are much too large to print out each time. For this a test is used which sums the squares of the differences between the components of each successive eigenvector. To be more concrete, if the eigenvector at the ith step is

$$|\psi^i\rangle = \sum_j c_j^{(i)} |j\rangle \ , \tag{3.38}$$

then the test is

$$A_i = \sum_{j=1}^{N_s} |c_j^{(i-1)} - c_j^{(i)}|^2 \ . \tag{3.39}$$

This provides a way of seeing how much the eigenvector has changed at each step of its construction.

It was found in all cases that the eigenvalue converged below the set tolerance,

and this occurred in a shorter number of steps than the eigenvector test of Eq. (3.39). For example, at the point when the eigenvalue had converged below the tolerance, it was found A_i was still of the order $10^{-1} - 10^{-2}$. In all cases it was found that A_N (i.e.: A_i computed at the Nth step) was of the order set for the tolerance. After completing studies of larger lattice sizes, it was found that A_N was one order of ten greater than the tolerance. This suggests a size dependence for the convergence of the vectors consistent with the size dependence mentioned above.

Additionally, when constructing the ground state eigenvector the value

$$\theta_i^{approx} = \langle \psi^i | H | \psi^i \rangle \tag{3.40}$$

is also computed in order to see how close the eigenvector at the ith step, $|\psi^i\rangle$, is to yielding the desired eigenvalue, θ. This also provides another confirmation that the code is yielding correct results, as this provides a direct way of viewing the gradual convergence of the eigenvector. However, the values found for θ_i^{approx} never converge exactly to those of the eigenvalue computed directly in the Lanczos code, θ, but they do converge to a degree of accuracy of the order of the tolerance.

As a concluding note, it was found that for the quantities of interest in this study, i.e. the superconducting correlations and susceptibility (discussed in the next chapter), there was no difference in the results found when the tolerance was changed from 10^{-7} to 10^{-4}. However, a tolerance of 10^{-7} was retained, as a tolerance of 10^{-4} did not provide much of an improvement in the length of time it took to find the results, and, most importantly, a tolerance of 10^{-7} ensured correct results each time.

Chapter 4

Numerical Results

In superconducting materials, an effective attractive interaction produces a condensate of electron pairs, with a large overlap between pairs. The superconducting state is thought to be a fluid of these electron pairs. In conventional superconductors this pairing is understood via the BCS theory [2], but for the HTSCs this is not the case. A more sophisticated explanation is needed. The first step towards an explanation is to find a model Hamiltonian which mimics the observed properties of the systems. The key property for superconductivity is that under certain conditions, e.g. electron filling, temperature, etc., the electrons tend to be found grouped in pairs, and that these pairs tend to remain bound throughout the lattice. To this effect one is searching for correlations between electron pairs, or *pair-pair* correlations.

In this chapter the numerical results of the pairing correlations and susceptibility as function of $\frac{J}{t}$ of the $t-J$ model found in this study are presented. First, a general discussion of electron pairing is given where the pair-pair correlation and susceptibility functions are introduced[1]. Then our results for the one dimensional chain and the

[1]Appendix D contains a further discussion, as well as some background information, of the topic

two-dimensional honeycomb lattice are discussed.

4.1 Pair-Pair Correlations

To search for correlations one considers the pair-pair correlation function

$$C(\mathbf{m}) = \left(\frac{1}{N_{sites}}\right) \sum_{i=0}^{\frac{N_{sites}}{2}} \langle \Delta_i^\dagger \Delta_{i+\mathbf{m}} \rangle \ . \tag{4.1}$$

The operator Δ_i is the pair operator, and $\mathbf{m}$ is a parameter that measures the separation between pairs. From the correlation function a susceptibility may be found, given by

$$\chi_{sus} = \sum_{\mathbf{m}} C(\mathbf{m}) \ . \tag{4.2}$$

Since this function essentially adds up all of the correlations in the system, as the range of correlation increases this number would get increasingly large. This would imply if the system achieves a superconducting state, i.e. the system has condensed into a sea of correlated pairs at all distances, the susceptibility would then appear to diverge, or at least reach some sort of maximum for a finite system.

The exact form of the pair operator, Δ_i, depends on the type of pairing that one is searching for. The $t-J$ model considers only interactions between electrons residing on nearest neighbour sites, favouring the anti-ferromagnetic alignment of electrons. It follows then that pairing would be expected between opposite-spin electrons on nearest neighbour sites, as is the case for a singlet state. In one dimension for two sites and two electrons, a singlet would be given by the state $\frac{1}{\sqrt{2}}\left(c_{1,\uparrow}^\dagger c_{2,\downarrow}^\dagger - c_{1,\downarrow}^\dagger c_{2,\uparrow}^\dagger\right)$.

discussed in this section.

By analogy one can define the singlet pair operator as [23]

$$\Delta_i = \frac{1}{\sqrt{2}} \left(c_{i,\uparrow} c_{i+1,\downarrow} - c_{i,\downarrow} c_{i+1,\uparrow} \right) \ . \tag{4.3}$$

Extending this to two dimensions on the square lattice, the pairing operator is defined as [23]

$$\Delta_i = c_{i,\uparrow} \left(c_{i+\hat{\mathbf{x}},\downarrow} + c_{i-\hat{\mathbf{x}},\downarrow} \pm c_{i+\hat{\mathbf{y}},\downarrow} \pm c_{i-\hat{\mathbf{y}},\downarrow} \right) \ , \tag{4.4}$$

where $\hat{\mathbf{x}}$ and $\hat{\mathbf{y}}$ indicate a translation of one lattice site along the appropriate lattice vector. The plus sign of the $\pm$ corresponds to extended s-wave, and the minus sign to $d_{x^2-y^2}$ wave. It is the general consensus that $d_{x^2-y^2}$ wave pairing is responsible for HTSC, whereas s-wave pairing occurs in the conventional superconductors [12, 11].

For the honeycomb lattice with a two-site basis, calculating the correlations is a little more complicated. A direct application of (4.4) cannot be used, so a simpler pair operator is considered,

$$\Delta_{\mathbf{r}_i} = c_{i,\uparrow} c_{i+\delta_i,\downarrow} \ . \tag{4.5}$$

Here δ_i refers to a nearest neighbour to site i, and the positions $\mathbf{r}_i = \frac{\mathbf{r}_i + \mathbf{r}_{i+\delta_i}}{2}$ refer to the center of the ith pair. The correlation function is then computed as

$$C\left(|\mathbf{r}_{i,j}|\right) = \frac{1}{2N_{sites}} \sum_{<i,\delta_i>} \langle \Delta^\dagger_{\mathbf{r}_i + \mathbf{r}_{i,j}} \Delta_{\mathbf{r}_j} \rangle \ , \tag{4.6}$$

where $|\mathbf{r}_{i,j}| = |\mathbf{r}_i - \mathbf{r}_j|$ refers to the minimum distance between the pairs (once periodic boundaries are taken into account). In the honeycomb case, with a more complicated lattice structure, it is simpler to perform the sum over the entire lattice. This results in counting each correlation twice, hence the factor of $\frac{1}{2}$ in front of Eq. (4.6). From

this, the so-called superconducting susceptibility is calculated through

$$\chi_{sus} = \sum_{|r_{i,j}|} C\left(|r_{i,j}|\right) \ . \tag{4.7}$$

Note, however, that this susceptibility is not the sum over a specific pair-pair correlation, e.g. s- or d-wave of a square lattice, but effectively sums up all correlations for each unique absolute distance between all possible pairs of electrons.

4.2 One Dimensional Studies

Initially a one-dimensional system with periodic boundary conditions was studied. A system of length $L = 16$ would have been ideal since it would have allowed a direct comparison to the results given in [23]. However, the Hilbert space of such a system was much too large for our computational resources, as there are 900,900 states present at quarter-filling. (Given the sophistication of the code written, with this many states it could take anywhere in the range of two to three weeks to find a single ground state, and there simply was not enough time to carry out a full study of this system.) Instead a somewhat smaller system of length $L = 12$ was used[2], which at quarter-filling has 18,480 states. For each filling the susceptibility was found and plotted over a range of values for $\frac{J}{t}$. Afterwards, for each filling the correlations were analyzed at particular values of $\frac{J}{t}$ to search for evidence of long range correlations which might suggest superconductivity, as well as other interesting features that may be present.

The results for the susceptibility vs. $\frac{J}{t}$ for this system, for various fillings, are

[2]A system of this length is preferable over, for instance, $L = 14$ because it has an even number of electrons at quarter-filling.

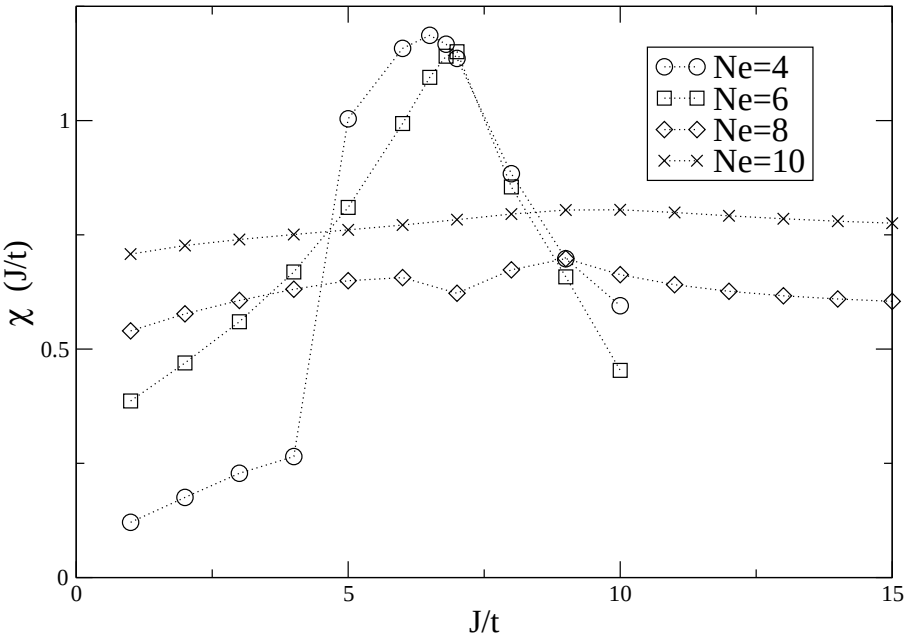

Figure 4.1: Susceptibility vs. $\frac{J}{t}$ for the $L = 12$ system. The four different fillings are plotted together for comparison. The dotted line is included as a guide to the eye to provide an indication of how the susceptibility is changing for each filling. Note that both the four and six electron fillings show strong peaks, whereas the other fillings remain flat. This is supportive of the results given in [23].

presented in Fig. 4.1. Both fillings of four and six electrons exhibit an appreciable peak in their susceptibility curves. The curve for four electrons achieves a maximum at $\frac{J}{t} = 6.5$, which is a slightly larger susceptibility than found for the maximum susceptibility of six electrons at $\frac{J}{t} = 6$. However, six electrons presents a sharper peak than the four electron system, and closely resembles the results presented in [23]. Both of these fillings should therefore have appreciable correlations at and around these $\frac{J}{t}$, suggesting the existence of superconductivity.

The susceptibility vs. $\frac{J}{t}$ relationships for the other two fillings remain relatively flat. However, they do have somewhat larger values for the susceptibility, in particular

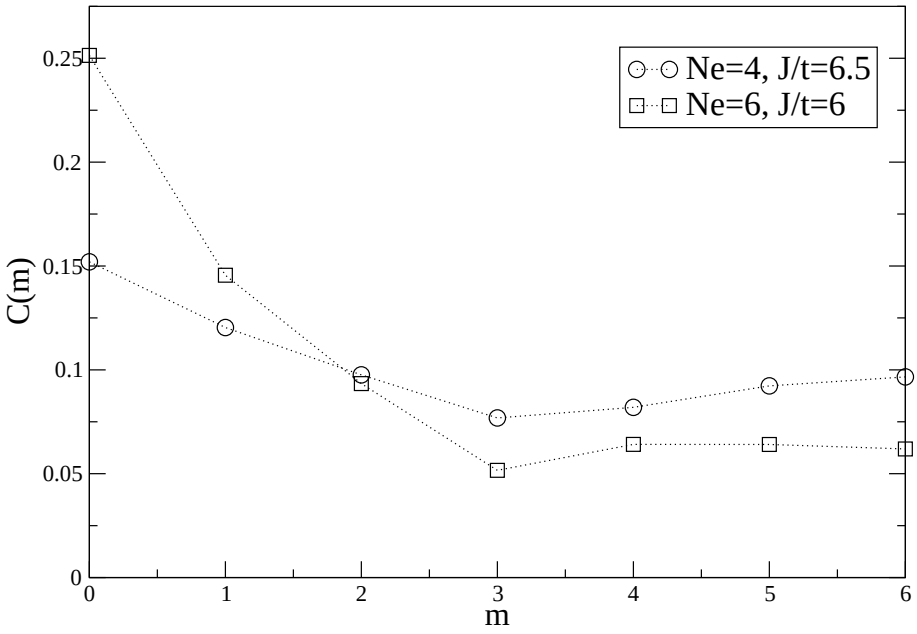

Figure 4.2: The correlations for the four and six electron fillings. The plots are given at the values of $\frac{J}{t}$ where susceptibility vs. $\frac{J}{t}$ is a maximum. Both fillings show non-zero correlations throughout the entire system, a key indication of possible superconductivity.

when compared with other fillings at lower values of $\frac{J}{t}$. This is interesting since $\frac{J}{t} = \frac{4t}{U}$ when U is large, implying $\frac{J}{t} < 1$, so it is interesting to see what, if any, indications of superconductivity might exist at low values of $\frac{J}{t}$.

In a study by Dagotto and Riera [23], which focused on a one-dimensional quarter-filled system of length $L = 16$, it was found that the susceptibility vs. $\frac{J}{t}$ was sharply peaked, and plots of the correlations for $\frac{J}{t}$ where the susceptibility is a maximum showed appreciable, non-zero values for all correlation lengths. Similar results are found here for $L = 12$ at sixth-filling (four electrons) and quarter-filling (six electrons). In fact, the appearance of the peak found for the quarter-filled case is almost identical

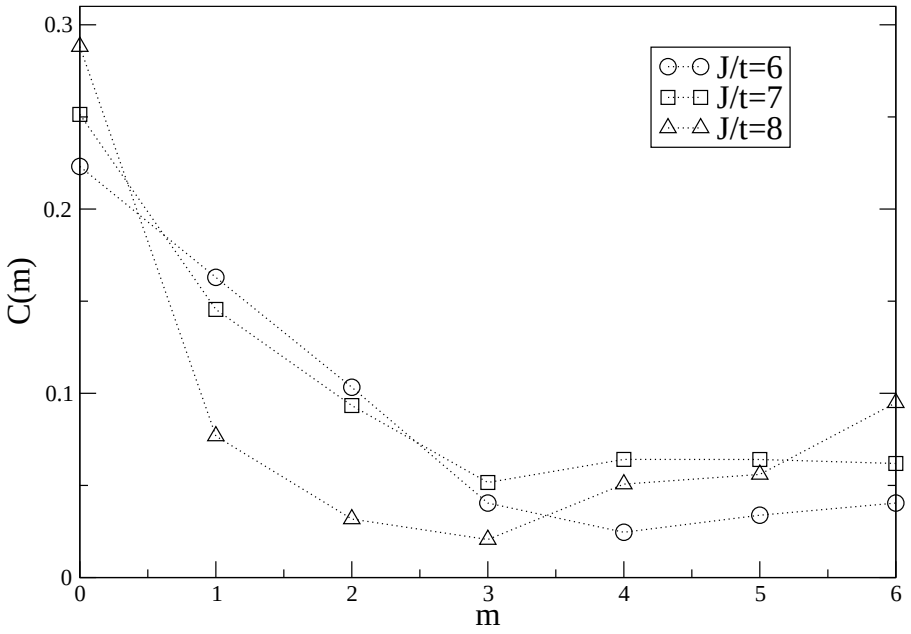

Figure 4.3: Plots of the correlations for the quarter-filled system for values of $\frac{J}{t}$ around which the susceptibility vs. $\frac{J}{t}$ reaches the maximum. All plots show strong superconducting correlations, none of which come close to zero. This supports the suggestion in [23] that in the region around which the susceptibility vs. $\frac{J}{t}$ reaches maximum superconducting correlations should dominate.

to the results given in [23].

A plot of the correlations at the maximum value of $\frac{J}{t}$ for the susceptibility as a function of $\frac{J}{t}$ for both the quarter-filled and sixth-filled cases are given in Fig. 4.2. Note that both curves display strong, non-zero superconducting correlations throughout the entire lattice. This is indicative of superconductivity for reasons given in Appendix D.

Also, in [23] it is suggested that phase separation occurs in the region of $\frac{J}{t}$ immediately after the peak in susceptibility. Furthermore, as a result of phase separation,

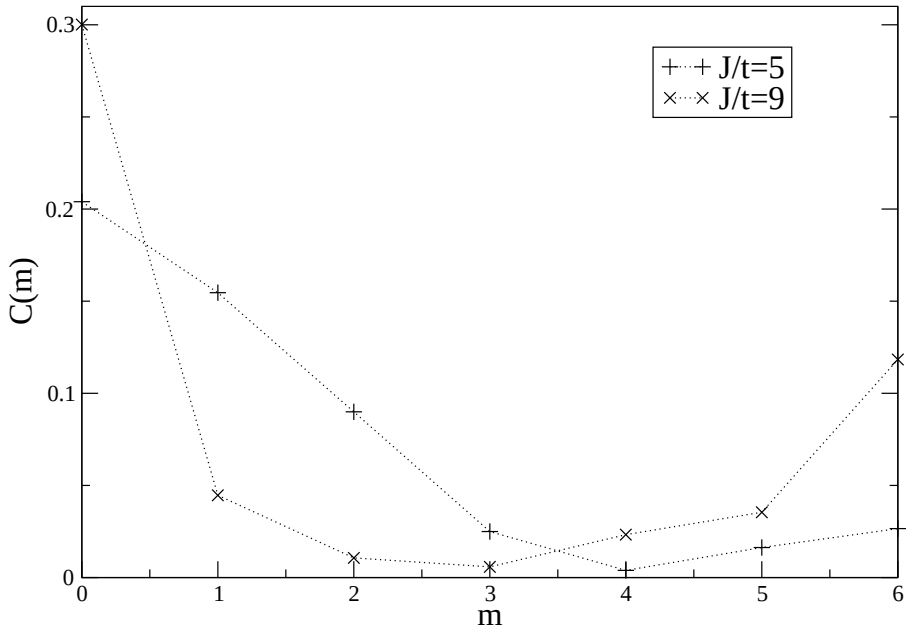

Figure 4.4: Plots of the correlations for the six electron case for values of $\frac{J}{t}$ just outside those plotted in Fig.4.3. The purpose is to show that as one moves further way from the maximum $\frac{J}{t}$ the correlations become less dominant, some of which come close to zero for some values of m.

it is claimed around the maximum values of $\frac{J}{t}$ superconducting correlations will dominate. This behaviour can be seen in Fig. 4.3 for the quarter-filled case where the correlations maintain relatively large, non-zero for all values of m for $\frac{J}{t} = 6$, 7, and 8. To illustrate this point further, plots of the correlations for $\frac{J}{t} = 5$ and 9 are included in Fig. 4.4 to show that the correlations become smaller further away from the maximum $\frac{J}{t}$. It is clear that the correlations are decreasing, since for some values of m the correlations are very close to zero.

The four-electron system yields results similar to those found for six electrons. Shown in Fig. 4.5 are plots of the correlations for values of $\frac{J}{t}$ around the maximum of susceptibility vs. $\frac{J}{t}$. Again much like the six-electron case the correlations are strong

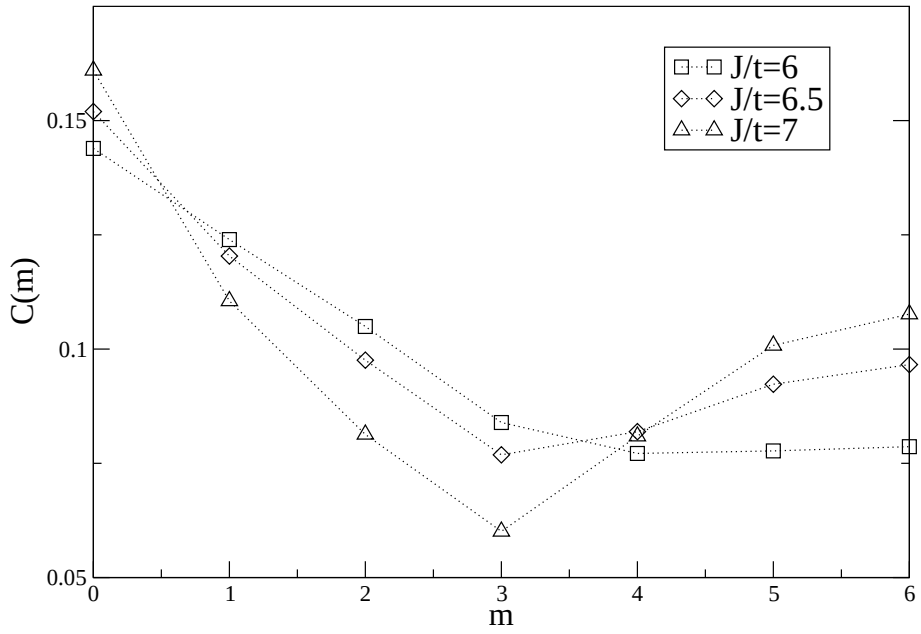

Figure 4.5: Plots of the correlations for the four electron filling for values of $\frac{J}{t}$ around which the susceptibility vs. $\frac{J}{t}$ reaches the maximum. Note the y-axis does not start at zero. All plots show strong superconducting correlations, none of which come close to zero. This supports the suggestion in [23] that in the region around which the susceptibility vs. $\frac{J}{t}$ reaches maximum superconducting correlations should dominate.

and non-zero in this region, suggestive of superconductivity. Plots for values outside this region are shown in Fig. 4.6, showing the correlations are much less pronounced. In fact, for $\frac{J}{t} = 4$ they are negative for larger values of m.

In addition to superconducting correlations, evidence of phase separation in the system can be seen in these plots. It is most blatantly displayed in the four-electron plots of Figs. 4.5 and 4.6, especially the latter. In Fig. 4.6 it is clear there has been a drastic change in the preferred separations of the pairs between the two $\frac{J}{t}$ plots shown. Initially the correlations start out as an exponentially decaying function, as expected when there are no long range correlations. Then gradually the correlations flatten

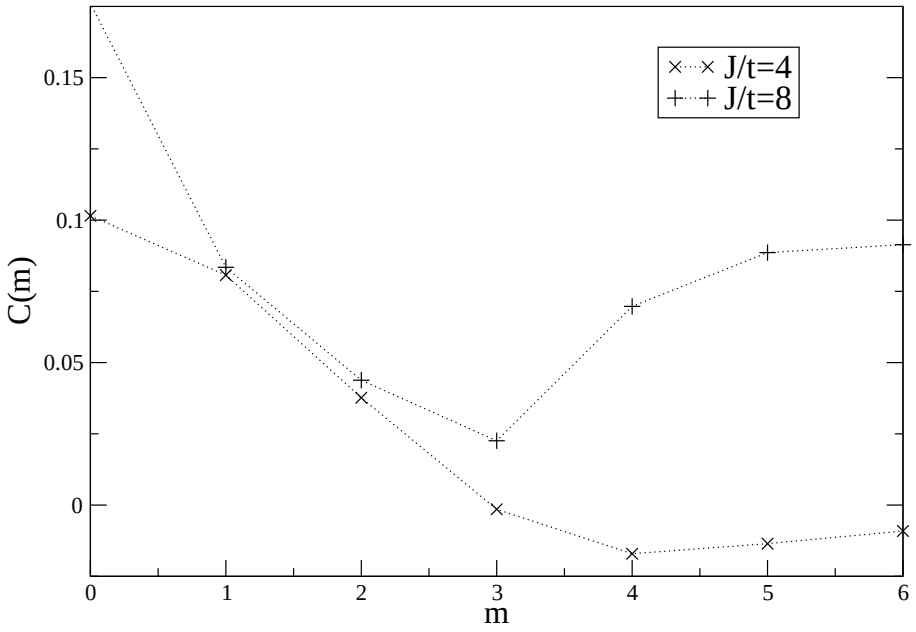

Figure 4.6: Plots of the correlations for the quarter-filled system for values of $\frac{J}{t}$ just outside those plotted in Fig.4.5. The purpose is to show that as one moves further way from the maximum $\frac{J}{t}$ the correlations become less dominant, some of which actually become negative for some values of m.

out as the values of $\frac{J}{t}$ move through the maximum, as seen in Fig. 4.5, gaining long range correlations necessary for the presence of superconductivity. Beyond this region of $\frac{J}{t}$, the long range correlations remain strong while the shorter range correlations decrease. Eventually the correlations settle on the form displayed in Fig. 4.6 for $\frac{J}{t} = 8$, which is markedly different from that found in the $\frac{J}{t} = 4$ curve. A similar, yet subtler trend can be seen in Figs. 4.3 and 4.4 when the system contains six electrons. This indeed suggests that something has occurred in moving through this region, as there has been a definite shift in the relative values of the correlations at each m. The interesting thing here is that the correlations at the lengths of $m = 2$ and 3

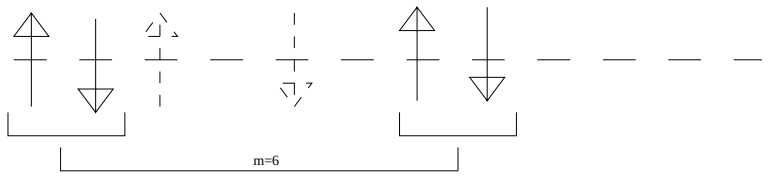

Figure 4.7: An example of one possible preferred alignment of the six electron case for the correlations found in Fig. 4.4 for $\frac{J}{t} = 9$. The lines represent the lattice sites, and the electrons are given by the arrows, the direction of which indicates the spin direction. The $m = 6$ correlation seem to be dominant, suggesting the other, non-paired electrons (the dashed-lined arrows) might be found anywhere.

become much smaller than the rest, with the longer-ranged correlations maintaining the largest values. This is especially evident in the quarter-filled system at $\frac{J}{t} = 8$ and 9 where $m = 6$ displays the largest correlations. One explanation is that the electron pairs are now in some state where pairs are being found but prefer to remain as far away as possible from each other given the periodic boundary conditions, as the large $m = 6$ correlations would suggest. See Fig. 4.7 for a diagrammatic representation of this. This definitely suggests that phase separation has occurred, further supporting the claims made in Ref. [23].

Moving on to higher fillings, the situation is quite different. The system maintains higher susceptibilities for the fillings $N_e = 8$ and 10 than for the lower fillings of $N_e = 4$ and 6 (shown in Fig. 4.1), at the low values of $\frac{J}{t}$. These higher fillings, however, do not display a peak and remain relatively flat throughout. The susceptibility vs. $\frac{J}{t}$ for $N_e = 8$ has the strange feature of having two peaks and one local minimum, which as discussed below does seem to coincide with some interesting features of the correlations.

A plot of the correlations in the $N_e = 10$ system for some values of $\frac{J}{t}$ is shown in Fig. 4.8. Despite having a large susceptibility at $\frac{J}{t} = 1$ there is no indication of

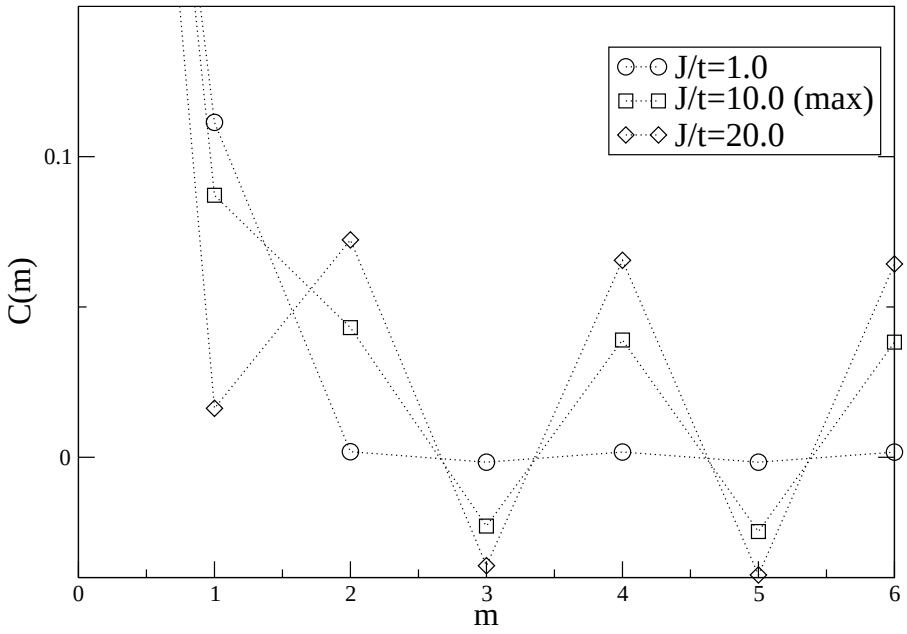

Figure 4.8: Plots of the correlations for the $N_e = 10$ system for the two values $\frac{J}{t} = 1$, 10 and 20. This shows as $\frac{J}{t}$ is increased the electrons become locked in a preferred spatial alignment indicative the anti-ferromagnetic nature of the $t - J$ model.

long range correlations. The plot for $\frac{J}{t} = 10$, where the susceptibility vs. $\frac{J}{t}$ reaches a maximum, shows the odd values of m become smaller, and indeed negative, and the even m become larger. This trend continues as $\frac{J}{t}$ is increased further to 20. When one considers the system as having only two empty sites, this makes sense. At low values of $\frac{J}{t}$ the system would be in any number of arrangements with roughly equal weighting, where near neighbour bonds will not be particularly strong and thus the electrons will not necessarily have a preferred spatial alignment. However, as $\frac{J}{t}$ is increased up to 20, owing to the anti-ferromagnetic nature of the $\frac{J}{t}$-term, the system would prefer to align itself so that each nearest neighbour bond is anti-ferromagnetic such that the electrons become bunched together in an alternating ...up, down, up,

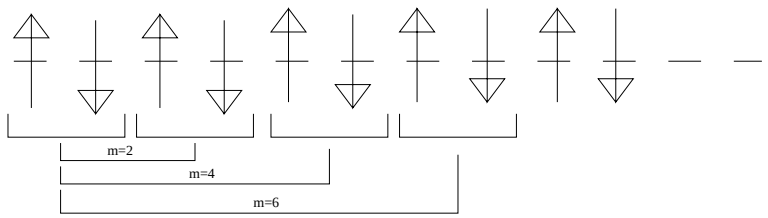

Figure 4.9: The probable alignment of the electrons for the ten electron case corresponding to the correlations shown in Fig. 4.8 at $\frac{J}{t} = 20$. The lines represent the lattice sites, and the electrons are given by the arrows which indicate the spin direction. The indicated values of m correspond to the large values seen in Fig. 4.8.

down... fashion; see Fig. 4.9. Hence, the even values of m are large since pairs would necessarily be separated by two lattice sites.

The correlations for a filling of eight electrons are presented in Fig. 4.10 for the two values of the susceptibility vs. $\frac{J}{t}$ which are a maximum, $\frac{J}{t} = 6$, which is a local maximum, and $\frac{J}{t} = 9$, which is the global maximum. In Fig. 4.11 a plot of the correlations at $\frac{J}{t} = 7$, the point of the minimum of the susceptibility vs. $\frac{J}{t}$, and $\frac{J}{t} = 8$ are also included since they occur between the two peaks, and help to illustrate some of the points discussed below. Overall there does not appear to be any evidence of long range superconductivity, the $\frac{J}{t} = 8$ plot seems to give the most promising indications of superconductivity, thus ruling out long range correlations. However, it is at $\frac{J}{t} = 8$ that the correlations have their most appreciable values.

The most interesting feature of this particular filling is the appearance of the two peaks, which seem to coincide with some interesting features of the correlations. For example, the $m = 1$ and $m = 4$ correlations seem to act in opposition to one another. The $m = 4$ correlations drop to a minimum at $\frac{J}{t} = 6$, the point where the $m = 1$ correlations maximize. At the local minimum of the susceptibility vs. $\frac{J}{t}$, $\frac{J}{t} = 7$, all long range correlations become negative, as seen in Fig. 4.11 . Immediately

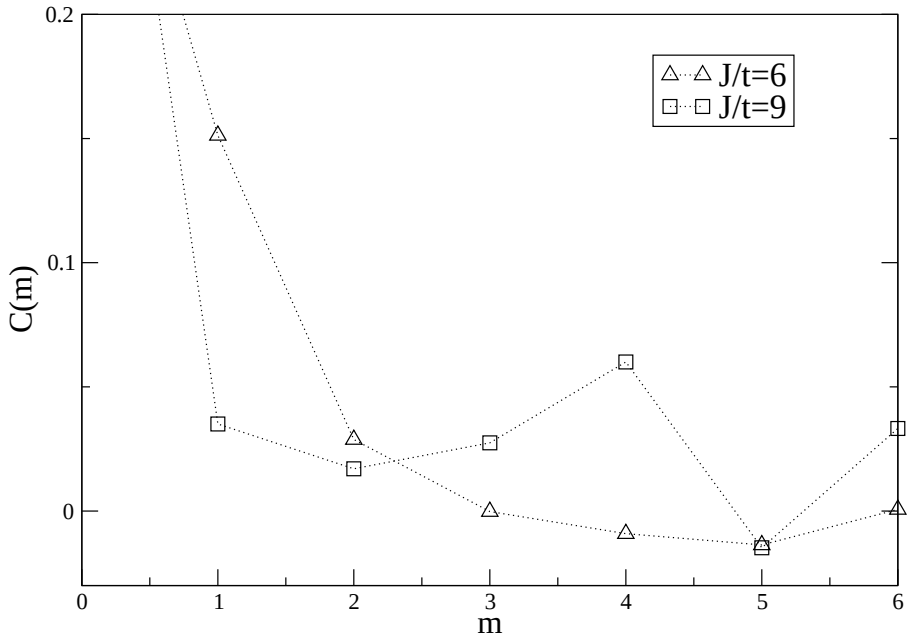

Figure 4.10: Plots of the correlations for the $N_e = 8$ system at the points where the susceptibility vs. $\frac{J}{t}$ reaches a maximum. $\frac{J}{t} = 6$ corresponds to the local maximum, and $\frac{J}{t} = 9$ corresponds to the global maximum. Note in particular the relative shift in the values of the correlations at $m = 1$ and $m = 4$ between the two $\frac{J}{t}$ plots. Suggesting a possible phase separation.

afterwards, at $\frac{J}{t} = 8$, the $m = 1$ correlations drop drastically while all values $m > 1$ rise. At $\frac{J}{t} = 9$ the $m = 4$ correlations make a sudden jump, while the rest seem to fall. It is worth noting that the $m = 6$ correlation seems to mimic the $m = 4$ correlations, but to a lesser degree. It would appear from all this that electrons make a shift from being closer together to being largely separated, again suggesting a change in the order of the arrangement of the electrons has taken place, much like for $N_e = 4$ and 6.

In conclusion, the claim found in [23] that the quarter-filled system exhibits the most conclusive indication of superconducting pairing is supported by our results for

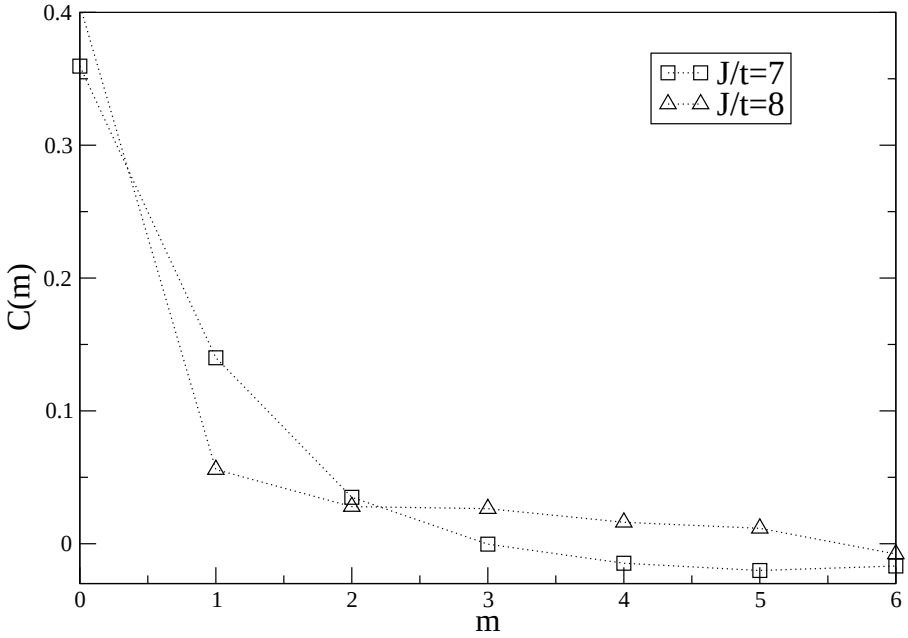

Figure 4.11: Plots of the correlations for the $N_e = 8$ system at the points in between the maximums of the susceptibility vs. $\frac{J}{t}$. Note how the correlation go from being almost all negative at $\frac{J}{t} = 7$ to almost all positive, and relatively large at $\frac{J}{t} = 8$, suggesting a change of ordering has taken place.

a shorter system. Of particular interest to this study is the fact that $LiTi_2O_4$ is a quarter-filled system in its ground state, the point at which it superconducts. This lends support to extending this study to the CTSL, the structure of the conduction sites in $LiTi_2O_4$, using the $t - J$ model. Furthermore, the analysis of the correlations also support the claims in [23] of phase separation occurring in these models.

4.3 Two Dimensional Studies on the Honeycomb Lattice

We now discuss our results for the honeycomb lattice. As mentioned in the introduction, a large amount of the work done on two-dimensional systems has been done on square lattice systems. This is partly due to its simplicity and partly because the copper-oxide planes of the cuprate superconductors form a square lattice. However, some work has been carried out on honeycomb lattices [47, 59, 60, 61, 62], mainly due to the recent discoveries of superconductivity in $Na_xCoO_2yH_2O$, as well as the fascinating properties of graphite [48]. To reiterate, the main point in studying the honeycomb lattice is as a preliminary step towards a study of a CSTL, which is structurally similar to the honeycomb lattice. It is then instructive to see what, if any, indications of pairing correlations exist in this structure.

A system of length $L = 3$ was considered with two different fillings of four and six electrons. Anything larger was not possible due to system size considerations. With two basis sites a honeycomb lattice of length $L = 3$ in both the x- and y- directions has eighteen sites. $L = 3$ was chosen since it contains the maximum number of unit cells (nine) such that two different fillings (more than one) could be studied. With length $L = 3$ and six electrons there are $371,280$ states in the Hilbert space. The next even filling is eight electrons, and this yields a Hilbert space of over one million states, which is much too large to study here. For the next larger size having 32 sites, only a filling of four electrons could be considered, which has slightly over $215,000$ states, because for six electrons this brings the Hilbert space to over eighteen million states. This is obviously too large. With only one filling possible on that system, not

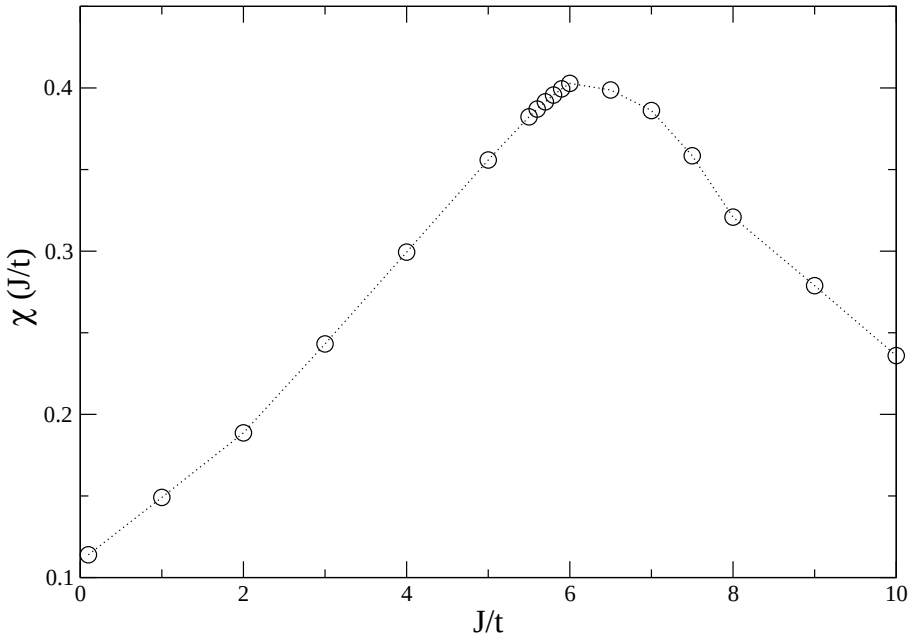

Figure 4.12: Plots of the susceptibilities vs. $\frac{J}{t}$ for the filling of $N_e = 4$. Like the quarter- and sixth-filled one-dimensional chains shown in the last section, this shows a marked rise in susceptibility as $\frac{J}{t}$ is increased. However, the system does not exhibit the sharp peaks seen in the one-dimensional case, but it is a rather smooth transition through the maximum.

much information could be gathered for a qualitative study.

Another important point to mention is that with eighteen sites, having exactly quarter-filling is impossible. The two fillings considered come as close to quarter filling as possible, with four electrons being $\frac{2}{9}$-filled and six electrons being one third-filled. These being slightly smaller and larger, respectively, than a quarter-filled system allows an indirect look at a quarter-filled system.

The four electron system is considered first. Shown in Fig. 4.12 is the susceptibility vs. $\frac{J}{t}$, using the correlation function found in Eq. (4.6), for this filling. Like the four and six electron cases in one dimension shown in the last section, this shows a marked

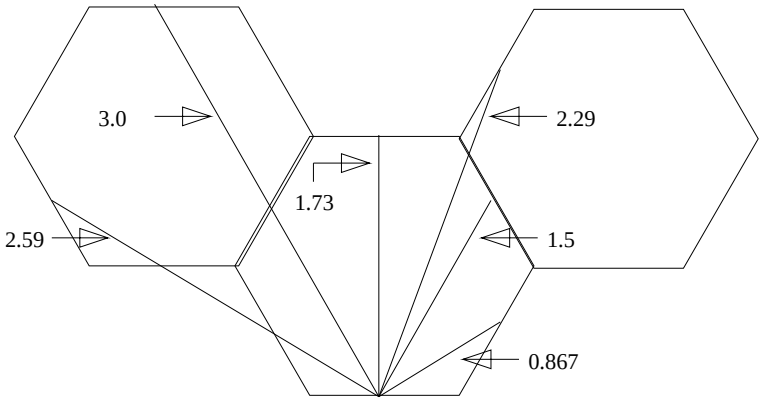

Figure 4.13: The unique nearest-neighbour distances on the $L = 3$ honeycomb lattice. The sites of the atoms are located on the corners of the hexagons. Note the distances between pairs, $|\mathbf{r}_{i,j}|$, are measured from the point in between the sites. Not all of the distances have the same weight as some distances occur more than others. For instance $|\mathbf{r}_{i,j}| = 2.29$ occurs eight times while and $|\mathbf{r}_{i,j}| = 2.59$ occurs only twice.

rise in susceptibility as $\frac{J}{t}$ is increased. However, the system does not exhibit the sharp peaks seen in those one-dimensional cases, but a rather smooth transition through the maximum.

To discuss the spatial correlations, refer to Fig. 4.13, which demonstrates the unique nearest-neighbour distances on the honeycomb lattice. Note this describes only the $L = 3$ system, as a larger or shorter lattice would either create new, or eliminate some, distances. Also, not all of the distances have the same weight, as some distances occur more than others. For instance, $|\mathbf{r}_{i,j}| = 2.29$ occurs eight times while $|\mathbf{r}_{i,j}| = 2.59$ occurs only twice.

Plots of the correlations corresponding to the values of $\frac{J}{t} = 0.1$, 6 (the point at which the susceptibility vs. $\frac{J}{t}$ reaches a maximum), and 10 are shown in Fig. 4.14. The correlations for $\frac{J}{t} = 0.1$ are small, the largest of which reaches no greater than 0.02. At $\frac{J}{t} = 6$, the maximum of the susceptibility vs. $\frac{J}{t}$, all correlations have risen, except the separation of $|\mathbf{r}_{i,j}| = 3$ which becomes negative. At $\frac{J}{t} = 10$ all long range

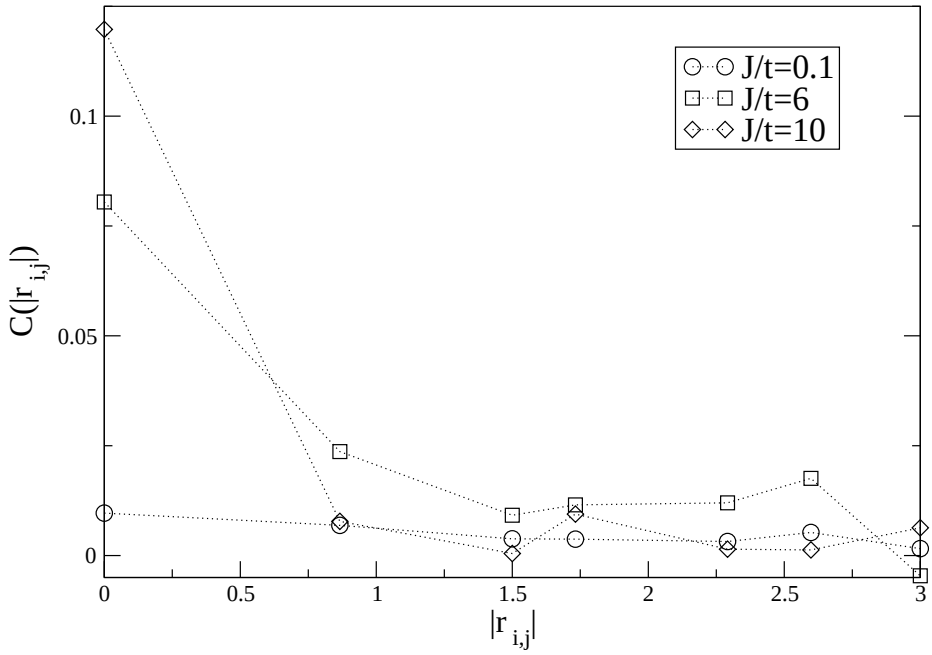

Figure 4.14: The correlations plotted at the values of $\frac{J}{t} = 0.1$ and 10, and the point where the susceptibility vs. $\frac{J}{t}$ reaches a maximum, $\frac{J}{t} = 6$.

correlations have settled down again to roughly the same values as $\frac{J}{t} = 0.1$, and interestingly the correlation of $|\mathbf{r}_{i,j}| = 3$ is again positive. The fluctuation of the $|\mathbf{r}_{i,j}| = 3$ correlation is interesting, since at $\frac{J}{t} = 6$ the remainder of the points would suggest superconductivity is present. Perhaps if superconductivity is present this suggests it is also accompanied by a preference for particular spatial arrangements. A more detailed study, perhaps taking into account symmetries arising from the geometry of the lattice, could shed further light on this.

The other filling considered was six electrons, or a third-filling, which is slightly larger than a quarter filling. The susceptibility vs. $\frac{J}{t}$ for this filling is shown in Fig. 4.15. It is is very similar to the four electron case, except for the strange "bump"

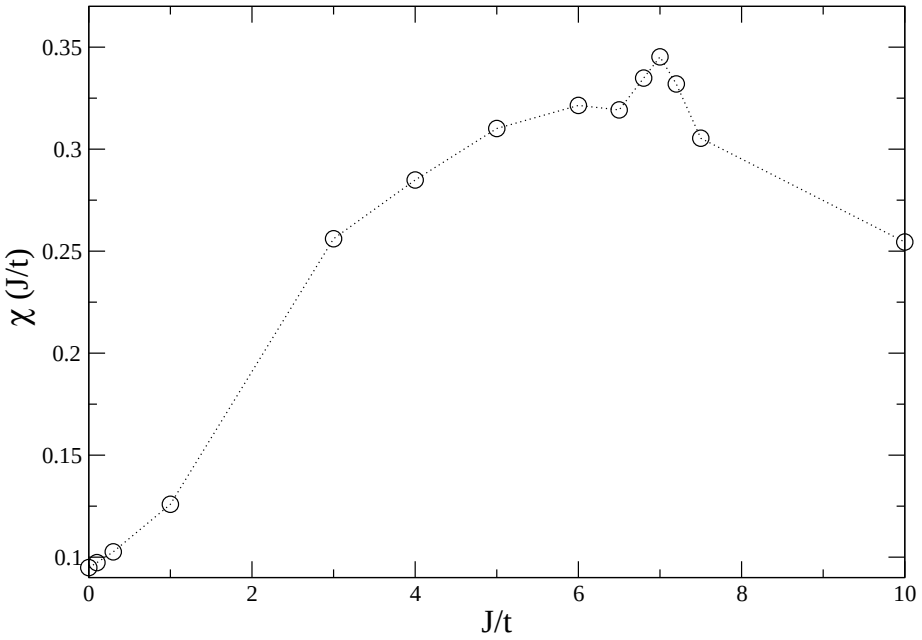

Figure 4.15: Plots of the susceptibilities vs. $\frac{J}{t}$ for the filling of $N_e = 6$. This curve has the strange "bump" feature around the point $\frac{J}{t} = 7$, not present in the $N_e = 4$ case. Barring this anomaly the graph is very similar to the $N_e = 4$ case.

feature around the point $\frac{J}{t} = 7$. This feature gives the susceptibility two maxima, like the eight electron case in one-dimension. However, unlike that case, this curve is not flat.

In Fig. 4.16 the correlations for the values $\frac{J}{t} = 0.1$, 6, and 10 are shown. The overall behaviour is very similar to the filling of $N_e = 4$. The correlations for $\frac{J}{t} = 0.1$ are relatively flat, and most are close to zero. At the point $\frac{J}{t} = 6$ the correlations rise, except this time it is the distance $|\mathbf{r}_{i,j}| = 1.5$ which becomes negative, again suggesting a preferred spatial arrangement. When $\frac{J}{t}$ is raised to 10 the correlations drop back down, becoming lower than the values for $\frac{J}{t} = 0.1$. At $\frac{J}{t} = 10$ the curve takes the form of a decaying exponential. Again the rise in most correlations for

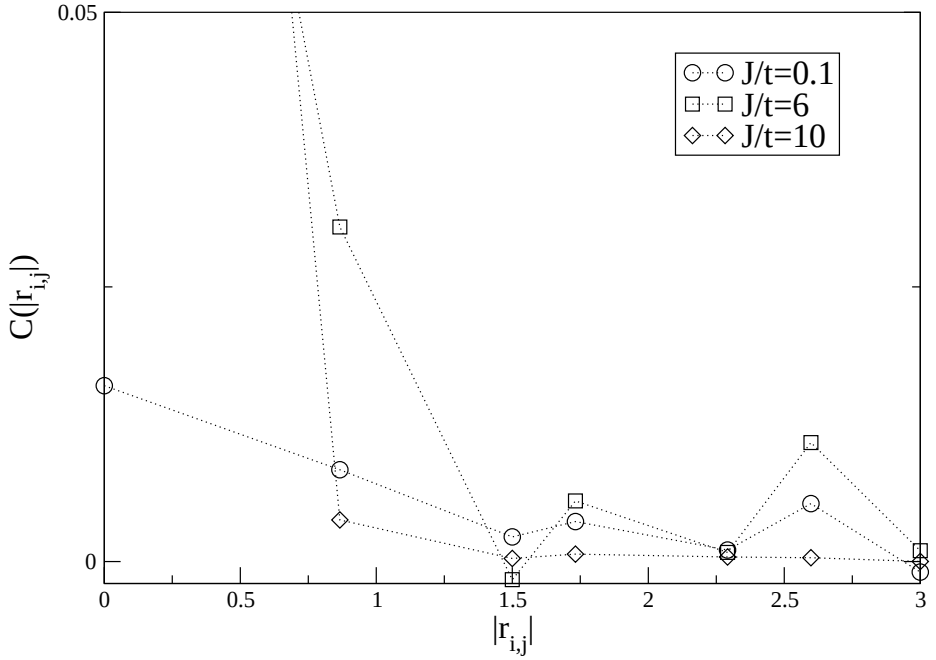

Figure 4.16: The correlations plotted at the values of $\frac{J}{t} = 0.1$ and 10, and the point where the susceptibility vs. $\frac{J}{t}$ reaches a local maximum, $\frac{J}{t} = 6$.

the local maximum value of $\frac{J}{t} = 6$ suggests the possibility of superconductivity, as well as the possibility of symmetry effects in the negative correlations for $|\mathbf{r}_{i,j}| = 1.5$. Symmetry might also be the reason why there is almost no change in the correlations at $|\mathbf{r}_{i,j}| = 2.59$. Indeed, a more detailed study should be carried out.

Figure 4.17 shows a comparison of the correlations for the values of $\frac{J}{t} = 6$ and 7, the points of two maxima in the susceptibility vs. $\frac{J}{t}$. The only notable difference is a rise in the $|\mathbf{r}_{i,j}| = 1.73$ and 2.29 correlations from $\frac{J}{t} = 6$ to $\frac{J}{t} = 6.5$, accompanied by a slight decline $|\mathbf{r}_{i,j}| = 1.5$ to an even more negative value. However, since the values are small and there is really very little change between the values, this would suggest there is nothing interesting occurring between these two points. Perhaps the

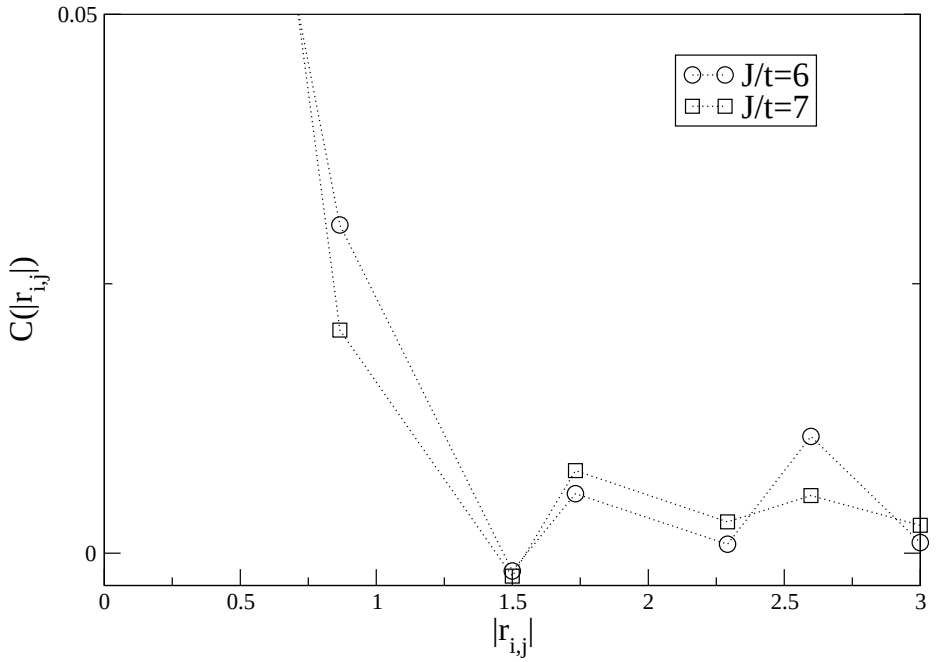

Figure 4.17: The correlations plotted for the two values of the maxima of the susceptibility vs. $\frac{J}{t}$ found at $\frac{J}{t} = 6$ and 7, for the six electron case.

rise in susceptibility at $\frac{J}{t} = 7$ is simply a finite size effect. A further study using a more sophisticated correlation function than Eq. (4.6) could possibly eliminate this bump, or provide some additional insight into the reason for its appearance.

The two fillings studied appear to show the same behaviour. Both start off flat at low $\frac{J}{t}$. As $\frac{J}{t}$ is increased both gain some appreciable long range correlations suggestive of superconductivity at the point where the susceptibility vs. $\frac{J}{t}$ reaches a maximum. Eventually both settle down to an exponentially decaying form at large $\frac{J}{t}$, with no long range correlations. Both of the susceptibilities vs. $\frac{J}{t}$ are roughly the same; however, the $N_e = 6$ case has that anomalous bump in it.

There is little work already done on this system with which to compare to, and

there is no work to directly compare, i.e. we found no source which carried out a Lanczos study of the honeycomb lattice. However, there are Lanczos studies on other lattices, such as the square lattice studied in [23] and in a paper the following year [24]. In these papers Dagotto and Riera considered a two dimensional 4×4 square lattice system for various electronic densities. Some larger systems were also considered, for instance with twenty and twenty-four sites. In Dagotto and Riera's study, they found results similar to the one-dimensional results presented in [23], where quarter-filling presented the most dominant correlations, and the susceptibility vs. $\frac{J}{t}$ was sharply peaked, again suggesting phase separation. It was determined that the most dominant correlations were of $d_{x^2-y^2}$ symmetry, as opposed to s- or d_{xy}-wave. In general, their results for two-dimensions seemed consistent with those for one-dimension.

The results for the honeycomb lattice did not compare well to the results found for the one-dimensional chain. The susceptibility vs. $\frac{J}{t}$ curves for both the one-dimensional chain and the honeycomb lattice did show some similarity in the low-density filling regime, but there were differences. The one-dimensional case the susceptibility vs. $\frac{J}{t}$ curves achieved a sharper peak than the corresponding curves for the honeycomb lattice, which were were smooth, with no sudden jumps (barring the bump in the $N_e = 6$ case). However, in both one and two dimensions, at low filling, the susceptibility vs. $\frac{J}{t}$ curves yielded a distinct rise in the susceptibility as a function of $\frac{J}{t}$ to a maximum which is much larger than the initial low $\frac{J}{t}$ values. Comparing the correlations for the honeycomb system with the correlations for the one-dimensional system, the two systems had some considerable differences. In two-dimensions at low $\frac{J}{t}$, the correlations are very close to zero for most distances, while in one dimension they have an exponential form. In one dimension at large values of $\frac{J}{t}$, the long range

correlation appear to be larger than those at shorter distances. However, in the honeycomb system these longer range correlations die off and are roughly the same size as the shorter correlation lengths. The correlations rise, as $\frac{J}{t}$ is increased, to the maximum value found for susceptibility vs. $\frac{J}{t}$, but then begin to get smaller. There is no shift in the relative weights of each throughout this process, as seen in one dimension where there was a definite shift in the relative weights of the correlations as $\frac{J}{t}$ was increased. Again, a more detailed correlation function and taking the symmetry of the lattice into account could yield more conclusive results.

As mentioned at the beginning of the section, recently there have been some studies on the honeycomb lattice. A recent study [62] considered the $t - J - U - V$ model on a honeycomb lattice using a functional renormalization group technique, the specifics of which are not discussed here. Away from half filling, f-wave and $d_{x^2-y^2} + id_{xy}$-wave singlet pairing was found. In another recent study [59] it is found that in addition to s-wave pairing that a p-wave phase appears at half filling in their derived mean-field phase diagram. This is supported by a later study [60] in which a $t - J$ model study of a honeycomb lattice near half-filling found p-wave symmetry in bound pairs of electrons.

It was not possible to compare to these results as this study neither considered any sort of symmetry in the pairing, or a system near half-filling. However, it does provide a possible starting point for further work. As this is a work in progress, there is still much work to be done with the honeycomb system before more complex lattices, e.g. kagomé and CTSL, can be considered.

Chapter 5

Conclusions and Future Work

5.1 Summary and Conclusions

In this thesis, superconducting correlations on both a one-dimensional chain and a honeycomb lattice were investigated by diagonalizing the $t - J$ model Hamiltonian using the Lanczos method. The one-dimensional results obtained were compared with previously studied results. The honeycomb results were compared to the one-dimensional results, as well as previously studied results considering two-dimensional square lattices.

This thesis is the first step in a larger theoretical examination of lithium titanate, $LiTi_2O_4$, a superconducting TMO with the spinel structure. It was found that the metal-to-insulator transition of this material may be a result of strong electronic correlations [6], suggesting that perhaps the superconducting properties are also a result of strong electronic correlations.

The conducting sites of $LiTi_2O_4$ reside on the Ti atoms which form a corner-sharing tetrahedral lattice (CSTL). Unfortunately, the CSTL is too large and complicated to consider with the available computational resources, and, for reasons given in Chapter 2, the honeycomb lattice was studied instead.

To investigate the superconducting properties of the honeycomb lattice and the one-dimensional chain the $t - J$ model Hamiltonian was used, which is introduced along with the Hubbard model in Chapter 2. This was followed by a demonstration of the important result that the Hubbard model at half-filling, with large on-site energy U and restricted double-occupancy, becomes equivalent to the $t - J$ model.

In Chapter 3, the Hilbert space of the problem considered is shown to be too large to diagonalize by conventional methods. For this reason the Lanczos method, discussed in Chapter 3, was employed to find the ground state eigenvalues and eigenvectors. Testing and diagnostics of the code, as well as other numerical aspects of the study, were discussed in Chapter 3.

Once the ground state was found, it was analyzed to find indications of superconducting correlations. For this, the superconducting correlation function and the corresponding superconducting susceptibility were defined and discussed in Chapter 4, as well as in Appendix D. The results of this analysis for the one-dimensional chain were consistent with those found in the literature, e.g. Ref. [23]. Strong superconducting correlations were found for the quarter- and sixth-filled systems. The higher fillings also showed indications of superconducting correlations; however, these indications were not as strong as for lower fillings. For the honeycomb lattice a slightly simplified correlation function was defined due to the complicated nature of the lattice. Two fillings of four and six electrons were considered, of which neither

demonstrated strong indications of superconductivity. However, as the next section outlines, there is still much work to be done on this structure before this study can be considered to be complete.

5.2 Future Work

There are many steps which must be taken to reach the final goal of a full examination of the CSTL. Indeed, with each step being a study in and of itself, there is much future work which can be derived from this study.

First, as mentioned towards the end of Chapter 4, the work on the honeycomb lattice should be completed. This will provide a more complete picture of this system before moving on to other, more complicated systems. As a first step in completing the work on the honeycomb lattice, a proper singlet pairing function should be considered, as opposed to the general pairing, defined in Eq. (4.5), which was used in this study. After this, more complicated pairing functions, which take into account of *symmetry of the lattice*, could be considered; for example, many sources have found p-wave symmetry in the honeycomb structure, as mentioned in Chapter 4. Aside from numerical work, a two-band BCS analysis could also be carried out.

The next step in reaching a study of the CSTL would be to perform a thorough examination of the kagomé lattice. As was shown in Chapter 2 the CSTL is an ...ABCABC... stacking of kagomé lattices, making the kagomé an ideal intermediate structure. Also, the kagomé lattice will incorporate more details of the CSTL; for instance, geometrical frustration, which the honeycomb lattice did not have. Before moving onto the full study of the CSTL it would be prudent to broaden the theoretical treatment of both the honeycomb and kagomé lattices already given; for example, a

Monte Carlo study should be carried out, in addition to considering other model Hamiltonians.

Finally, before moving on to other larger and more complicated structures, it should be made possible to consider larger system sizes. This could also minimize possible finite-size effects from the present study, or allow larger electron fillings to be included. For this it is imperative to employ more analytical techniques to reduce the size of the Hilbert space. One such technique would be to incorporate translational symmetry into the system, since this allows a reduction of the Hilbert space on the order of N_{sites} [54]. Indeed, other symmetries, such as reflection, could be included also. In addition, the use of a parallel computing system could aid in the time consuming step of constructing the Hamiltonian every time it is needed, allowing quicker results and, in turn, larger systems could be examined. This is currently being investigated.

Bibliography

[1] J. Bednorz and K. Müller. Possible high-T_c superconductivity in the $Ba - La - Cu - O$ system. *Z. Phys. B*, 64:188, 1986.

[2] J. Bardeen, L. N. Cooper, and J. R. Schrieffer. Theory of superconductivity. *Phys. Rev.*, 108(5):1175, Dec. 1957.

[3] Elbio Dagotto. Correlated electrons in high-temperature superconductors. *Rev. Mod. Phys.*, 66(3):763, July 1994.

[4] Micheal Tinkham. *Introduction to Superconductivity, Second Edition.* Dover Publications, Inc., 1996.

[5] E. W. Carlson, V. J. Emery, S. A. Kivelson, and D. Orgad. Concepts in high temperature superconductivity. www.arXiv.org//cond-mat.0206217v1.

[6] Farhad Fazileh. *The metal-to-insulator transition in disordered* $LiTi_2O_4$. PhD thesis, Queen's University, 1995.

[7] J. E. Hirsch and H. Q. Lin. Pairing in the two-dimensional Hubbard model: A Monte Carlo study. *Phys. Rev. B*, 37(10):5070, 1988.

[8] S. Wang, J. Carlson, and J. E. Gubernatis. Pairing correlations in the two-dimensional Hubbard model. *Phys. Rev. Lett.*, 78(23):4486, 1997.

[9] A. G. Petukhov, J. Galán, and J. A. Vergés. Bound states of two electrons described by the $t - J$ model. *Phys. Rev. B*, 46(10):6212, 1992.

[10] S. R. White et. al. Numerical study of the two-dimensional Hubbard model. *Phys. Rev. B*, 40(1):506, 1989.

[11] D. J. Scalapino. The case for $d_{x^2-y^2}$ pairing in the cuprate superconductors. *Phys. Rep.*, 250:329, 1995.

[12] D. J. Sacalpino and S. R. White. Numerical results for the Hubbard model: Implications for the high-t_c pairing mechanism. *Found. Phys.*, 31(1):27, 2001.

[13] J. E. Hirsch. Attractive interaction and pairing in fermion systems with strong on-site repulsion. *Phys. Rev. Lett.*, 54(12):1317, 1985.

[14] L. N. Cooper. Bound electron pairs in a degenerate Fermi gas. *Phys. Rev.*, 104(4):1189, Nov. 1956.

[15] P. W. Anderson. The resonating valence bond state in La_2CuO_4 and superconductivity. *Science*, 235:1196, 1987.

[16] J. R. Schreiffer, X. G. Wen, and S. C. Zhang. Dynamic spin fluctuations and the bag mechanism of high-T_c superconductivity. *Phys. Rev. B*, 39(16):11663, 1989.

[17] F. F. Assaad and D. Würtz. Charge and spin structures in the one-dimensional $t - J$ model. *Phys. Rev. B*, 44(6):2681, 1991.

[18] J.-Y. P. Delannoy, M. J. P. Gingras, P. C. W. Holdsworth, and A.-M. S. Tremblay. Néel order, ring exchange, and charge fluctuations in the half-filled Hubbard model. *Phys. Rev. B*, 72(11):115114, 2005.

[19] K. A. Chow, J. Spalek, and A. M. Oleś. Canonical perturbation expansion of the Hubbard model. *Phys. Rev. B*, 18(7):3453, 1978.

[20] A. H. MacDonald, S. M. Girvin, and D. Yoshioka. $\frac{t}{U}$ expansion for the hubbard model. *Phys. Rev. B*, 37(16):9753, 1988.

[21] J. D. Reger and A. P. Young. Monte Carlo simulations of the spin-$\frac{1}{2}$ Heisenberg antiferromagnet on a square lattice. *Phys. Rev. B*, 37(10):5978, 1988.

[22] S. Chakravarty, B. I. Halperin, and D. R. Nelson. Two-dimensional quantum heisenberg antiferromagnet at low temperatures. *Phys. Rev. B*, 39(4):2344, 1989.

[23] E. Dagotto and J. Riera. Superconductivity in the two-dimensional $t-J$ model. *Phys. Rev. B*, 46(18):12084, 1992.

[24] E. Dagotto and J. Riera. Indications of $d_{x^2-y^2}$ superconductivity in the two-dimensional $t-J$ model. *Phys. Rev. Lett.*, 70(5):682, 1993.

[25] M. Ogata, M. U. Luchini, S. Sorella, and F. F. Assaad. Phase diagram of the one-dimensional $t-J$ model. *Phys. Rev. Lett.*, 66(18):2388, 1991.

[26] T. Prucshke and H. Shiba. Superconducting correlations in the one dimensional $t-J$ model. *Phys. Rev. B*, 46(1):356, 1992.

[27] M. Troyer, H. Tsunetsugu, T. M. Rice, J. Riera, and E. Dagotto. Spin gap and superconductivity in the one-dimensional $t - J$ model with coulomb repulsion. *Phys. Rev. B*, 48(6):4002, 1993.

[28] S. Sorella, G. B. Martins, F. Becca, C. Gazza, L. Capriotti, A. Parola, and E. Dagotto. Superconductivity in the two-dimensional $t - J$ model. *Phys. Rev. Lett.*, 88(11):117002, 2002.

[29] J. Emery V, S. A. Kivelson, and H. Q. Lin. Phase separation in the $t - J$ model. *Phys. Rev. Lett.*, 64(4):475, 1990.

[30] H. Q. Lin. Dilute gas of electron pairs in the $t - J$ model. *Phys. Rev. B*, 44(9):4674, 1991.

[31] L. P. Pryadko, S. A. Kivelson, and O. Zachar. Incipient order in the $t - J$ model at high temperatures. *Phys. Rev. Lett.*, 92(6):067002–1, 2004.

[32] T. K. Lee, C. T. Shih, Y. C. Chen, and H. Q. Lin. Comment on: Superconductivity in the two-dimensional $t - J$ model. *Phys. Rev. Lett.*, 89(27):279702, 2002.

[33] S. Sorella, G. B. Martins, F. Becca, C. Gazza, L. Capriotti, A. Parola, and E. Dagotto. Dilute gas of electron pairs in the $t - J$ model. *Phys. Rev. Lett.*, 89(27):279703, 2002.

[34] W. O. Putikka and M. U. Luchini. Broad peak in the $d_{x^2-y^2}$ superconducting correlation length as a function of hole concentration in the two-dimensional $t-J$ model. *Phys. Rev. Lett.*, 96(24):247001, 2006.

[35] Sashi Satpathy and Richard M. Martin. Electronic structure of the superconducting oxide spinel $LiTi_2O_4$. *Phys. Rev. B*, 36:7269, 1987.

[36] S. Massidda, Jaejun Yu, and A. J. Freeman. Electronic structure and properties of superconducting $LiTi_2O_4$. *Phys. Rev. B*, 38:11352, 1988.

[37] D. C. Johnson, H. Prakash, W. H. Zachariasen, and R. Viswanathan. High temperature superconductivity in the Li-Ti-O ternary system. *Mater. Res. Bull.*, 8:777, 1973.

[38] Evagelia G. Moshopoulou. Superconductivity in the spinel compound $LiTi_2O_4$. *J. Am. Ceram. Soc.*, 82(12):3317, 1999.

[39] R. W. McCallum, D. C. Johnson, C. A. Luengo, and M. B. Maple. Superconducting and normal state properties of $Li_{1+x}Ti_{2x}O_4$ spinel compounds. ii. low-temperature heat capacity. *J. Low Temp. Phys.*, 25(1):177, 1976.

[40] F. Fazileh, R. J. Gooding, and D. C. Johnson. Examining the metal-to-insulator transitions in $Li_{1+x}Ti_{2-x}O_4$ and $LiAl_yTi_{2-y}O_4$ with a quantum site percolation model. *Phys. Rev. B*, 69:104503, 2004.

[41] M. R. Harrison, P. P. Edwards, and J. B. Goodenough. *Phil. Mag. B*, 52:679, 1985.

[42] J. M. Heintz et. al. Superconductivity of $LiTi_2O_4$ and related systems. *Cond. Mat.: Z. Phys B*, 76:303, 1989.

[43] P. M. Lambert, P. P. Edwards, and M. R. Harrison. Magnetism, superconductivity, and the metal-nonmetal transition in the spinel $LiM_xTi_{2-x}O_4$: $M = Al$, Cr. *J. Sol. St. Chem.*, 89:345, 1990.

[44] Patrick Fazekas. *Lecture notes on electron correlation and magnetism.* World Scientific, 1999.

[45] Assa Auerbach. *Interacting electrons and quantum magnetism.* Springer-Verlag New York, Inc., 1994.

[46] J.E. Greedan. Geometrically frustrated magnetic materials. *J. Mater. Chem.*, 11:37, 2001.

[47] Andreas Lüscher, Andreas Läuchli, Weihong Zheng, and Oleg P. Sushkov. Single-hole properties of the $t - J$ model on the honeycomb lattice. *Phys. Rev. B*, 73(15):155118, 2006.

[48] Y. Kopelevich, P. Esquinazi, J.H.S. Torres, and S. Moehlecke. Ferromagnetic- and superconducting-like behaviour of graphite. *J. Low Temp. Phys.*, 119:691, 2000.

[49] J. Hubbard. Electron correlations in narrow energy bands. *Proc. Roy. Soc. A*, 276:238, 1963.

[50] C. Lanczos. An iterative method for the solution of the eigenvalue problem of linear differential and integral operators. *J. Res. Nat. Bur. Stand.*, 45:255, 1950.

[51] Gene H. Golub and Charles F. Van Loan. *Matrix Computations, Third Edition.* John Hopkins University Press, 1996.

[52] C. C. Paige. Computational variants of the Lanczos method for the eigenproblem. *J. Inst. Math. Its Appl.*, 10:373, 1972.

[53] H. Q. Lin and J. E. Gubernatis. Exact diagonalization methods for quantum systems. *Comp. in Phys.*, 7(4):400, Jul/Aug 1993.

[54] P. W. Leung and Paul E. Oppenheimer. Implementation of the Lanczos algorithm for the Hubbard model on the connected machine system. *Comp. in Phys.*, 6(6):603, Nov/Dec 1992.

[55] H. Q. Lin. Exact diagonalization of quantum spin models. *Phys. Rev. B*, 42(10):651, October 1990.

[56] Jane K. Cullum and Ralph A. Willoughby. *Lanczos Algorithms for Large Symmetric Eigenvalue Computations, Part 1: Theory.* Society for Industrial and Applied Mathematics, 2002.

[57] Gerard Meurant. *The Lanczos and Conjugate Gradient Algorithms, From Theory to Finite Precision Computations.* Society for Industrial and Applied Mathematics, 2006.

[58] Private communication with P. W. Leung.

[59] Bruno Uchoa and A. H. Castro Neto. Superconducting states of pure and doped graphene. *Phys. Rev. Lett.*, 98(14):146801, 2007.

[60] P. Wróbel and W. Suleja. Unconventional pairing in a weakly doped antiferromagnet on the honeycomb lattice: Mechanism of symmetry selection. *Phys. Rev. B*, 75(17):174522, 2007.

[61] C. Y. Kadolkar and S. Basu. Phase diagram of the $t - J$ model on a honeycomb lattice. *Phys. Rev. B*, 73(10):104501, 2006.

[62] C. Honerkamp. Density waves and Cooper pairing on the honeycomb lattice. www.arXiv.org//cond-mat.0711.1259v1.

[63] E. Maxwell. Isotope effect in the superconductivity of mercury. *Phys. Rev.*, 78(4):477, May 1950.

[64] C. A. Reynolds, B. Serin, W. H. Wright, and L. B. Nesbitt. Superconductivity of isotopes of mercury. *Phys. Rev.*, 78(4):487, May 1950.

[65] Neil W. Ashcroft and N. David Mermin. *Solid State Physics*. Thompson Learning, Inc., 1976.

[66] Michael Plishke and Birger Bergerson. *Equilibrium Statistical Physics, Second Edition*. World Scientific, 1994.

Appendix A

Bloch's Theorem

In free space, the energy of a single electron of mass m_e and wave vector $\mathbf{k}$ is given by

$$E_{\mathbf{k}} = \frac{\hbar^2 |\mathbf{k}|^2}{2m_e} \ , \tag{A.1}$$

and forms a continuum. For electrons in a lattice with a periodic potential, $U(\mathbf{r}+\mathbf{R}) = U(\mathbf{r})$, where $\mathbf{R} = \mathbf{R}_{m,n}$ is the period of the Bravais lattice, the energy levels no longer form a single continuum. They are broken into a family of continuous functions called energy bands

$$E_{n_b,\mathbf{k}+\mathbf{G}} = E_{n_b,\mathbf{k}} \ , \tag{A.2}$$

labelled by the band index, n_b. The parameter $\mathbf{G}$ is a reciprocal lattice vector. Each $E_{n_b,\mathbf{k}}$ is continuous in $\mathbf{k}$, and has an upper and lower bound such that all of the levels within a given n_b lie in a band of energies existing between these limits.

The eigenstates are of the form of a plane wave multiplied by a function which

has the periodicity of the Bravais lattice called Bloch waves,

$$\psi_{n,\mathbf{k}}(\mathbf{r}) = \exp(i\mathbf{k}\cdot\mathbf{r})u_{n_b,\mathbf{k}}(\mathbf{r}) \tag{A.3}$$

where,

$$u_{n_b,\mathbf{k}}(\mathbf{r}+\mathbf{R}) = u_{n_b,\mathbf{k}}(\mathbf{r}). \tag{A.4}$$

This is Bloch's Theorem and electrons with wave functions that satisfy Eq. (A.3) are referred to as Bloch electrons.

In both the free electron and Bloch electron cases, each one-electron level is labelled[1] by $\mathbf{k}$ and a spin label, σ, which is either up ($\uparrow$) or down ($\downarrow$). In the absence of an applied magnetic field the energy is degenerate with respect to the spin spin label, in which case two electrons of opposite spin may occupy a single $\mathbf{k}$-level. The ground state of an N-electron system, at temperature $T = 0$K, is constructed by filling all of the one-electron levels up to the Fermi energy, E_F.

In the case of Bloch electrons, with the continuum broken up into bands, two possible situations result determined by the electronic density and the Fermi energy. The first is where a given number of bands are completely filled, while the rest remain completely empty. The difference in energy between the top of the highest occupied band and bottom of lowest unoccupied band is called the band gap. Under various circumstances pertaining to the nature of the band gap this gives rise to either insulators or semi-conductors. The second situation is when one or more bands are partially filled. This leaves the Fermi energy within the range of one or more of the bands. There is a surface in $\mathbf{k}$-space for each partially filled band that separates the

[1]For Bloch electrons the parameter $\mathbf{k}$ is no longer the free wave vector, but $\hbar\mathbf{k}$ is now an analogous parameter referred to as the crystal momentum.

occupied and unoccupied levels. Collectively, the set of these surfaces is known as the Fermi surface, the existence of which leads to metallic properties.

Appendix B

Cooper Pairs

The central idea of the BCS theory of superconductivity is that a weak, attractive interaction can form a bound state out of a pair of electrons [14], called a Cooper pair. No matter how weak this interaction is, a filled Fermi sea[1] will form at least one bound pair of electrons. The mechanism for this attractive potential is an over-screening of the ion cores, as a result of which the ions respond to the motion of the electrons. As an electron moves through the lattice it distorts the lattice, which, in turn, effects the motion of another electron. The electrons effectively interact through a phonon, which under certain circumstances leads to an attractive interaction. The experimental proof of this is the isotope effect[2] [63, 64]. Below is a simple example illustrating the Cooper problem.

The ground state energy of this system will be measured from the Fermi energy,

[1] A state in which all of the lowest energy states have been filled up to the Fermi energy.

[2] When the isotope of the superconducting material changes the critical temperature also changed. Since changing the isotope changes the mass of the atoms it would then effect how readily movable they are within the material. It is found that T_c is proportional to the square root of the mass for isotopes of the same element [4].

ϵ_F. and the ground state will be taken to be the filled Fermi sea

$$|F\rangle = \prod_{|\mathbf{k}|<\mathbf{k}_f,\sigma} c^\dagger_{\mathbf{k},\sigma}|0\rangle \ . \tag{B.1}$$

The lowest energy state of a pair of electrons acting under an attractive potential is the singlet state in which the electrons have equal and opposite momenta $(\mathbf{k}, -\mathbf{k})$ and spin ($S_z = \frac{\hbar}{2} \equiv\uparrow, S_z = -\frac{\hbar}{2} \equiv\downarrow$). Consider such a pair added to the Fermi sea at $T = 0$, the resulting wave function is

$$|\psi_{pair}\rangle = \sum_{|\mathbf{k}|>k_f} g_{\mathbf{k}} c^\dagger_{\mathbf{k},\uparrow} c^\dagger_{-\mathbf{k},\downarrow}|F\rangle = \sum_{|\mathbf{k}|>k_f} g_{\mathbf{k}}|\mathbf{k},\uparrow;-\mathbf{k},\downarrow\rangle \ . \tag{B.2}$$

They interact with one another via some pairing interaction potential, and interact with those electrons in the Fermi sea only through the Pauli exclusion principal (PEP), which acts to exclude them from the states below the Fermi level. For a two particle bound state to exist in an attractive potential just above the Fermi energy (such that each electron has an energy roughly of the order of ϵ_F), there must be an eigenstate of this pair such that the two particles are bound with an energy $E < 2\epsilon_F$.

The Hamiltonian is given by

$$H = \sum_{|\mathbf{k}|>k_F,\sigma} \epsilon_{\mathbf{k}} c^\dagger_{\mathbf{k},\sigma} c_{\mathbf{k},\sigma} + \sum_{|\mathbf{k}|,|\mathbf{k}'|>k_F} V_{\mathbf{k},\mathbf{k}'} c^\dagger_{\mathbf{k},\uparrow} c^\dagger_{-\mathbf{k},\downarrow} c_{-\mathbf{k}',\downarrow} c_{\mathbf{k}',\uparrow} \tag{B.3}$$

where the $V_{\mathbf{k},\mathbf{k}'}$ are the interaction matrix elements between the states. In this interaction it is assumed that scattering can only occur such that, $(\mathbf{k},\uparrow) \rightarrow (\mathbf{k}',\uparrow)$ and $(-\mathbf{k},\downarrow) \rightarrow (-\mathbf{k}',\downarrow)$.

Substitution into the Schrödinger equation yields the condition

$$Eg_{\mathbf{k}} = 2g_{\mathbf{k}}\epsilon_{\mathbf{k}} + \sum_{|\mathbf{k}'|>k_F} g_{\mathbf{k}'}V_{\mathbf{k},\mathbf{k}'} \ . \tag{B.4}$$

If a set $g_{\mathbf{k}}$ can be found such that the above relation is satisfied for an energy $E < 2\epsilon_F$, then a bound-pair state exists. It will now be assumed that the interaction potential is attractive only in some small shell of width ϵ_c surrounding the Fermi sphere. In this shell the matrix elements $V_{\mathbf{k},\mathbf{k}'} = -V$ between states in the range of energy $R|R \in \{\epsilon_F \leq \epsilon_{\mathbf{k}} \leq \epsilon_F + \hbar\omega_c\}$, where ω_c is some cut-off frequency not too far from the Fermi surface. The relation found in Eq. (B.4) then becomes,

$$(E - 2\epsilon_{\mathbf{k}})g_{\mathbf{k}} = \begin{cases} -V\sum_{|\mathbf{k}'|>k_F} g_{\mathbf{k}'} & \text{if} \quad k \in R \\ 0 & \text{if} \quad k \notin R \end{cases} \ . \tag{B.5}$$

Working now only in the range R, rearranging the above gives

$$g_{\mathbf{k}} = V\frac{\sum_{|\mathbf{k}'|>k_F} g_{\mathbf{k}'}}{(2\epsilon_{\mathbf{k}} - E)} \tag{B.6}$$

Now, cancelling the $\sum_{|\mathbf{k}'|>k_F} g_{\mathbf{k}'}$ by summing both sides of this equation gives

$$\frac{1}{V} = \sum_{|\mathbf{k}|>k_F} \frac{1}{(2\epsilon_{\mathbf{k}} - E)} \tag{B.7}$$

Replacing the sum with an integral over R, $\sum_{|\mathbf{k}|>k_F} \rightarrow \int_{\epsilon_F}^{\epsilon_F+\hbar\omega_c} d\epsilon\rho(\epsilon)$ where $\rho(\epsilon) = \frac{\partial \mathbf{k}}{\partial \epsilon}$ is the density of states. In this range of integration if one assumes that the density

of states is constant, $\rho(\epsilon) \to \rho(\epsilon_F)$, hence

$$\frac{1}{V} = \rho(\epsilon_F) \int_{\epsilon_F}^{\epsilon_F + \hbar\omega_c} \frac{d\epsilon}{(2\epsilon - E)} \tag{B.8}$$

Performing this integral gives

$$\frac{1}{V} = \rho(\epsilon_F) \ln\left(\frac{2\epsilon_F - E - 2\hbar\omega_c}{2\epsilon_F - E}\right) , \tag{B.9}$$

which then in turn gives the energy

$$E \approx 2\epsilon_F - \hbar\omega_c \exp\left(-\frac{2}{\rho(\epsilon_F)v}\right) < 2\epsilon_F . \tag{B.10}$$

Where due to the weak attractive interaction, $-V$, assumed at the beginning, the approximation $\rho(\epsilon_F)V \ll 1$ has been used.

Therefore, in the presence of a weak attractive potential there exists an energy $E < 2\epsilon_F$, and there also exists a bound state of the electron pair with $k > k_F$.

Note also that similar results may also be found for two electrons on a one dimensional lattice, with periodic energy $\epsilon_{\mathbf{k}} = -2t\cos k$, where t is the usual hopping energy. From Eq. (B.6), the sum is again replaced by an integral over k where the density of states may be shown to reduce to

$$\rho(\epsilon) = \frac{L}{2\pi} \frac{1}{\sqrt{4t^2 - \epsilon_k^2}} . \tag{B.11}$$

This gives (compare to Eq. (B.8))

$$\frac{1}{V} = \frac{L}{2\pi} \int_{\epsilon_F}^{\epsilon_F + \hbar\omega_c} \frac{1}{\sqrt{4t^2 - \epsilon_k^2}(2\epsilon_{\mathbf{k}} - E)} d\epsilon_{\mathbf{k}} , \tag{B.12}$$

which integrates to

$$\frac{1}{V} = \frac{-L}{\pi} \frac{1}{\sqrt{16t^2 - E^2}} \ln(x) \ , \tag{B.13}$$

where

$$x = \frac{\left(8t^2 - E\left(\epsilon_F + \hbar\omega_c\right) + \sqrt{16t^2 - E^2}\sqrt{4t^2 - \left(\epsilon_F + \hbar\omega_c\right)^2}\right)\left(2\epsilon_F - E\right)}{\left(8t^2 - E\epsilon_F + \sqrt{16t^2 - E^2}\sqrt{4t^2 - \epsilon_f^2}\right)\left(2\left(\epsilon_F + \hbar\omega_c\right) - E\right)} \ . \tag{B.14}$$

Since a solution is sought where the value of E is slightly less than Fermi energy, this equation is solved analytically by making the substitution,

$$E = 2\epsilon_F - \Delta \tag{B.15}$$

where $\Delta \ll 1$.

A solution for Δ is found, where

$$\Delta \approx \hbar\omega_c \exp\left(\frac{-4\pi\sqrt{4t^2 - \epsilon_F}}{Lv}\right) \ . \tag{B.16}$$

It is seen from Eq. (B.15) that the condition $E < \epsilon_F$ is satisfied, since $\Delta > 0$. The energy is therefore

$$E \approx 2\epsilon_F - \hbar\omega_c \exp\left(\frac{-4\pi\sqrt{4t^2 - \epsilon_F}}{Lv}\right) \ . \tag{B.17}$$

Identifying the density of states in the above as

$$\rho(\epsilon) = \frac{L}{2\pi} \frac{1}{\sqrt{4t^2 - \epsilon_f^2}} \ , \tag{B.18}$$

we get for the energy,

$$E \approx 2\epsilon_F - \hbar\omega_c \exp\left(-\frac{2}{\rho(\epsilon_F)v}\right) < 2\epsilon_F \ . \tag{B.19}$$

This expression is seen to be identical to the expression already found for the free particle case in Eq. (B.10), showing that similar results are found for the Cooper-pairing of two electrons on a one dimensional lattice as for free space.

Appendix C

BCS Theory

The BCS theory [2] is an extension of the idea of a Cooper pair. In the BCS ground state all electrons are considered to have transformed into Cooper pairs, where each pair is in a singlet state. As the temperature rises through its critical value, T_c, all pairs become unbound, with a continuous conversion back to the normal ground state of the independent electron approximation.

Due to the low binding energy the Cooper pairs cannot be viewed as independent bosons. Rather the superconducting state consists of electrons which are intricately spatially interlocked [65]. Since the spatial extent of a pair, ζ_0, is of the order $10^3 \mathring{A}$ which is large compared with inter-particle spacing r_s, within ζ_0 there will be millions of pairs.

The BCS ground state is constructed by grouping the N electrons of the Fermi sea into $\frac{N}{2}$ Cooper pairs. It is defined as

$$|BCS\rangle = \prod_{\mathbf{k}} \left(u_{\mathbf{k}} + v_{\mathbf{k}} c^{\dagger}_{\mathbf{k},\uparrow} c^{\dagger}_{-\mathbf{k},\downarrow} \right) |0\rangle \ , \tag{C.1}$$

where $|u_{\mathbf{k}}|^2 + |v_{\mathbf{k}}|^2 = 1$. $|v_{\mathbf{k}}|^2$ gives the probability that the pair $(\mathbf{k}, \uparrow; -\mathbf{k}, \downarrow)$ is occupied, and $|u_{\mathbf{k}}|^2 = 1 - |v_{\mathbf{k}}|^2$ is the probability that it is unoccupied. The BCS wave function is then taken to be the new vacuum state, with the zero of energy set to be the Fermi energy, $\xi_{\mathbf{k}} = \epsilon_{\mathbf{k}} - \epsilon_F$. For simplicity this will be considered only at $T = 0$.

A change of basis is required to find new creation and annihilation operators such that $\gamma_{\mathbf{k},\sigma}|BCS\rangle = 0$. The new operators are related to the $c_{\mathbf{k}}$ through a Bogoliubov-Valatin transformation given by

$$c_{\mathbf{k},\uparrow} = u^*_{\mathbf{k}}\gamma_{\mathbf{k},\uparrow} + v_{\mathbf{k}}\gamma^\dagger_{-\mathbf{k},\downarrow} \tag{C.2}$$

$$c^\dagger_{-\mathbf{k},\downarrow} = -v^*_{\mathbf{k}}\gamma_{\mathbf{k},\uparrow} + u_{\mathbf{k}}\gamma^\dagger_{-\mathbf{k},\downarrow} \ . \tag{C.3}$$

The $\gamma_{\mathbf{k},\sigma}$ are called quasi-particle operators. Below it will be shown they do not conserve particle number, and so cannot be considered as conventional fermionic operators.

In order to find values for $u_{\mathbf{k}}$ and $v_{\mathbf{k}}$ we start with the standard second-quantized interaction Hamiltonian found in Eq. (B.3)

$$H = \sum_{\mathbf{k},\sigma} \epsilon_{\mathbf{k}} n_{\mathbf{k},\sigma} + \sum_{\mathbf{k},\mathbf{k}'} V_{\mathbf{k}\mathbf{k}'} \left(c^\dagger_{\mathbf{k},\uparrow} c^\dagger_{-\mathbf{k},\downarrow} c_{-\mathbf{k}',\downarrow} c_{\mathbf{k}',\uparrow} \right) \ . \tag{C.4}$$

The mean-field-like substitution $c_{-\mathbf{k},\downarrow}c_{\mathbf{k},\uparrow} = b_{\mathbf{k}} + c_{-\mathbf{k},\downarrow}c_{\mathbf{k},\uparrow} - b_{\mathbf{k}}$, such that $b_{\mathbf{k}} = \langle c_{-\mathbf{k},\downarrow}c_{\mathbf{k},\uparrow}\rangle$ is made and terms quartic in $c_{\mathbf{k}}$ are ignored. This yields

$$H' = \sum_{\mathbf{k},\sigma} \xi_{\mathbf{k}} c^\dagger_{\mathbf{k},\sigma} c_{\mathbf{k},\sigma} + \sum_{\mathbf{k},\mathbf{k}'} V_{\mathbf{k}\mathbf{k}'} \left(c^\dagger_{\mathbf{k},\uparrow} c^\dagger_{-\mathbf{k},\downarrow} b_{\mathbf{k}'} + b^\dagger_{\mathbf{k}} c_{-\mathbf{k}',\downarrow} c_{\mathbf{k}',\uparrow} - b^\dagger_{\mathbf{k}} b_{\mathbf{k}'} \right) \ . \tag{C.5}$$

Now, define

$$\Delta_{\mathbf{k}} = -\sum_{\mathbf{k}'} V_{\mathbf{k}\mathbf{k}'} b_{\mathbf{k}'} \tag{C.6}$$

and by substituting Eqs. (C.6) and (C.2) into Eq. (C.5) leads to a fully diagonalized Hamiltonian:

$$H' = \sum_{\mathbf{k}} \left(\xi_{\mathbf{k}} - E_{\mathbf{k}} + \Delta_{\mathbf{k}} b^*_{\mathbf{k}}\right) + \sum_{\mathbf{k}} E_{\mathbf{k}} \left(\gamma^*_{\mathbf{k},\uparrow}\gamma_{\mathbf{k},\uparrow} + \gamma^*_{-\mathbf{k},\downarrow}\gamma_{-\mathbf{k},\downarrow}\right) \ . \tag{C.7}$$

The first sum is a constant which corresponds to the condensation energy[1]. The second sum describes the elementary, quasi-particle excitations of the system. The excitations have energy $E_{\mathbf{k}} = \sqrt{\xi^2_{\mathbf{k}} + |\Delta_{\mathbf{k}}|^2}$ where $\Delta_{\mathbf{k}}$ is seen to be an energy gap; note that even at the Fermi level, where $\xi_{\mathbf{k}} = 0$, $E_{\mathbf{k}} = |\Delta_{\mathbf{k}}| > 0$.

The condition for diagonalization is governed by the relation

$$2\xi_{\mathbf{k}} u_{\mathbf{k}} v_{\mathbf{k}} + \Delta^\dagger_{\mathbf{k}} v^2_{\mathbf{k}} - \Delta^\dagger_{\mathbf{k}} u^2_{\mathbf{k}} = 0 \ . \tag{C.8}$$

This leads to an expression for the Bogoliubov-Valatin coefficients,

$$|v_{\mathbf{k}}|^2 = 1 - |u_{\mathbf{k}}|^2 = \frac{1}{2}\left(1 - \frac{\xi_{\mathbf{k}}}{E_{\mathbf{k}}}\right) \ . \tag{C.9}$$

Now, consider the action of a quasi-particle creation operator on the BCS ground state:

$$\gamma^\dagger_{\mathbf{k},\uparrow}|BCS\rangle = c^\dagger_{\mathbf{k},\uparrow} \prod_{\mathbf{k}\neq\mathbf{k}'} \left(u_{\mathbf{k}'} + v_{\mathbf{k}'} c^\dagger_{\mathbf{k}',\uparrow} c^\dagger_{-\mathbf{k}',\downarrow}\right)|0\rangle \ . \tag{C.10}$$

[1]The condensation energy is the difference in energy between the BCS ground state of Eq. (C.1) and the normal, Fermi sea state in Eq. (B.2).

Evidently, the quasi-particle operators do not conserve particle number, as this operation has removed the particle corresponding to $c^{\dagger}_{-\mathbf{k},\downarrow}$ from the state altogether. More importantly, however, is that both $c^{\dagger}_{\mathbf{k},\uparrow}$ as well as it Cooper pair $c^{\dagger}_{-\mathbf{k},\downarrow}$ have been blocked out of the BCS state. This reflects the idea that the transition from the superconducting state to the normal state consists of breaking pairs, as it is seen that an excitation of this system with respect to the quasi-particles corresponds to the removal a Cooper pair from the BCS state. However, this is not an entirely correct argument[2], the proper, number conserving excited state would be given be given by $|\Psi^1_{BCS}\rangle = \gamma_{\mathbf{k},\uparrow}\gamma_{-\mathbf{k},\downarrow}|\tilde{0}\rangle$. The energy of such an excitation would be

$$E = \langle \Psi^1_{BCS}|H|\Psi^1_{BCS}\rangle = 2E_{\mathbf{k}} \ . \tag{C.11}$$

Assuming the pair has an energy close to the Fermi energy, i.e. $\xi_{\mathbf{k}} = 0$, then $E = 2\Delta_{\mathbf{k}}$, which corresponds to the experimental fact [4] that the spectroscopic gap is 2Δ and not Δ.

[2]See Ref. [4] for a more thorough explanation.

Appendix D

The Pair-Pair Correlation Function

The pair-pair correlation function can be understood by first considering the spin-spin correlation function of the Ising model. For the Ising model the magnetization as $T \to T_c$ from below[1] has the asymptotic form [66]

$$m\left(T\right) \approx \left(T - T_c\right)^{\frac{1}{2}} \ . \tag{D.1}$$

The zero-field magnetic susceptibility can be shown to have the form

$$\chi\left(h = 0, T\right) = \left(\frac{\delta m}{\delta h}\right)_T \Big|_{h=0} = \sum_j \left(\langle \sigma_j \sigma_0 \rangle - \langle \sigma_j \rangle \langle \sigma_0 \rangle\right) \ . \tag{D.2}$$

The Ising spins $\sigma_j = \pm 1$ on site j. The susceptibility will diverge only if $\Gamma_j = \langle \sigma_j \sigma_0 \rangle - \langle \sigma_j \rangle \langle \sigma_0 \rangle$ is long-ranged [66].

The spin-spin correlation function is defined

$$C_j = \langle \sigma_j \sigma_0 \rangle \ . \tag{D.3}$$

[1]Here the critical temperature refers to the onset of a magnetically ordered state.

Consider the limit $j \to \infty$, i.e. when the spins are a large distance apart. In this limit the approximation $\langle \sigma_j \sigma_0 \rangle \approx \langle \sigma_j \rangle \langle \sigma_0 \rangle$ can be made. From this two conclusions may be drawn. The first is that when $\langle \sigma_j \rangle = 0$, i.e. the system has no magnetization, this implies

$$\langle \sigma_j \sigma_0 \rangle = 0 \ , \tag{D.4}$$

and the system is considered to be disordered. On the other hand if $\langle \sigma_j \rangle = m$, i.e. the system has some fixed magnetization, this implies

$$\langle \sigma_j \sigma_0 \rangle \neq 0 \ , \tag{D.5}$$

and the system is considered to be ordered.

For superconducting correlations the pair annihilation operator, Δ_j, is considered instead of the σ_j. It is related to the expression for the superconducting energy gap defined in Eq. (C.6), which represents the energy required to destroy a Cooper pair. The exact form of Δ_j depends on the type of singlet pairing one is expecting; this is discussed in Chapter 4.

The pair-pair correlation function is defined as,

$$C\left(\mathbf{m}\right) = \left(\frac{1}{N_{sites}}\right) \sum_i \langle \Delta_i^\dagger \Delta_{i+\mathbf{m}} \rangle \ . \tag{D.6}$$

Where $\mathbf{m}$ is a parameter that measures the separation between pairs. From the pair-pair correlation function a susceptibility as a function of the anti-ferromagnetic

super-exchange J of the Heisenberg model may be found

$$\chi_{sus}\left(\frac{J}{t}\right) = \sum_{\mathbf{m}} C\left(\mathbf{m}\right) \ . \tag{D.7}$$

Thus, for a finite system, such as the ones encountered in this thesis, one is interested in the case when $C\left(\mathbf{m}\right)$ maintains appreciable non-zero values for all possible values of $\mathbf{m}$. Ideally, there is a point where χ_{sus} will reach a maximum as more and more correlations are included in the sum in Eq. (D.7). It is suggested that phase separation occurs in the region of $\frac{J}{t}$ immediately after the peak in susceptibility [23]. In the infinite system limit χ_{sus} would diverge, indicating the system has gone through a change of ordering at the point where J has reached a critical J_c. The system at this point makes a change to the superconducting phase where all particles have become Cooper-paired, and are coherently correlated throughout the entire system.

Appendix E

The Lanczos Algorithm Code

Included in this Appendix is the code used to compute the eigenvalue using the Lanczos routine, plus two of the important subroutines which appear as included files within the main Lanczos routine. One subroutine generates the Hamiltonian, and the other generates the binary states. The code for finding the eigenvector via the Lanczos routine is almost identical to that for the eigenvalue, except for one step which performs Eq. (3.35), so it will not be included here.

There were some issues, however, that were addressed when writing the Lanczos code. The first was the high chance of floating point error, since during the Lanczos routine vectors are being continuously subtracted from and added to; BLAS has been utilized wherever possible to help reduce this. Another concern is the loss of orthogonality of the Lanczos vectors, there are several several ways around this [51], however, the method used here was to simply ignore the problem [53]. Another crucial aspect of the code mentioned in most references is finding an efficient matrix-vector multiplication routine for the step $H|w_i\rangle$ (see the outline of the Lanczos routine in § 3.1 of Chapter 3). Since the Hamiltonian is never written down, but generated at

each step of the algorithm, this is not a concern. An efficient routine was devised that generates each row of the Hamiltonian one at a time; then the dot product between this row and the current Lanczos vector, $|w_i\rangle$, is found.

E.1 Lanczos Routine for Finding the Eigenvalue

```
#include <string.h>
#include <math.h>
#include <stdio.h>
#include <stdlib.h>
#include <sys/resource.h>
#include <sys/types.h>
#include <gsl/gsl_rng.h>
#include <gsl/gsl_math.h>

// first define all BLAS function which will be used in the program

double daxpy_(unsigned long long int *N, double *SA, double *SX,
   int *INCX, double *SY, int *INCY); // finds SY=SA*SX+SY

double ddot_(unsigned long long int *N, double *SX, int *INCX,
   double *SY, int *INCY); // finds SX.SY

double dscal(unsigned long long int *N, double *SA, double *SX,
   int *INCX);
// finds SX=SA*SX

double dnrm2_(unsigned long long int *N, double *SX, int *INCX);
// finds SX.SX

double dcopy_(unsigned long long int *N,double *SX, int *INCX,
   double *SY, int *INCY); // finds SY=SX

double dsymv_( char *uplo, unsigned long long int *n, double *alpha,
    double *m, int *llda, double *w, int *incx, double *beta,
```

```
    double *y, int *incy);
// finds y=m*x+alpha*y

double dstevr_(char *jobz, char *range, unsigned long long int *N,
    double *d, double *e, double *vl, double *vu, int *il, int *iu,
    double *abstol, int *M, double *w, double *z, int *lldz,
    int *isuppz, double * work, int *lwork, int * iwork,
    int *liwork, int *info);
// finds eigenvalues of a symmetric tridiagonal matrix

int main ()
{

   int Ne, Nsi, Nehalf; /* size and state parameters */

   unsigned long long int Nst,Nst1; /* number of states */
   double t, J, J1, dist;   /* model parameters */
   int L; /*length of lattice */
   int i,j,k,l; /* counters */

   unsigned long long int k1,k2,k3,k4;

   /* input parameters */

   char line[100];

   printf("What is the length of the lattice?\n");
   fgets(line, sizeof(line),stdin);
   sscanf(line, "%d", &L);
   printf("How many electrons?\n");
   fgets(line, sizeof(line),stdin);
   sscanf(line, "%d", &Ne);
   printf("What is t?\n");
   fgets(line, sizeof(line),stdin);
   sscanf(line, "%lf", &t);
   printf("What is J?\n");
   fgets(line, sizeof(line),stdin);
   sscanf(line, "%lf", &J);

   /* find number of sites (to be changed for larger dimensions*/
```

```
Nsi = 2*L*L; // the number of sites for a honeycomb lattice
Nehalf = Ne/2;

/* now find the number of states */

unsigned long long int Nsifac, Nsifac1,Nehalffac;

// first find Nsi!

j=Nsi-1;
Nsifac=Nsi;
while(j>Nsi-Nehalf)
{
  Nsifac=Nsifac*j;
  j--;
}

// now find Nsi1!

j=Nsi-1;
Nsifac1=Nsi;
while(j>Nsi-Ne)
{
  Nsifac1=Nsifac1*j;
  j--;
}

// now find (Ne/2)!

j=Nehalf-1;
Nehalffac=Nehalf;
while(j>0)
{
  Nehalffac=Nehalffac*j;
  j--;
}

Nst1= Nsifac/Nehalffac;
Nst = Nsifac1/(Nehalffac*Nehalffac);
```

```
   /* now create the state numbers and the look up tables */

   unsigned long long int num, num1, num2, num3;
   /* used in binary labeling */

   /* now find the maximum number up to which binary
       numbers will be created */

   num = pow(2,Nsi);

   /* now define the maximum number of lanczos steps */
   /* this avoids using too much memory */

   int steps;

   printf("How many Lanczos Steps?\n");
   fgets(line, sizeof(line),stdin);
   sscanf(line, "%d", &steps);

   /* now create the binary states */

   unsigned long long int * statenumhalf, * statenum;

   statenumhalf = (unsigned long long int *)
               malloc(Nst1*sizeof(unsigned long long int));
   statenum = (unsigned long long int *)
               malloc(Nst*sizeof(unsigned long long int));

   int * bin,* bin_change;
   unsigned long long int tempnum;
   int elecct;
   unsigned long long int statenumrest;

#include "bin_create_nodoubocc.c"

   /* the states have been created */

   /* now the Lanczos routine will begin */
```

```
   /* variables used in the BLAS & LAPACK routines */

   int    lda = Nst;
   int    INCX = 1;
   int    INCY = 1;
   char   jobz, range, uplo;
   int    il, iu, M, lwork, liwork, *isuppz, *iwork, info;
   unsigned long long int ldz;
   double  vl, vu, *work, abstol,  *ZT;
   double WT;
   int ldz1;
   int lwork1;
   int liwork1;

   jobz = 'V';
   range = 'I';
   uplo    = 'U';
   il = 1;
   iu = 1;
   M = iu - il + 1;
   abstol = 0.000001;

// define vectors used in Lanczos

   double *w; // the initial normalised trial vector
   double *a;  // the diagonal matrix element vector
               //   of the tridiagonal matrix
   double *b; // the diagonal matrix element vector
              // of the tridiagonal matrix
   double *q; // the initial "eigenvector"
   double *y; // an extra vector used in the
              // matrix multiplication
   double *t1; // an extra vector used in the code to
               // copy vectors
   double * cons;  // a vector containing some constants
                   // used in Lanczos routine
   double *Hamvec; // the row matrix used in the
                   // Hamiltonian generation
```

```
// quantities used in the hamiltonian code

   int oldsite, newsite, i1, i2, j1, phase1,phase2,phaset;
   unsigned long long int upper,lower,search;

   int * bin_sign;
   int * dist_arr;

//  now define other quantities

   unsigned long long int lan; // the lanczos step count
   double * grndst;  // the groundstate vector
   double diff; // the difference between the eigenvalues
   double check;
   int comp;
   double norm;
   double norm1;

// specify the tolerance

   printf("What is difference in the eigenvalues?\n");
   fgets(line, sizeof(line),stdin);
   sscanf(line, "%lf", &diff);

// specify the step at which to start diagonalization

   printf("When to start diagonalizing?\n");
   fgets(line, sizeof(line),stdin);
   sscanf(line, "%d", &comp);

// first intialise the random number generator

   gsl_rng *NUM= gsl_rng_alloc(gsl_rng_taus);
   gsl_rng *PN= gsl_rng_alloc(gsl_rng_taus2);

// now seed the rng

   int SEED, SEED1; // the seeds for the generators

   printf("Enter an integer\n");
```

```
   fgets(line, sizeof(line),stdin);
   sscanf(line, "%d", &SEED);
   printf("Enter another integer\n");
   fgets(line, sizeof(line),stdin);
   sscanf(line, "%d", &SEED1);

// open a file to save diagnostic information

   char data[100];
   char data1[100];
   char data2[100];

   FILE *fp;
   sprintf(data, "t_J_Honeycomb_LanczosRunInfo
      _L=%d_Ne=%d_J=%2.3lf_tol=%2.1e.txt",L,Ne,J,diff);
   fp=fopen(data, "w");

// gsl will now generate a random normalised trial vector

#include "rand.c"

// now define the lattice

#include "distance_honeycomb.c"

// the Lanczos routine now begins

// first allocate space for the diagonal
// and subdiagonal matrix elements

   a = (double *) malloc (steps*sizeof(double));
   b = (double *) malloc (steps*sizeof(double));

// vectors which will be constantly rewritten over and over again

   cons = (double *) calloc (2, sizeof(double));
   y = (double *) calloc (Nst, sizeof(double));
   q = (double *) calloc (Nst, sizeof(double));

#include "tJ_mat_unref_vec.c" /* the Hamiltonian generation */
```

```
   cons[0] = 1.0;
   daxpy_(&Nst, &cons[0], y, &INCX, q, &INCY);
      //q[i]=q[i]+y[i](completing q=q+M*w)
   free(y);
   a[0] = ddot_(&Nst, w, &INCX, q, &INCY); // a[k]=w[i]*q[i]
   cons[1] = -a[0];
   daxpy_(&Nst, &cons[1], w, &INCX, q, &INCY);
       //q[i]=q[i]-a[k]*w[i]
   b[0] = dnrm2_(&Nst, q, &INCX); // b[k]=q[i]*q[i]
   free(cons);

   for ( lan=1; lan<steps; lan++)
   {
      cons = (double *) calloc (4, sizeof(double));
      t1 = (double *) calloc (Nst, sizeof(double));
      dcopy_(&Nst, w, &INCX, t1, &INCY);  //t=w[i]
      free(w);
      w = (double *) calloc (Nst, sizeof(double));
      cons[0] = (1/b[lan-1]);
      daxpy_(&Nst,  &cons[0], q, &INCX, w, &INCY);
         //w[i]=q[i]/b[k-1]
      free(q);
      q = (double *) calloc (Nst, sizeof(double));
      cons[1] = -b[lan-1];
      daxpy_(&Nst,  &cons[1], t1, &INCX, q, &INCY);
        //q[i]=-b[k-1]*t
      free(t1);
      y = (double *) calloc (Nst, sizeof(double));

#include "tJ_mat_unref_vec.c" /* the Hamiltonian generation */

      cons[2] = 1.0;
      daxpy_(&Nst,  &cons[2], y, &INCX, q, &INCY);
        // q[i]=q[i]+y[i]
      free(y);
      a[lan] = ddot_(&Nst, w, &INCX, q, &INCY);
        // a[k]=w[i]*q[i]
      cons[3] = -a[lan];
      daxpy_(&Nst, &cons[3], w, &INCX, q, &INCY);
```

```
  //q[i]=q[i]-a[k]*w[i]
b[lan] = dnrm2_(&Nst, q, &INCX); // b[k]=q[i]*q[i]
free(cons);

// now after a given number of lanczos loops
//  begin finding the groundstate T[i,j]

if (lan>comp)
{

  // first copy the diagonal and subdiagonal vectors
  // since they will be over written upon diagonalization

   double *d;  // diag components
   d = (double *) calloc (lan, sizeof(double));
   double *e;  // sub diag components
   e = (double *) calloc (lan-1, sizeof(double));
   dcopy_(&lan, a, &INCX, d, &INCY);
   k1=lan-1;
   dcopy_(&k1, b, &INCX, e, &INCY);
   lwork1  = 33*lan;
   liwork1 = 10*lan;
   ldz1= lan;
   ZT   = (double *) malloc(ldz1*1*sizeof(double));
          // the lanczos groundstate
   isuppz = (int *) malloc(2*lan*sizeof(int));
   work   = (double *) malloc(33*lan*sizeof(double));
   iwork  = (int *) malloc(10*lan*sizeof(int));

   dstevr_(&jobz, &range, &lan, d, e, &vl, &vu, &il,
             &iu, &abstol, &M, &WT, ZT, &ldz1, isuppz,
              work, &lwork1, iwork, &liwork1, &info);

   free(d);
   free(e);

   // now find the tolerance condition

   check = fabs(b[lan-1]*ZT[lan-1]);
```

```
// save the results to the diagonstic file

fprintf(fp,"%lld\t",lan);
fprintf(fp,"%+2.10e\t",check);
fprintf(fp,"%+2.10e\n",WT);
fflush(fp);

// now test the tolerance condition

if (check <= diff)
{
   steps = lan; // set the max steps for the vector code
   break;
}

// save some important info every tenth step
// in case something happens which terminates
// the code prematurely

if(lan%10==0)
{
   FILE *fp4;
   sprintf(data1,
      "Z_t_J_Honeycomb_LanczosVector
            _L=%d_Ne=%d_J=%2.3lf.txt",L,Ne,J);
   fp4=fopen(data1, "w");

   for(i=0; i<lan; i++)
   {
      fprintf(fp4,"%+2.10e\n", ZT[i]);
   }

   fclose(fp4);

   FILE *fp5;
   sprintf(data2,
       "t_J_Honeycomb_RestartInfo
             _L=%d_Ne=%d_J=%2.3lf.txt",L,Ne,J);
   fp5=fopen(data2, "w");
```

```
          for(i=0; i<Nst; i++)
          {
             fprintf(fp5,"%+2.10e\n", w[i]);
          }

          for(i=0; i<Nst; i++)
          {
             fprintf(fp5,"%+2.10e\n", q[i]);
          }

          for(i=0; i<lan; i++)
          {
             fprintf(fp5,"%+2.10e\n", a[i]);
          }

          for(i=0; i<lan; i++)
          {
             fprintf(fp5,"%+2.10e\n", b[i]);
          }

          fclose(fp5);
      } // end file save if
    } // end if
} // end lan

fclose(fp);

// now print the groundstate energy to a file

FILE *fp2;
sprintf(data,
     "t_J_Honeycomb_GSNRG_L=%d_Ne=%dJ=%2.3lf
               _tol=%2.1e.txt",L,Ne,J,diff);
fp2=fopen(data, "w");
fprintf(fp2,"%+2.10e\n\n", WT);
fclose(fp2);

FILE *fp4;
sprintf(data1, "Z_t_J_Honeycomb_LanczosVector
              _L=%d_Ne=%d_J=%2.3lf.txt",L,Ne,J);
```

```
fp4=fopen(data1, "w");

// create input file for vector code

char datav[100];

FILE *fpv;
sprintf(datav, "in1_%d%d%2.1lf",L,Ne,J);
fpv=fopen(datav, "w");

fprintf(fpv, "%d\n%d\n%2.1lf\n%2.1lf\n%d\n%d\n%lld\n",
               L,Ne,t,J,SEED,SEED1,lan);

for(i=0; i<lan; i++)
{
   fprintf(fp4,"%+2.10e\n", ZT[i]);
   fprintf(fpv, "%+2.10e\n",ZT[i]);
}
fclose(fp4);
fclose(fpv);

FILE *fp5;
sprintf(data2, "t_J_Honeycomb_RestartInfo
           _L=%d_Ne=%d_J=%2.3lf.txt",L,Ne,J);
fp5=fopen(data2, "w");

for(i=0; i<Nst; i++)
{
   fprintf(fp5,"%+2.10e\n", w[i]);
}

for(i=0; i<Nst; i++)
{
   fprintf(fp5,"%+2.10e\n", q[i]);
}

for(i=0; i<lan; i++)
{
   fprintf(fp5,"%+2.10e\n", a[i]);
}
```

```
   for(i=0; i<lan; i++)
   {
      fprintf(fp5,"%+2.10e\n", b[i]);
   }

   fclose(fp5);

   // noe free vectors used durign Lanczos routine

   free(w);
   free(a);
   free(b);
   free(q);
   free(ZT);

  return 0;
}
```

E.2 Generation of the Hamiltonian Matrix

```
for (k1=0; k1<Nst; k1++)
{

   Hamvec = (double *) calloc (Nst, sizeof(double));

   // first convert state to binary form

   bin = (int *)calloc(2*Nsi,sizeof(int));
   num=statenum[k1];
   for (i1=0; i1<2*Nsi; i1++)
   {
      if (num % 2 == 0)
      {
         num=num/2;
      }
      else
      {
         bin[i1]=1;
```

```
      num = (num-1)/2;
   }
}

// determine the possibility of a diagonal entry
// by analysing the state itself

J1=0;
for (i1=0; i1<Nsi; i1++)
{
   l=(i1+1)%Nsi;
   J1=J1+(bin[i1]-bin[i1+Nsi])*(bin[l]-bin[l+Nsi]);
}

// now find the matrix element

Hamvec[k1] = J*J1/4;

// now find all off-diagonal elements
  // connected to the state
// consider first the up spins
// first search for t-terms in the up spin state
// first sort through the binaries to find the
   // other possible arrangments

elecct = 0;
for (i1=0; i1<Nsi; i1++)
{

// first find a site with an electron on it

   if (elecct==Nehalf){break;}
   if (bin[i1]==1)
   {

      // now find all possible nearest neighbours
      // by sorting through the distance matrix
      //for non-zero entries

      elecct++; // count electrons to avoid sorting
```

```
          // through empty sites
oldsite = i1;
for (i2=0; i2<Nsi; i2++)
{
   if(dist_arr[i1*Nsi+i2]==1)
   {

      // search through the binary state to make sure
      // there is no electron on the site

      if((bin[i2]==0)&&(bin[i2+Nsi]==0))
      {
         // now form the new state number

         newsite =i2;
         tempnum = statenum[k1]
                -pow(2,oldsite)+pow(2,newsite);

         // find the state this is connected to

         upper = Nst; lower = 0;
         search =lower+upper;

         for (k3=0; k3<Nst/2; k3++)
         {
            if(search%2==0)
            {
               search = search/2;
            }
            else
            {
               search = (search-1)/2;
            }
            if(tempnum == statenum[search])
            {
               num = statenum[search];
               k2=search;
               break;
            }
            else if(tempnum < statenum[search])
```

```
   {
      upper = search;
      search = lower + upper;
   }
   else
   {
      lower = search;
      search = lower + upper;
   }
}

// now find the sign on the hopping, t

bin_sign = (int *)calloc(2*Nsi,sizeof(int));

for (j1=0; j1<2*Nsi; j1++)
{
   if (num % 2 == 0)
   {
      num=num/2;
   }
   else
   {
      bin_sign[j1]=1;
      num = (num-1)/2;
   }
}

// now calculate the sign on the hopping term
phase1=0;
phase2=0;

for(j1=oldsite; j1<Nsi; j1++)
{
   phase1 = phase1 + bin[j1];
}

for(j1=newsite; j1<Nsi; j1++)
{
   phase2 = phase2 + bin_sign[j1];
```

```
                }
                free(bin_sign);

                phaset = pow(-1,phase1+phase2);

                Hamvec[k2]=-phaset*t;
             }

                // now search for J-terms

             else if ((bin[i2]==0)&&(bin[i2+Nsi]==1))
             {

// see if there is a down spin on the nearest neighbour site
// make the site it is moving to is empty

                if(bin[i1+Nsi]==1){continue;}
                newsite =i2;
                tempnum = statenum[k1]-pow(2,oldsite)
                  +pow(2,newsite)-pow(2,Nsi+newsite)
                  +pow(2,Nsi+oldsite);

                // now find the state this is connected to

                upper = Nst; lower = 0;
                search =lower+upper;

                for (k3=0; k3<Nst/2; k3++)
                {
                   if(search%2==0)
                   {
                      search = search/2;
                   }
                   else
                   {
                      search = (search-1)/2;
                   }
                   if(tempnum == statenum[search])
                   {
                      num = statenum[search];
```

```
                        k2=search;
                        break;
                     }
                     else if(tempnum < statenum[search])
                     {
                        upper = search;
                        search = lower + upper;
                     }
                     else
                     {
                        lower = search;
                        search = lower + upper;
                     }
                  }
                  Hamvec[k2]=-J/2;
               } // end down spin find if
               else
               {
                  continue;
               }

            } // end distance if
         } // end i2-loop

      } // end electron search if bin[i1]
   } // end i1-for

      // now do it over again for the down spin
      // only need to find t-term

   elecct=0;
   for (i1=0; i1<Nsi; i1++)
   {

    // first find a site with an electron on it

      if(elecct==Nehalf){break;}
      if (bin[Nsi+i1]==1)
      {
         // find all possible nearest neighbours
```

```
// by sorting through the distance matrix
// for non-zero entries

elecct++;
oldsite = i1;
for (i2=0; i2<Nsi;i2++)
{
   if(dist_arr[i1*Nsi+i2]==1)
   {
      // make sure there is no electron on the site

      if((bin[i2]==1)||(bin[i2+Nsi]==1)){continue;}

      // now form the new state number

      newsite =i2;
      tempnum = statenum[k1]-pow(2,Nsi+oldsite)
                  +pow(2,Nsi+newsite);

      // find the new state this is connected to

      upper = Nst; lower = 0;
      search =lower+upper;

      for (k3=0; k3<Nst/2; k3++)
      {
         if(search%2==0)
         {
            search = search/2;
         }
         else
         {
            search = (search-1)/2;
         }
         if(tempnum == statenum[search])
         {
            num = statenum[search];
            k2=search;
            break;
         }
```

```
   else if(tempnum < statenum[search])
   {
      upper = search;
      search = lower + upper;
   }
   else
   {
      lower = search;
      search = lower + upper;
   }
}

// find the sign on the t

bin_sign = (int *)calloc(2*Nsi,sizeof(int));
for (j1=0; j1<2*Nsi; j1++)
{
   if (num % 2 == 0)
   {
      num=num/2;
   }
   else
   {
      bin_sign[j1]=1;
      num = (num-1)/2;
   }
}

// now calculate the sign on the hopping term

phase1=0;
phase2=0;
for(j1=(Nsi+oldsite); j1<2*Nsi; j1++)
{
   phase1 = phase1 + bin[j1];
}
for(j1=(Nsi+newsite); j1<2*Nsi; j1++)
{
   phase2 = phase2 + bin_sign[j1];
}
```

```
                free(bin_sign);
                phaset = pow(-1,phase1+phase2);
                Hamvec[k2]=-phaset*t;
             } // end distance if
          } // end i2-loop
       } // end electron search if bin[i1]
    } // end i1-for

    // now multiply the Hamiltonian row by the current Lanczos vector

    y[k1] = ddot_(&Nst, Hamvec, &INCX, w, &INCY);

    /* now free the Hamvec */

    free(Hamvec);

    /* now free the bin */

    free(bin);

} // end main (i - for)
```

E.3 Generation of the Binary States

```
    k1=0;
    for (num1=1; num1<num; num1++)
    {
       elecct = 0;
       num2=num1;
       for (i=0; i<Nsi; i++)
       {
          if (num2 % 2 == 0)
          {
             num2=num2/2;
          }
          else
          {
             elecct++;
             num2 = (num2-1)/2;
```

```
      }
   }

   /* now decide whether or not the statenum will be recorded
         based on if the number of electrons is proper */

   if (elecct == Nehalf)
   {
      statenumhalf[k1]=num1;
      k1++;
      if(k1==Nst){break;}
   }
}

/* now create the full state by multiplying
      every statenumhalf by each other */

k1=0;
for(k2=0; k2<Nst1; k2++)
{
   num=statenumhalf[k2];
   statenumrest=0;
   for (k=0; k<Nsi; k++)
   {
      if (num % 2 == 0)
      {
         num=num/2;
      }
      else
      {
         statenumrest = statenumrest+pow(2,Nsi+k);
         num = (num-1)/2;
      }
   }

   for(k3=0; k3<Nst1; k3++)
   {
       num3=statenumhalf[k3]+statenumrest;

       // convert the temp_state to a binary to count the ones
```

```
        bin = (int *)calloc(2*Nsi,sizeof(int));
        for (k=0; k<2*Nsi; k++)
        {
           if (num3 % 2 == 0)
           {
              bin[k]=0;
              num3=num3/2;
           }
           else
           {
              bin[k]=1;
              num3 = (num3-1)/2;
           }
        }

        // now count the ones

        tempnum = 0;
        for (k4=0; k4<Nsi; k4++)
        {
           tempnum = tempnum + bin[k4]*bin[k4+Nsi];
        }
        free(bin);
        if(tempnum==0)
        {
           statenum[k1]=statenumhalf[k3]+statenumrest;
           k1++;
        }
     }
  }
  free(statenumhalf);
```